**Article:**
Aad, G., Aakvaag, E., Abbott, B. et al. (2025) Search for tt H /A → ttt t production in proton–proton collisions at √s = 13 TeV with the ATLAS detector. The European Physical Journal C, 85 (5). 573. ISSN: 1434-6044

https://doi.org/10.1140/epjc/s10052-025-14041-z

Eur. Phys. J. C (2025) 85:573
https://doi.org/10.1140/epjc/s10052-025-14041-z

THE EUROPEAN PHYSICAL JOURNAL C

Regular Article - Experimental Physics

# Search for $t\bar{t}H/A \to t\bar{t}t\bar{t}$ production in proton–proton collisions at $\sqrt{s} = 13$ TeV with the ATLAS detector

**ATLAS Collaboration**[⋆]

CERN, 1211 Geneva 23, Switzerland

Received: 2 September 2024 / Accepted: 8 March 2025


**Abstract** A search is presented for a heavy scalar ($H$) or pseudo-scalar ($A$) predicted by the two-Higgs-doublet models, where the $H/A$ is produced in association with a top-quark pair ($t\bar{t}H/A$), and with the $H/A$ decaying into a $t\bar{t}$ pair. The full LHC Run 2 proton–proton collision data collected by the ATLAS experiment is used, corresponding to an integrated luminosity of 139 fb$^{-1}$. Events are selected requiring exactly one or two opposite-charge electrons or muons. Data-driven corrections are applied to improve the modelling of the $t\bar{t}$+jets background in the regime with high jet and $b$-jet multiplicities. These include a novel multi-dimensional kinematic reweighting based on a neural network trained using data and simulations. An $H/A$-mass parameterised graph neural network is trained to optimise the signal-to-background discrimination. In combination with the previous search performed by the ATLAS Collaboration in the multilepton final state, the observed upper limits on the $t\bar{t}H/A \to t\bar{t}t\bar{t}$ production cross-section at 95% confidence level range between 14 fb and 5.0 fb for an $H/A$ with mass between 400 GeV and 1000 GeV, respectively. Assuming that both the $H$ and $A$ contribute to the $t\bar{t}t\bar{t}$ cross-section, $\tan\beta$ values below 1.7 or 0.7 are excluded for a mass of 400 GeV or 1000 GeV, respectively. The results are also used to constrain a model predicting the pair production of a colour-octet scalar, with the scalar decaying into a $t\bar{t}$ pair.

## Contents



## 1 Introduction

The discovery of the Higgs boson by the ATLAS and CMS collaborations at the Large Hadron Collider (LHC) completes the list of elementary particles in the Standard Model (SM) [1,2]. Shortcomings of the SM remain, such as quadratic divergences arising from radiative corrections to the Higgs boson mass [3] and the nature of non-baryonic dark matter [4]. As a result, many beyond the Standard Model (BSM) theories have been proposed with extended Higgs sectors, such as two-Higgs-doublets models (2HDM) [5], hMSSM [6–8], and models with Higgs boson triplets [9–14]. A search is presented for additional heavy Higgs bosons using a four-top-quark ($t\bar{t}t\bar{t}$) final state. In Type-II 2HDM models, the Higgs boson sector consists of two complex doublets of Higgs boson fields and generates five scalar states including CP-even neutral Higgs bosons $h$ and $H$, a CP-odd neutral Higgs boson, $A$, and two charged Higgs boson states $H^{\pm}$. There are five free parameters including three Higgs boson masses, the mixing angle of the two CP-even Higgs boson states ($\alpha$) and the ratio of the vacuum expectation values of the Higgs boson doublets ($\tan\beta$). In what is called the 'alignment limit', where $\sin(\beta-\alpha) = 1$, the $h$ couplings in 2HDM matches those of the SM Higgs boson.

⋆ e-mail: atlas.publications@cern.ch

Published online: 26 May 2025

Direct searches for heavy neutral bosons were carried out by the ATLAS and CMS collaborations [15–22], and also indirect searches using precision measurements of the production cross-sections and decay rates of the SM Higgs boson [23]. These searches and measurements effectively restrict the available parameter space to the alignment limit [24].

In the 2HDM model, for $H/A$ masses $> 500$ GeV and modest values of $\tan\beta$, the predominant decay mode is into a $t\bar{t}$ pair. Searches for $H/A \to t\bar{t}$ produced via a gluon–gluon initiated loop are difficult because of destructive interference with the SM $t\bar{t}$ background that distorts the Breit–Wigner peak in the $t\bar{t}$ mass spectrum [25,26]. Both the ATLAS experiment (20.3 fb$^{-1}$ at $\sqrt{s} = 8$ TeV) and the CMS experiment (36 fb$^{-1}$ at $\sqrt{s} = 13$ TeV) searched for $gg \to A/H \to t\bar{t}$ taking the interference term into account [20,27]. The ATLAS experiment recently published results in the same channel using the full Run 2 data set at $\sqrt{s} = 13$ TeV [19]. Alternatively, $H/A$ production in association with a $t\bar{t}$ pair, followed by $H/A \to t\bar{t}$, is much less susceptible to interference effects with the SM $t\bar{t}t\bar{t}$ production. An illustrative Feynman diagram for $t\bar{t}H/A \to t\bar{t}t\bar{t}$ production is shown in Fig. 1. Searches for $H/A$ production in the $t\bar{t}t\bar{t}$ final state are therefore promising, especially given that the SM $t\bar{t}t\bar{t}$ production has now been observed by both the ATLAS [28] and CMS experiments [29]. The measured cross-sections using final states with two leptons with the same electric charge or at least three leptons (2LSS/ML) are $22.5^{+4.7}_{-4.3}(\text{stat.})^{+4.6}_{-3.4}(\text{syst.})$ fb by the ATLAS experiment and $17.7^{+3.7}_{-3.5}(\text{stat.})^{+2.3}_{-1.9}(\text{syst.})$ fb by the CMS experiment. Both of the measurements are consistent with the latest SM prediction of $13.4^{+1.0}_{-1.8}$ fb, computed at next-to-leading-order (NLO) with full electroweak (EW) corrections including threshold resummation at next-to-leading-logarithm (NLL′) accuracy [30]. With the present uncertainties, both the measurements leave room for additional contributions to SM $t\bar{t}t\bar{t}$ production. Both the ATLAS and CMS experiments have searched for $t\bar{t}H/A \to t\bar{t}t\bar{t}$ production in the 2LSS/ML final state at $\sqrt{s} = 13$ TeV [21,22,31,32].

A search is presented for $t\bar{t}H/A \to t\bar{t}t\bar{t}$ in the $H/A$ mass ($m_H$) range of 400−1000 GeV. The search uses events with exactly one lepton (electron or muon) or two leptons with opposite electric charge (1L/2LOS), and multiple heavy-flavour jets selected from the 139 fb$^{-1}$ of proton–proton ($pp$) collision data at $\sqrt{s} = 13$ TeV collected by the ATLAS experiment during 2015–2018. The analysis adopts similar baseline strategies to those used in the $t\bar{t}t\bar{t}$ cross-section measurement in the 1L/2LOS channel [33], with improved physics object reconstruction and identification, advanced background modelling of $t\bar{t}$+jets with multivariate data-driven corrections, and a new $m_{H/A}$-parameterised multivariate discriminant. The cross-section of SM $t\bar{t}t\bar{t}$ production is taken to be the latest NLO+NLL′ prediction from Ref. [30] in the search. Due to the smallness of the SM $t\bar{t}t\bar{t}$ production cross-section and the little discrimination between SM $t\bar{t}t\bar{t}$ and $t\bar{t}H/A \to t\bar{t}t\bar{t}$ production with $m_{H/A}$ close to 400 GeV, a simultaneous measurement of the SM $t\bar{t}t\bar{t}$ cross-section is infeasible. Limits are produced on the $t\bar{t}H/A$ production cross-section times branching ratio of $H/A \to t\bar{t}$ as a function of $m_{H/A}$. A combination with a previous search using the 2LSS/ML final state and the same data sample [21] is performed. The upper limits on the cross-sections are interpreted in the context of a Type-II 2HDM in the alignment limit. The analysis also sets limits on a model predicting the pair production of a colour-octet scalar, usually known as a sgluon, where the sgluons decay into $t\bar{t}$ pairs [34].

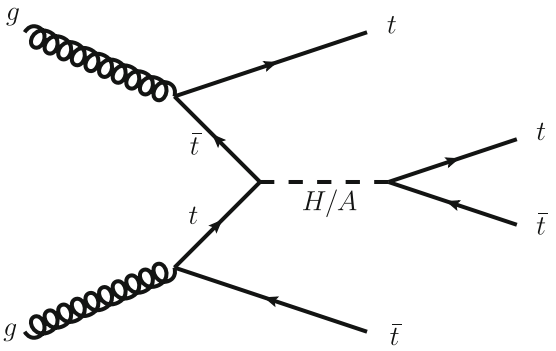


**Fig. 1** Illustrative Feynman diagram showing the production of a heavy scalar or pseudo-scalar Higgs boson, $H/A$, produced in association with a pair of top quarks and the Higgs boson decaying into a pair of top quarks

## 2 ATLAS detector

The ATLAS detector [35] at the LHC covers nearly the entire solid angle around the collision point.[1] It consists of an inner tracking detector surrounded by a thin superconducting solenoid, electromagnetic and hadronic calorimeters, and a muon spectrometer incorporating three large superconducting air-core toroidal magnets.

The inner-detector system (ID) is immersed in a 2 T axial magnetic field and provides charged-particle tracking in the range of $|\eta| < 2.5$. The high-granularity silicon pixel detector covers the vertex region and typically provides four

[1] ATLAS uses a right-handed coordinate system with its origin at the nominal interaction point (IP) in the centre of the detector and the $z$-axis along the beam pipe. The $x$-axis points from the IP to the centre of the LHC ring, and the $y$-axis points upwards. Polar coordinates $(r, \phi)$ are used in the transverse plane, $\phi$ being the azimuthal angle around the $z$-axis. The pseudorapidity is defined in terms of the polar angle $\theta$ as $\eta = -\ln\tan(\theta/2)$ and is equal to the rapidity $y = \frac{1}{2}\ln\left(\frac{E+p_z c}{E-p_z c}\right)$ in the relativistic limit. Angular distance is measured in units of $\Delta R \equiv \sqrt{(\Delta y)^2 + (\Delta\phi)^2}$.

measurements per track, the first hit generally being in the insertable B-layer (IBL) installed before Run 2 [36,37]. It is followed by the SemiConductor Tracker (SCT), which usually provides eight measurements per track. These silicon detectors are complemented by the transition radiation tracker (TRT), which enables radially extended track reconstruction up to $|\eta| = 2.0$. The TRT also provides electron identification information based on the fraction of hits (typically 30 in total) above a higher energy-deposit threshold corresponding to transition radiation.

The calorimeter system covers the pseudorapidity range of $|\eta| < 4.9$. Within the region of $|\eta| < 3.2$, electromagnetic calorimetry is provided by barrel and endcap high-granularity lead/liquid-argon (LAr) calorimeters, with an additional thin LAr presampler covering $|\eta| < 1.8$ to correct for energy loss in material upstream of the calorimeters. Hadronic calorimetry is provided by the steel/scintillator-tile calorimeter, segmented into three barrel structures within $|\eta| = 1.7$, and two copper/LAr hadronic endcap calorimeters. The solid angle coverage is completed with forward copper/LAr and tungsten/LAr calorimeter modules optimised for electromagnetic and hadronic energy measurements respectively.

The muon spectrometer (MS) comprises separate trigger and high-precision tracking chambers measuring the deflection of muons in a magnetic field generated by the superconducting air-core toroidal magnets. The field integral of the toroids ranges between 2.0 and 6.0 T m across most of the detector. Three layers of precision chambers, each consisting of layers of monitored drift tubes, cover the region of $|\eta| < 2.7$, complemented by cathode-strip chambers in the forward region, where the background is highest. The muon trigger system covers the range of $|\eta| < 2.4$ with resistive-plate chambers in the barrel, and thin-gap chambers in the endcap regions.

The luminosity is measured mainly by the LUCID–2 [38] detector that records Cherenkov light produced in the quartz windows of photomultipliers located close to the beampipe.

Events are selected by the first-level trigger system implemented in custom hardware, followed by selections made by algorithms implemented in software in the high-level trigger [39]. The first-level trigger accepts events from the 40 MHz bunch crossings at a rate below 100 kHz, which the high-level trigger further reduces in order to record complete events to disk at about 1 kHz.

A software suite [40] is used in data simulation, in the reconstruction and analysis of real and simulated data, in detector operations, and in the trigger and data acquisition systems of the experiment.

## 3 Object and event preselection

The analysis uses $pp$ collision data collected between 2015 and 2018 by the ATLAS detector at $\sqrt{s} = 13$ TeV. The full data sample corresponds to an integrated luminosity of 139 fb$^{-1}$ [41] after applying data quality requirements [42]. Events were collected using single-lepton triggers, with minimum $p_{\mathrm{T}}$ thresholds varying from 20 to 26 GeV depending on the lepton flavour and the data-taking period [43,44]. Events are required to have a collision vertex matched with at least two ID tracks, each with transverse momentum $p_{\mathrm{T}} > 0.5$ GeV. The vertex with the largest sum of $p_{\mathrm{T}}^2$ over all matched ID tracks is referred to as the primary vertex [45].

Electron candidates are reconstructed from energy deposits in the electromagnetic calorimeter matched to a track in the ID [46] and are required to be within $|\eta| = 2.47$, excluding the calorimeter transition region $1.37 < |\eta| < 1.52$. Muon candidates are reconstructed by combining tracks in the ID with tracks in the MS [47] and are required to be within $|\eta| = 2.5$. Both the electron and muon candidates are required to have $p_{\mathrm{T}} > 10$ GeV. Electrons must satisfy the 'TightLH' identification criterion [46] and are required to be well isolated using criteria based on the sum of the energies of the topological clusters in the calorimeter and $p_{\mathrm{T}}$ of ID tracks around the reconstructed electron. Muons must meet the 'Medium' identification criterion [47] and are required to satisfy isolation requirements based on the $p_{\mathrm{T}}$ sum of the ID tracks around the reconstructed muon. The transverse impact parameter divided by its estimated uncertainty, $|d_0|/\sigma(d_0)$, is required to be lower than five (three) for electron (muon) candidates. The longitudinal impact parameter must satisfy $|z_0 \sin\theta| < 0.5$ mm for both the lepton flavours.

Jets are reconstructed by combining measurements from both the ID and the calorimeter using a particle-flow algorithm [48]. The anti-$k_t$ algorithm [49,50] with a radius parameter of $R = 0.4$ is used. These jets are referred to as 'small-$R$ jets' (or jets for simplicity). They are calibrated as described in Ref. [51] and are required to have $p_{\mathrm{T}} > 25$ GeV and $|\eta| < 2.5$. A jet-vertex tagger (JVT) [52] is applied to jets with $p_{\mathrm{T}} < 60$ GeV and $|\eta| < 2.4$ to reduce the effect of additional $pp$ collisions in the same or a nearby bunch crossing, collectively referred to as pile-up. A set of quality criteria are also applied to reject events containing at least one jet arising from non-collision sources or detector noise [53].

Jets containing $b$-hadrons are identified ($b$-tagged) using the DL1r algorithm [54]. A jet is $b$-tagged if the DL1r score is above a certain threshold, referred to as an operating point (OP). Four OPs are defined with average expected efficiencies for $b$-jets of 60%, 70%, 77% and 85%,

as determined in simulated $t\bar{t}$ events. An integer pseudo-continuous $b$-tagging (pcb) score ranging from five to one is assigned to each jet. Each score value represents that the jet satisfies one OP but fails to meet the adjacent tighter one. The largest score of five is assigned to jets satisfying the tightest OP of 60%. A score of one is assigned if a jet does not satisfy any of the OPs.

The selected and calibrated small-$R$ jets are used as inputs for jet reclustering [55], using the anti-$k_t$ algorithm with a radius parameter of $R = 1.0$. These reclustered jets are referred to as 'large-$R$ jets'. The calibration corrections and uncertainties for the reclustered large-$R$ jets are inherited from the small-$R$ jets. To suppress the contribution from pile-up, a trimming procedure is applied to the reclustered jets to remove all the matched small-$R$ jets that have $p_{\mathrm{T}}$ below 5% of the $p_{\mathrm{T}}$ of the reclustered jet. Large-$R$ jets are required to have $p_{\mathrm{T}} > 200$ GeV and $|\eta| < 2.0$.

A sequential overlap removal procedure identical to that used in Ref. [21] is applied to ensure that the same calorimeter energy deposit or the same track is not matched with two or more different reconstructed objects.

The missing transverse momentum of the event, whose magnitude is denoted by $E_{\mathrm{T}}^{\mathrm{miss}}$, is defined as the negative vector sum of the $p_{\mathrm{T}}$ of all reconstructed and calibrated objects in the event. This sum includes a term to account for the transverse momenta of ID tracks matched to the selected primary vertex but not matched with any of the selected objects in the event [56].

Events are preselected by requiring either exactly one lepton (electron or muon) and at least seven jets (1L channel) or exactly two opposite-charge leptons and at least five jets (2LOS channel). The highest-$p_{\mathrm{T}}$ (leading) lepton must have $p_{\mathrm{T}} > 28$ GeV. In the 2LOS channel, the events with two same-flavour leptons must have a dilepton invariant mass above 15 GeV and outside the $Z$ boson mass window of 83–99 GeV. Events must contain at least two $b$-tagged jets passing the 70% OP. After the preselection, ∼91% of the background events come from $t\bar{t}$+jets production, estimated by using the simulated samples described in Sect. 4 with data-driven corrections discussed in Sect. 6.

## 4 Monte Carlo simulations

Monte-Carlo (MC) simulated samples were generated for all signal and background processes [57]. The predictions are based on simulations produced with POWHEG [58–61] or MadGraph5_aMC@NLO [62] as the matrix element (ME) generator, interfaced with Pythia8 [63] or Herwig7 [64,65] for the simulation of parton shower (PS) including fragmentation and hadronisation, or combined simulations of ME and PS produced with the Sherpa2 [66] generator following the MEPS@NLO prescription [67–71]. The masses of the top quark and the SM Higgs boson in the relevant samples were set to 172.5 and 125 GeV, respectively. The A14 set of tuned parameters (tune) [72] was implemented in Pythia8 whereas for Herwig7 and Sherpa the generator-specific tuned parameters were used. Unless otherwise specified, the NNPDF2.3lo [73] and NNPDF3.0nlo [74] sets of parton distribution functions (PDF) were used for samples generated with leading-order (LO) and NLO accuracy in QCD, respectively. Pile-up events were simulated using Pythia8.186 [75] with the NNPDF2.3lo PDF set and the A3 tune [76], and overlaid on each hard-scattering event. EvtGen1.2.0 or 1.6.0 [77] were used to model heavy-flavour hadron decays in Pythia8 and Herwig7. The detector geometry and response were simulated using either Geant4 [78] or a fast simulation (AFII) which parameterises the calorimeter response [79]. All simulated samples were processed through the same reconstruction software as used for data.

The signal samples were simulated assuming a 2HDM Type-II model in the alignment limit ($\sin(\beta - \alpha) = 1$). Events of $t\bar{t}H \to t\bar{t}t\bar{t}$ were simulated assuming the on-shell production of $H$. The simulation was performed at LO accuracy in the ME using MadGraph5_aMC@NLO with the NNPDF3.1lo [74] PDF set. The decay of the top quarks is simulated in the ME generation to include spin correlations. The value of $\beta$ was found to yield no change in the event kinematics. No mixing between $H$ and $A$ was considered. No dedicated $t\bar{t}A \to t\bar{t}t\bar{t}$ samples were simulated given that the kinematic distributions of interest differ by less than 1% between $t\bar{t}H \to t\bar{t}t\bar{t}$ and $t\bar{t}A \to t\bar{t}t\bar{t}$. Seven signal samples were generated for $m_H$ from 400 to 1000 GeV spaced with 100 GeV steps. For each assumed $m_H$ value, the $H$ width was set to values consistent with the scenario of $\tan\beta \sim 1$, ranging from 5 GeV for $m_H = 400$ GeV to 30 GeV for $m_H = 1000$ GeV. Varying the width up to 75% of $m_H$ yields a change of less than 10% in only the lepton and jet $p_{\mathrm{T}}$ distributions and negligible changes in the other distributions. The interference with the SM $t\bar{t}t\bar{t}$ production was not taken into account. For the $(\tan\beta, m_{H/A})$ parameter space that this search is sensitive to, both the effects of the interference and the non-resonant production are smaller than a few percent, and are therefore neglected.

An additional BSM signal corresponding to the pair production of a colour-octet scalar ($S_8$), a sgluon, was considered, where both the $S_8$ decay into a $t\bar{t}$ pair. The production of $S_8S_8$ events was simulated at LO with MadGraph5_aMC@NLO using the simplified model from Ref. [34] with the NNPDF3.0nlo PDF set, interfaced with Pythia8. The decay of $S_8 \to t\bar{t}$ was handled by MadSpin [80,81]. Simulated samples were generated for $m_{S_8}$ ranging between 0.4 and 2 TeV, with a spacing of 100 GeV for $m_{S_8} \in [0.4, 1.5]$ TeV, and 250 GeV for $m_{S_8} \in [1.75, 2.0]$ TeV. The $S_8t\bar{t}$ coupling parameter $y_{S_8}$ was set to 0.1, ensuring that $S_8S_8$ production dominates over $t\bar{t}S_8$

production. For $y_{S_8} < 0.1$ and $m_{S_8} < 2$ TeV, the interference with the SM background and the $t\bar{t}S_8$ production contribute less than 10% to the total cross-section of $t\bar{t}t\bar{t}$ production via $S_8$ and were thus not simulated. The kinematics of $S_8S_8 \to t\bar{t}t\bar{t}$ production do not depend on the value of $y_{S_8}$.

The simulated $t\bar{t}$+jets events are classified into different groups. This classification is used to construct a detailed model of theoretical systematic uncertainties affecting this process. The events are classified as $t\bar{t}+\geq 1b$, $t\bar{t}+\geq 1c$ and $t\bar{t}$+light according to the flavour of the particle jets not originating from top-quark decays.[2] The flavour and origin of the particle jets are determined by checking whether any $b$- or $c$-hadron with $p_{\mathrm{T}} > 5$ GeV not originating from top-quark decays falls within $\Delta R = 0.3$ around the jet axis. Events with at least one particle jet matched to such $b$-hadrons are classified as $t\bar{t}+\geq 1b$ events. Those that are not classified as $t\bar{t}+\geq 1b$ events but contain at least one particle jet matched to $c$-hadrons are classified as $t\bar{t}+\geq 1c$ events. The $t\bar{t}+\geq 1b$ and $t\bar{t}+\geq 1c$ events are collectively referred to as '$t\bar{t}$+HF' events (HF for 'heavy flavour'). The remaining are classified as $t\bar{t}$+light events. The $t\bar{t}+\geq 1b$ events are further classified into $t\bar{t}+b$, $t\bar{t}+b\bar{b}$, $t\bar{t}+B$ and $t\bar{t}+\geq 3b$ events, where the $b$ or $\bar{b}$ refers to a particle jet matched to a single $b$-hadron, and $B$ refers to a particle jet matched to more than one $b$-hadron. The $t\bar{t}+\geq 3b$ events contain more than two particle jets matched to any number of $b$-hadrons.

The nominal $t\bar{t}$+jets prediction is based on a sample simulated using Powheg Box2 at NLO in QCD using the five-flavour scheme (5FS). The $h_{\mathrm{damp}}$ parameter, which regulates the $p_{\mathrm{T}}$ of the first additional emission beyond the Born configuration, is set to 1.5 times the top-quark mass of $m_t = 172.5$ GeV. The renormalisation and factorisation scales were set to $\frac{1}{2}\Sigma_{i=t,\bar{t}} m_{\mathrm{T},i}$, where $m_{\mathrm{T},i}$ is the transverse mass of a given parton $i$. Several samples in addition to the nominal Powheg Box+ Pythia8 samples were generated to evaluate systematic uncertainties, including samples generated with alternative ME or PS generators, MadGraph5_aMC@NLO+ Pythia8 and POWHEG+ Herwig7. Furthermore, a dedicated $t\bar{t}b\bar{b}$ sample was produced using Powheg Box Res [82,83] and OpenLoops [84–86] with the NNPDF3.0nlo_nf4 [74] PDF set, interfaced with Pythia8. This sample was produced using the four-flavour scheme (4FS) with the additional $b$-quarks in the ME generation. The $h_{\mathrm{damp}}$ parameter was set to $\frac{1}{2}\Sigma_{i=t,\bar{t},b,\bar{b}} m_{\mathrm{T},i}$. The renormalisation and factorisation scales were set to $\sqrt[4]{\prod_{i=t,\bar{t},b,\bar{b}} m_{\mathrm{T},i}}$ and $\frac{1}{2}\Sigma_{i=t,\bar{t},b,\bar{b},j} m_{\mathrm{T},i}$ (where $j$ stands for extra partons), respectively. These $t\bar{t}$+jets samples were previously studied in detail and compared in Ref. [87].

[2] Particle jets are constructed from simulated stable particles (with mean lifetime $\tau > 3\times10^{-11}$ s) using the anti-$k_t$ algorithm with $R = 0.4$ and are required to have $p_{\mathrm{T}} > 15$ GeV and $|\eta| < 2.5$.

The SM $t\bar{t}t\bar{t}$ background has an important impact on the search despite its small yield. The nominal $t\bar{t}t\bar{t}$ sample was simulated using MadGraph5_aMC@NLO at NLO in QCD with the NNPDF3.1nlo PDF set. The decay of the top quarks was simulated using MadSpin. The renormalisation and factorisation scales were set to $\frac{1}{4}\Sigma_{i=t,\bar{t},j} m_{\mathrm{T},i}$ following Ref. [88]. Two alternative samples were generated, one with Sherpa2.2.11, and another by replacing the Pythia8 parton shower of the nominal sample by Herwig7. The Sherpa sample was simulated at NLO in QCD. The renormalisation and factorisation scales were set to half of the scalar sum of the $p_{\mathrm{T}}$ of all final state particle. All $t\bar{t}t\bar{t}$ samples were normalised to the latest cross-section prediction of $13.4^{+1.0}_{-1.8}$ fb [30].

Other backgrounds constitute less than 8% of the total background. Most of these events come from $t\bar{t}H$, $t\bar{t}W$, $t\bar{t}Z$, single-top-quark and $V$+jets productions. The $t\bar{t}H$ and $t\bar{t}W/Z$ samples were simulated at NLO in QCD using Powheg Box2 and MadGraph5_aMC@NLO, respectively. For the $t\bar{t}W$ background, a dedicated sample containing only EW corrections was produced at LO in QCD, and combined with the NLO QCD sample. Alternative samples for $t\bar{t}H$ and $t\bar{t}W$ were simulated using MadGraph5_aMC@NLO+ Pythia8 and Sherpa2.2.10, respectively. The production of single-top quarks was modelled using the same generators as the ones used for the inclusive $t\bar{t}$+jets sample, including the alternative samples for systematic uncertainties. The 'diagram removal' scheme was used to treat the overlap between $tW$ and $t\bar{t}$ production. An alternative sample was simulated using the 'diagram subtraction' scheme [89]. The $V$+jets samples were simulated using Sherpa2.2.1 with the NNPDF3.0nnlo PDF set. The generation considered ME at NLO in QCD with up to two additional jets and at LO with up to four additional jets. The remaining events comprise less than 1% of the total background. These include events from $t\bar{t}WW$, $tWZ$, $tZ$, $t\bar{t}t$ production (simulated using MadGraph5_aMC@NLO) and $VV$ production (simulated using Sherpa2).

## 5 Analysis strategy and event categorisation

The $t\bar{t}H/A \to t\bar{t}t\bar{t}$ events feature high jet and $b$-jet multiplicities. The main background affecting the 1L/2LOS final states is $t\bar{t}$+jets, where several additional jets beyond the $t\bar{t}$ born level are required to give topologies similar to the $t\bar{t}t\bar{t}$ signal. Two known issues affect the modelling of the $t\bar{t}$+jets background from the simulations described in Sect. 4. The kinematics are mismodelled in the regime of high jet multiplicities and high $p_{\mathrm{T}}$ of the $t\bar{t}$ system [90] and the cross-section of $t\bar{t}$+HF production is underestimated [91,92]. Both of the issues affect the phase space populated by signal events. Data-driven corrections are adopted to mitigate

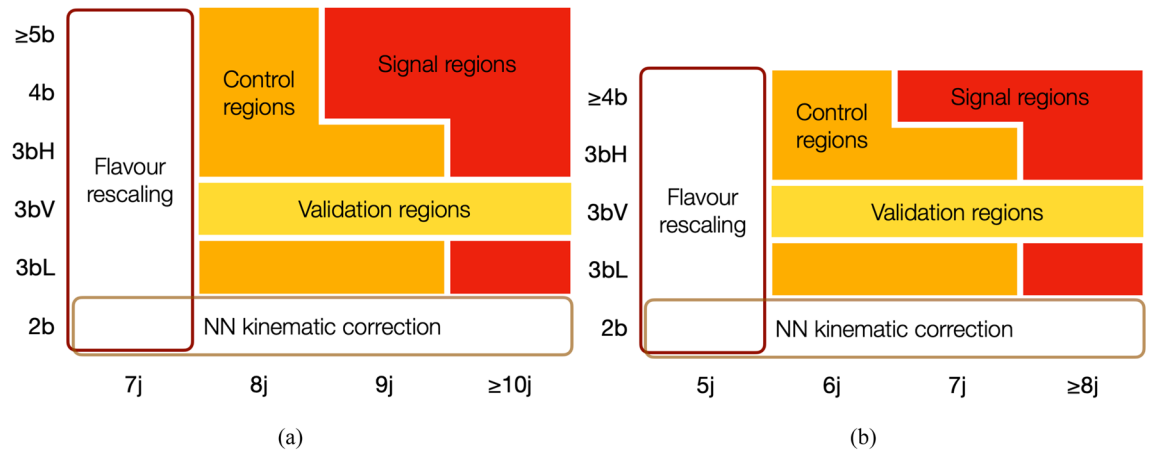


**Fig. 2** Schematic view of the event categorisation for the **a** 1L and **b** 2LOS channels. The axes represent the jet multiplicities and $b$-tagging requirements defined in Table 1. Control, signal and validation regions are shaded with different colours. The regions used to derive the flavour rescaling and NN kinematic corrections are highlighted using rectangles

the mismodelling. Rescaling factors are derived to correct the fractions and normalizations of $t\bar{t}$+light, $t\bar{t}+\geq 1c$ and $t\bar{t}+\geq 1b$, referred to as the 'flavour rescaling'. After applying the flavour rescaling, a neural network (NN) is then trained to correct the kinematic mismodelling. The details of the data-driven corrections are described in Sect. 6. Events passing the preselection are categorised into orthogonal regions. These include regions used to derive the data-driven corrections, and the control and signal regions (CR/SR) used in a profile likelihood fit (see Sect. 9) to extract and set a limit on the signal strength. In the SRs, a multivariate analysis based on $m_{H/A}$-parameterised graph neural networks (GNN) is performed to optimise the separation between the signals and the largest background, $t\bar{t}$+jets, detailed in Sect. 7.

Figure 2 illustrates the event categorisation. Events are categorised in bins of jet multiplicity, from seven jets (7j) to at least ten jets (≥10j) in the 1L channel and from five jets (5j) to at least eight jets (≥8j) in the 2LOS channel. Each jet multiplicity bin is further separated according to the $b$-tagging requirements listed in Table 1. Events are first split according to the number of $b$-tagged jets using the 70% OP ($N_b^{70\%}$), from two to at least five (four) in the 1L (2LOS) channel. The events with three $b$-tagged jets are further separated into 3bL, 3bH and 3bV regions given the number of jets passing the 60% and 85% OPs ($N_b^{60\%}$ and $N_b^{85\%}$). The 3bL (3bH) requirement aims to select events with lower (higher) purity of jets originating from $b$-quarks in events with three jets tagged at the 70% OP. This is verified in simulated samples using MC generator-level $b$-jets, defined as jets that are matched to $b$-hadrons. The 3bV requirement is used to define the validation regions (VR). The resulting six VRs have a signal contamination of $< 2\%$. The categorisation yields six (five) CRs and six (four) SRs in the 1L (2LOS) channel. The events in the 2b regions are used to derive the NN kinematic corrections to the $t\bar{t}$+jets background. The events in the 7j (5j) bin in the 1L (2LOS) channel are used to obtain the $t\bar{t}$+jets flavour rescaling factors. These regions used to derive the data-driven corrections all have negligible signal contaminations. The two sets of corrections are applied to the CRs, VRs and SRs.

**Table 1** Summary of the $b$-tagging requirements used for the event categorisation. Events in each category must satisfy all requirements listed in the columns. $N_b^{60\%}$, $N_b^{70\%}$ and $N_b^{85\%}$ are defined as the numbers of $b$-tagged jets obtained using $b$-tagging operating points with average expected efficiencies of 60%, 70% and 85%, respectively. The symbol '–' indicates that no requirement is applied

| Name | $N_b^{60\%}$ | $N_b^{70\%}$ | $N_b^{85\%}$ |
|---|---|---|---|
| 2b | – | $= 2$ | – |
| 3bL | $\leq 2$ | $= 3$ | – |
| 3bH | $= 3$ | $= 3$ | $> 3$ |
| 3bV | $= 3$ | $= 3$ | $= 3$ |
| ≥4b (2LOS) | – | $\geq 4$ | – |
| 4b (1L) | – | $= 4$ | – |
| ≥5b (1L) | – | $\geq 5$ | – |

The categorisation using $b$-tagging requirements creates regions enriched with different classes of $t\bar{t}$+jets events. In the profile likelihood fit to data, these regions provide constraints on each background class. The 3bH regions are mainly populated by $t\bar{t}+b$, $t\bar{t}+B$ and $t\bar{t}+b\bar{b}$ events, whereas the 3bL regions are populated by more $t\bar{t}$+light and $t\bar{t}+\geq 1c$ events. The ≥5b regions in the 1L channel provide unique constraints on the $t\bar{t}+\geq 3b$ background. The 2LOS channel has a lower number of events and therefore the ≥4b region is not further separated. The VRs defined using the 3bV requirement are mostly populated by $t\bar{t}+\geq 1b$ events, which are the

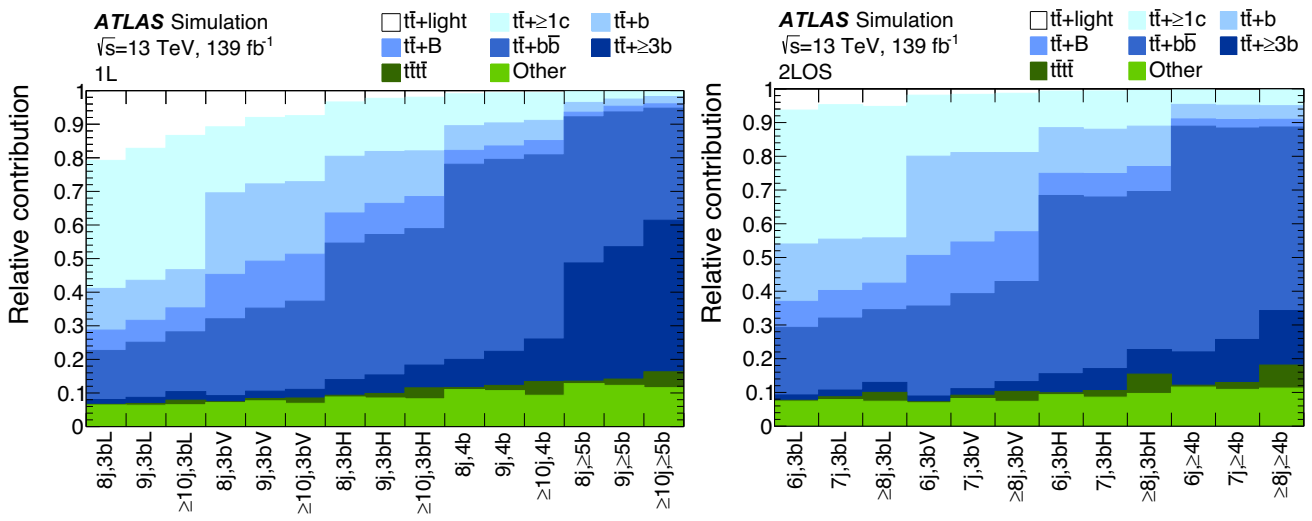


(a) (b)

**Fig. 3** The relative contribution of the different background classes in the control, validation and signal regions in the **a** 1L and **b** 2LOS channels

most important background events in the SRs. Figure 3 illustrates the background fractions in all the CRs, VRs and SRs.

## 6 Modelling of $t\bar{t}$+jets background

The flavour rescaling factors are determined as corrections to the overall normalisation of the $t\bar{t}$+light, $t\bar{t}$+$\geq$1$c$ and $t\bar{t}$+$\geq$1$b$ backgrounds. These factors correct the fraction of the three components and the overall acceptance of the $t\bar{t}$+jets background. To derive the flavour rescaling factors, events in the 7j and 5j bins respectively in the 1L and 2LOS channels are categorised into regions containing events with two, three or at least four $b$-tagged jets at the 70% OP. The predictions from the simulations are fit to data simultaneously in these six regions. The fit observable is the sum of the $b$-tagging pcb scores (defined in Sect. 3) of the third and fourth jets in descending order of the score. Systematic uncertainties arising from the calibration of the tagging efficiencies of $b$-jets and the mis-tag rates of $c$-jets and light-flavour jets are considered [93–95]. For the $t\bar{t}$+light background, two separate rescaling factors are assigned to the 1L and the 2LOS channels. This is to reduce the tension due to the different acceptance effects of the two channels. The resulting rescaling factors are $0.84 \pm 0.04$ ($0.87 \pm 0.03$) for the $t\bar{t}$+light background in the 1L (2LOS) channel, $1.61 \pm 0.13$ for the $t\bar{t}$+$\geq$1$c$ background and $1.18 \pm 0.03$ for the $t\bar{t}$+$\geq$1$b$ background. The central values are used to correct the $t\bar{t}$+jets simulations in the VRs, CRs and SRs. The fitted uncertainties in the rescaling factors are not considered in the profile likelihood fit determining the signals. Instead, more conservative uncertainties are assigned that cover the residual mis-modelling and the extrapolation from the low to high jet multiplicity bins. For $t\bar{t}$+$\geq$1$b$ and $t\bar{t}$+$\geq$1$c$, a normalisation uncertainty of 50% is assigned to each of them, based on the discrepancies observed in previous measurements [91,92]. For $t\bar{t}$+light events, a normalisation uncertainty of 5% is considered which covers both the uncertainties in the individual rescaling factors for the 1L and 2LOS channels, and the difference between the two channels.

The NN kinematic corrections are derived from multi-dimensional probability density functions of data and simulations estimated by using a feed-forward NN [96,97]. The NN is trained as a binary classifier between data and simulation. The output of the NN ($\mathcal{O}$) as a function of the input vector ($\mathbf{x}$) can be interpreted in terms of the a-posteriori Bayesian probability of data and simulations, $P_{\text{data}}(\mathbf{x})$ and $P_{\text{sim}}(\mathbf{x})$:

$$\mathcal{O}(\mathbf{x}) = P(\text{data}|\mathbf{x}) = \frac{\alpha_{\text{data}} P_{\text{data}}(\mathbf{x})}{\alpha_{\text{data}} P_{\text{data}}(\mathbf{x}) + \alpha_{\text{sim}} P_{\text{sim}}(\mathbf{x})}, \quad (1)$$

where $\alpha_{\text{data}}$ and $\alpha_{\text{sim}}$ are the proportions of data and simulated events used in the training, satisfying $\alpha_{\text{data}} + \alpha_{\text{sim}} = 1$. Event-by-event reweighting factors can therefore be obtained as:

$$w(\mathbf{x}) = \frac{\alpha_{\text{data}} P_{\text{data}}(\mathbf{x})}{\alpha_{\text{sim}} P_{\text{sim}}(\mathbf{x})} = \frac{\mathcal{O}(\mathbf{x})}{1 - \mathcal{O}(\mathbf{x})}. \quad (2)$$

The weights $w(\mathbf{x})$ can be used to reweight the simulations to match the probability density function of data. The training aims to correct only $t\bar{t}$+jets simulations, therefore other background events are subtracted from data during the training. This is done by labelling simulated non-$t\bar{t}$+jets events as 'data' events but with negative event weights. The events labelled as 'simulation' in the training are exclusively $t\bar{t}$+jets events, corrected with the flavour rescaling factors. To improve the performance of the training in the regime

with small training sample size, an exponential loss function is used [97]:

$$\mathcal{L} = P_{\text{data}}(\mathbf{x})e^{-\frac{\mathcal{O}(\mathbf{x})}{2}} + P_{\text{sim}}(\mathbf{x})e^{\frac{\mathcal{O}(\mathbf{x})}{2}}. \quad (3)$$

The resulting reweighting factors after the minimisation of $\mathcal{L}$ become $w(\mathbf{x}) = e^{\mathcal{O}(\mathbf{x})}$. The input variables to the training include the $p_{\text{T}}$ of all leptons and jets, the number of jets ($N_{\text{jets}}$) and large-$R$ jets ($N_{\text{LR-jets}}$) and $E_{\text{T}}^{\text{miss}}$. The training is performed in the inclusive 2b regions with $N_{\text{jets}} \geq 7$ (1L) and $N_{\text{jets}} \geq 5$ (2LOS) separately.

Figure 4 illustrates the effect of the data-driven corrections in the inclusive region containing all CRs, VRs and SRs, separately for the 1L and 2LOS channels. The correction improves significantly the agreement between data and the prediction in both the overall normalisation and the shape of the most relevant kinematic variables for signal-to-background discrimination.

## 7 Multivariate analysis

A multivariate discriminant is built based on a novel GNN structure [98] parameterised as $m_{H/A}$ [99]. The graphs representing the events are constructed using the reconstructed leptons, jets and $E_{\text{T}}^{\text{miss}}$ as 'nodes', encoding information about their type, four-momenta excluding $\phi$, and jet pcb scores. 'Edges' connecting all pairs of objects in the events encode their relative $\Delta\phi$, $\Delta\eta$ and $\Delta R$. In addition, event-level observables are introduced as 'global features' of each graph, covering jet $b$-tagging information, object multiplicities, event shape and kinematics, and the substructure information of the large-$R$ jets. These global features are listed in Table 2. The GNNs are built with the PyTorch library [100] and trained as a binary classifier with the signal samples at all mass points together against the $t\bar{t}$+jets background. The training is performed separately for the 1L and 2LOS channels, using events from the inclusive regions with $N_{\text{jets}} \geq 9$ (1L) and $N_{\text{jets}} \geq 6$ (2LOS) and $N_b^{70\%} \geq 3$. To balance the resulting performance against different signal masses, the signal samples at the different mass points are normalised to the same yields in the defined inclusive regions. The output of the GNN is used as the discriminant in the SRs. The 3bV regions with $\geq 9$ ($\geq 7$) jets in the 1L (2LOS) channel are used to validate the modelling of the GNN output. The $m_{H/A}$ parameterisation is done by including $m_{H/A}$ as an input to the training alongside the graphs. For the signal samples, this corresponds to the generated $m_{H/A}$. In the $t\bar{t}$+jets samples, a pseudo-$m_{H/A}$ is assigned to each event randomly taking the values from the generated signal $m_{H/A}$ with a uniform prior. The parameterisation allows for a smooth interpolation between the results at different $H/A$ mass points [99].

The training achieves an area under the receiver-operator-characteristic curve of 85% for the 400 GeV mass point and 94% for 1000 GeV mass point. The dominant feature for the training is the node-$p_{\text{T}}$ for both the channels, followed by $\sum_{i\in[1,6]} \text{pcb}_i$ and the pcb scores of the jet-nodes. Collectively, the global features $H_{\text{T}}$, $N_{\text{jets}}$ and $H_{\text{T}}^{\text{ratio}}$ and the edge feature $\Delta R$ also contribute significantly. The distributions of the GNN output evaluated at 400 GeV and 1000 GeV for both the 1L and 2LOS channels are shown in Fig. 5. The signal is compared with the SM $t\bar{t}t\bar{t}$ and $t\bar{t}$+jets backgrounds. The distributions of the signal and SM $t\bar{t}t\bar{t}$ production is similar for $m_H = 400$ GeV. The discrimination is significantly better for large $m_H$.

## 8 Systematic uncertainties

Systematic uncertainties in the results arise from uncertainties in experimental procedures, signal and background cross-sections, and the modelling of the relevant physics processes. Each uncertainty can affect either or both the normalisation and shape of the predictions. The largest uncertainties are from the modelling of the $t\bar{t}$+jets background, especially $t\bar{t}+\geq 1b$ events. The uncertainties in the modelling of the SM $t\bar{t}t\bar{t}$ production also have a sizeable contribution. The impact of the experimental uncertainties is small. The effects of the post-fit uncertainties on the results are summarised in Table 3 in Sect. 9.

### 8.1 Experimental uncertainties

All of the individual experimental uncertainties have a small impact on the analysis. The leading group of experimental uncertainties arises from the calibration of the jet energy scale and resolution [51]. The most important components are related to the modelling of the composition of gluon- and quark-jets and their detector response. The calibration of the $b$-tagging efficiencies and $c$- and light-jet rejection rates have smaller effects amongst the experimental uncertainties [93–95]. Other experimental uncertainties have minor contributions. The uncertainty in the integrated luminosity of the data sample is 1.7% [41], measured using the LUCID-2 detector [38] with complementary measurements using the ID and calorimeters. An uncertainty in the correction of the pile-up profile in the simulations to match that in data is considered. An uncertainty is applied to the corrections on the JVT selection efficiencies in simulations [52]. Uncertainties in electrons and muons arise from the calibration of the efficiencies of the trigger, reconstruction, identification and isolation requirements, and the energy scale and resolution [56]. Uncertainties in the measurement of $E_{\text{T}}^{\text{miss}}$ arise from a possible mis-calibration of its soft-track component [101].

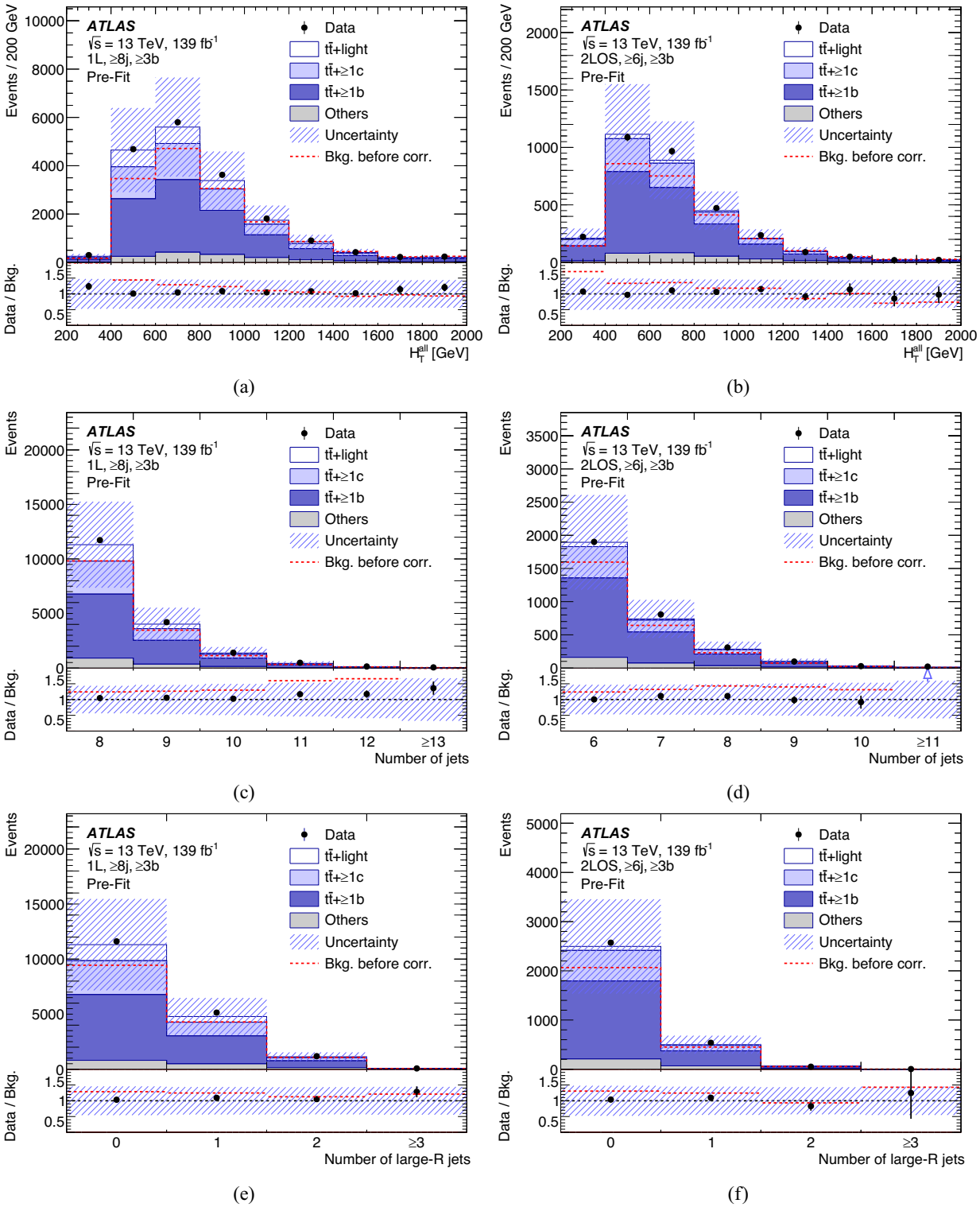


**Fig. 4** The comparison of (**a**, **b**) $H_{\mathrm{T}}$, (**c**, **d**) $N_{\mathrm{jets}}$ and (**e**, **f**) $N_{\mathrm{LR\text{-}jets}}$ distributions between data and background predictions before the likelihood fit to data (Pre-Fit), and before and after applying the data-driven corrections, separately for the 1L and 2LOS channels. The background prediction after applying the data-driven corrections is shown in coloured stacks, whilst the one before applying the corrections is shown with the red dashed line. The hashed area represents the total uncertainty in the background. The last bin in each distribution contains the overflow

**Table 2** The list of global features used in the GNN training in descending order of importance in the training of the 1L GNN. The importance is evaluated according to the fractional change in loss when removing the feature from the training

| Variable | Description |
|---|---|
| $\sum_{i\in[1,6]} \text{pcb}_i$ | Sum of the pcb scores of the six jets with the highest scores |
| $H_{\text{T}}$ | $p_{\text{T}}$ sum of all reconstructed leptons and jets |
| $N_{\text{jets}}$ | Number of jets |
| $H_{\text{T}}^{\text{ratio}}$ | $p_{\text{T}}$ sum of the four leading jets in $p_{\text{T}}$ divided by the $p_{\text{T}}$ sum of the remaining jets |
| $dR_{jj}^{\text{avg.}}$ | Average $\Delta R$ across all jet pairs |
| $m_{\text{T}}^{W}$ | $W$ boson transverse mass calculated using the lepton four-momenta and $E_{\text{T}}^{\text{miss}}$ (1L only) |
| $\Delta R_{bb}^{\text{min.}}$ | Minimum $\Delta R$ between any pair of jets $b$-tagged at the 70% OP |
| $\Delta R_{\ell b}^{\text{min.}}$ | Minimum $\Delta R$ between any pair of lepton and jet $b$-tagged at the 70% OP |
| $m_{bbb}^{\text{avg.}}$ | Average invariant mass of all triplets of jets $b$-tagged at the 70% OP |
| $m_{jjj}^{\text{avg.}}$ | Average invariant mass of all triplets of jets with an angular separation of $\Delta R < 3$ |
| $\sum d_{12}$ | Sum of the first $k_t$ splitting scale $d_{12}$ over all large-$R$ jets |
| $\sum d_{23}$ | Sum of the second $k_t$ splitting scale $d_{23}$ over all large-$R$ jets |
| $N_{\text{LR-jets}}$ | Number of large-$R$ jets with a mass greater than 100 GeV |
| Centrality | $\sum_i p_{\text{T}}^i / \sum_i E_i$ where the sums are performed over all reconstructed jets and leptons |
| $m_{\ell\ell}$ | Invariant mass of the two leptons (2LOS only) |

### 8.2 Uncertainties in the signals, SM $t\bar{t}t\bar{t}$ and $t\bar{t}$+jets

The uncertainties in signal modelling have minor impacts on the results. The uncertainties due to missing higher order QCD corrections and from PDF variations are considered. The former is evaluated by varying the renormalisation and factorisation scales in MadGraph5_aMC@NLO by a factor of two up and down, and comparing to the nominal prediction. The latter has an effect of up to 1% on the signal yields, estimated following the PDF4LHC recommendations [102].

The largest uncertainty in $t\bar{t}t\bar{t}$ modelling is evaluated by comparing the nominal sample simulated using MadGraph5_aMC@NLO+ Pythia8 with the one using Sherpa 2.2.11. This uncertainty covers the effects from the different matching schemes between the ME and PS, and different PS, hadronisation and fragmentation models. The uncertainty in the predicted $t\bar{t}t\bar{t}$ production cross-section, $^{+7.8\%}_{-13.3\%}$ from Ref. [30], has a smaller impact. Other uncertainties in $t\bar{t}t\bar{t}$ modelling have negligible impacts. These include an uncertainty evaluated by comparing the nominal sample with the one simulated using MadGraph5_aMC@NLO+ Herwig7, and the uncertainties from missing higher order QCD corrections and PDF variations evaluated in the same way as those for the signals.

The uncertainties in $t\bar{t}$+jets modelling are decomposed based on the $t\bar{t}$+jets event classification. The uncertainties for the different event classes are treated as independent. Uncertainties in the overall normalisation of $t\bar{t}$+light (5%), $t\bar{t}+\geq 1c$ (50%) and $t\bar{t}+\geq 1b$ (50%) are assigned as described in Sect. 6. Three sets of uncertainties are evaluated by comparing samples simulated using different generators. The effects from the ME-PS matching and the PS, hadronisation and fragmentation models are covered by the two uncertainties from the comparison of the nominal POWHEG+ Pythia8 sample with those simulated using MadGraph5_aMC@NLO+ Pythia8 and POWHEG+ Herwig7. For $t\bar{t}+\geq 1b$ events, another uncertainty is assigned by comparing the nominal prediction based on the 5FS with the one from the 4FS $t\bar{t}b\bar{b}$ sample. Each of these three uncertainties is first decomposed into components based on the finer classification that considers $t\bar{t}+\geq 1b$ subclasses. The component for each event class is further split into two, one controlling the shape of the fitted distributions in each region and another controlling the relative normalisation across the different regions. Other uncertainties are evaluated by varying the value of physics parameters used in the generation of the nominal sample. These are split into components for $t\bar{t}$+light, $t\bar{t}+\geq 1c$ and $t\bar{t}+\geq 1b$. The uncertainty from missing higher order QCD corrections is estimated by varying the factorisation and renormalisation scales individually or simultaneously by a factor of two up or down, and taking the largest up and down variations in any of the analysis bins. An uncertainty due to the chosen $h_{\text{damp}}$ value is estimated by varying its value up by a factor of two. The uncertainties in the amount of initial-state and final-state radiations (ISR/FSR) from the PS are evaluated, respectively, by varying the A14 tune parameter that controls the strong coupling and the FSR renormalisation scale by a factor of 2.0 and 0.625. The PDF uncertainties are estimated by using the same method as for the signals.

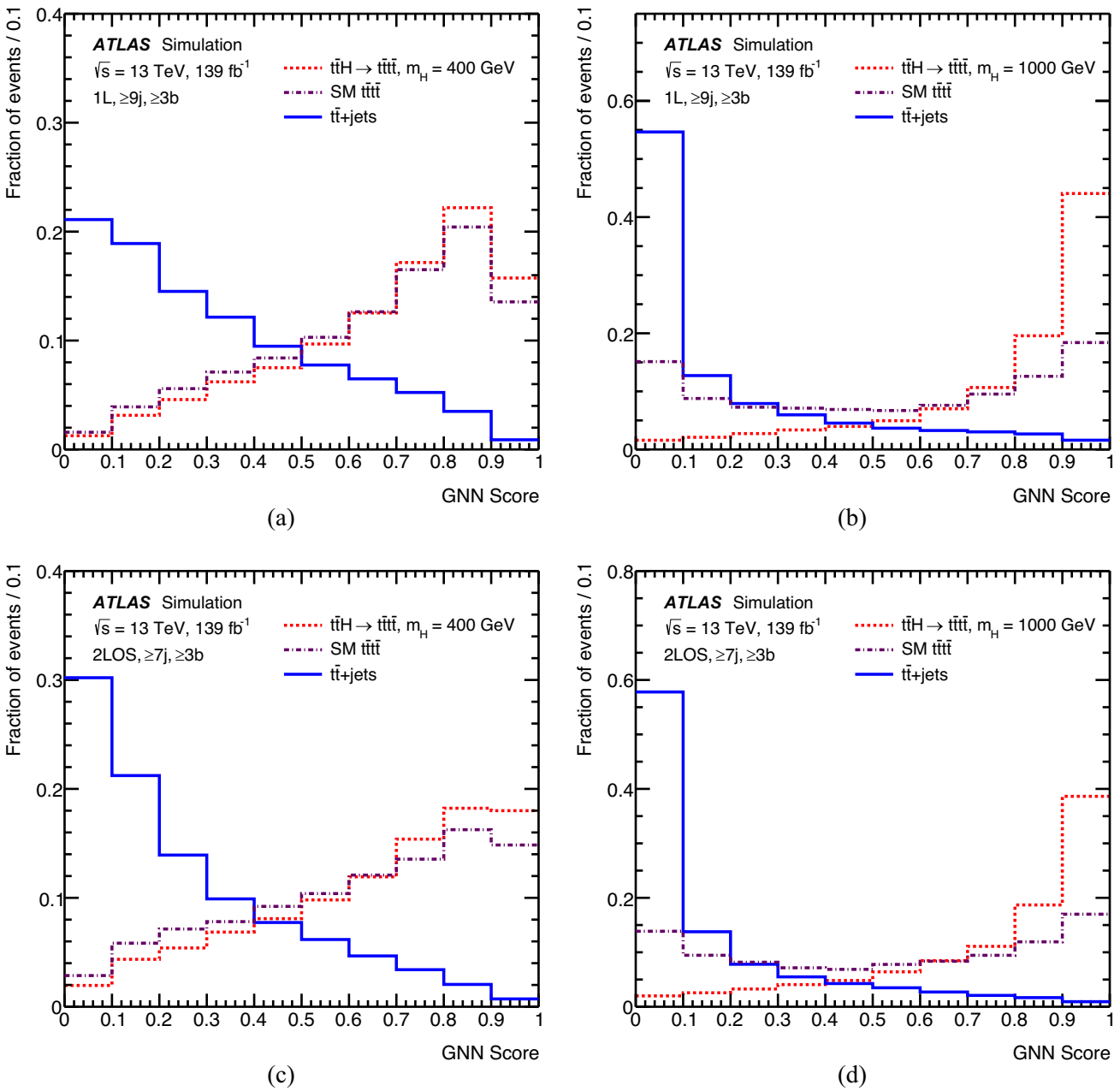


**Fig. 5** The distributions of the GNN output evaluated at 400 GeV and 1000 GeV for the (**a**, **b**) 1L and (**c**, **d**) 2LOS channels with inclusive selections close to the signal region. The distributions are compared for the signal, SM $t\bar{t}t\bar{t}$ production and $t\bar{t}$+jets production

#### *8.2.1 Flavour rescaling and NN kinematic corrections on $t\bar{t}$+jets modelling uncertainties*

The data-driven corrections described in Sect. 6 are consistently derived for and applied to the alternative $t\bar{t}$+jets predictions used to evaluate modelling uncertainties (Sect. 8.2). For each of these alternative predictions, dedicated flavour rescaling factors and NN kinematic corrections are derived. The flavour rescaling factors are derived such that the alternative predictions have the same $t\bar{t}+\geq 1b$, $t\bar{t}+\geq 1c$ and $t\bar{t}$+light yields as the nominal prediction after the flavour rescaling. The NN kinematic corrections are obtained from dedicated GNN trainings where the corresponding alternative $t\bar{t}$+jets simulations are used. These corrections reduce the size of the pre-fit uncertainties by exploiting the data. Evaluating dedicated flavour rescalings for each modelling uncertainty also avoids double counting effects from the acceptance and $t\bar{t}$+HF production cross-section, significantly reducing the correlations between these uncertainties and the $t\bar{t}+\geq 1b$, $t\bar{t}+\geq 1c$ and $t\bar{t}$+light normalisation uncertainties. For exper-

**Table 3** The list of impacts on the fitted $t\bar{t}H/A \to t\bar{t}t\bar{t}$ cross-sections from all sources of uncertainties, for $m_{H/A} = 400$ GeV, 700 GeV and 1000 GeV, grouped in categories according to their origin. The impacts are evaluated using the post-fit uncertainties in the $t\bar{t}H/A \to t\bar{t}t\bar{t}$ cross-sections (the total uncertainty) from the fit to data under the signal-plus-background hypothesis including all uncertainties (referred to as the nominal fit). The statistical uncertainty is evaluated as the post-fit uncertainty in the $t\bar{t}H/A \to t\bar{t}t\bar{t}$ cross-sections when fixing all systematic uncertainties to their post-fit values from the nominal fit. The impacts of systematic uncertainties are shown for groups of individual uncertainties of similar nature. The value for each group is obtained by fixing the group of uncertainties to their post-fit values from the nominal fit, and taking the quadratic difference between the resulting uncertainty in the $t\bar{t}H/A \to t\bar{t}t\bar{t}$ cross-section and the total uncertainty. The total systematic uncertainty is the quadratic difference between the total uncertainty and the statistical uncertainty. The sum in quadrature of all systematic uncertainties can be different from the total systematic uncertainty in the table due to the correlations amongst the uncertainties

| Uncertainty source | $\Delta\sigma_{t\bar{t}H/A\to t\bar{t}t\bar{t}}$ [fb] | | | | | |
|---|---|---|---|---|---|---|
| | $m_{H/A}$=400 GeV | | $m_{H/A}$=700 GeV | | $m_{H/A}$=1000 GeV | |
| **Signal Modelling** | | | | | | |
| BSM $t\bar{t}t\bar{t}$ modelling | < 1 | | +0.1 | < 0.1 | < 0.1 | |
| **Background Modelling** | | | | | | |
| $t\bar{t}$+≥1$b$ modelling | +11 | -10 | +3.7 | -3.4 | +1.9 | -1.7 |
| SM $t\bar{t}t\bar{t}$ modelling | +3 | -3 | +2.1 | -2.1 | +0.9 | -0.9 |
| $t\bar{t}$+jets reweighting | +3 | -3 | +1.0 | -1.0 | +0.5 | -0.5 |
| $t\bar{t}$+≥1$c$ modelling | +2 | -2 | +0.9 | -0.8 | +0.4 | -0.4 |
| $t\bar{t}$+light modelling | +1 | -1 | +0.2 | -0.2 | < 0.1 | |
| Other background modelling | < 1 | | +0.4 | -0.4 | +0.2 | -0.2 |
| **Experimental** | | | | | | |
| Jet energy scale and resolution | +4 | -2 | +1.3 | -0.8 | +0.5 | -0.3 |
| MC statistical uncertainties | +2 | -3 | +0.6 | -0.7 | +0.4 | -0.4 |
| $b$-tagging efficiency | +2 | -1 | +0.7 | -0.4 | +0.4 | -0.4 |
| Other uncertainties | < 1 | | +0.3 | -0.5 | +0.1 | -0.2 |
| Luminosity | < 1 | | +0.3 | -0.1 | < 0.1 | |
| **Total systematic uncertainty** | +13 | -12 | +4.8 | -4.6 | +2.5 | -2.4 |
| **Statistical uncertainty** | +6 | -6 | +3.3 | -3.2 | +2.3 | -2.2 |
| **Total uncertainty** | +14 | -13 | +5.6 | -5.4 | +3.2 | -3.0 |

imental uncertainties, given their small impact on the predictions, the nominal rescaling factors and NN kinematic corrections are used.

#### *8.2.2 Uncertainties in NN kinematic corrections*

Two sets of uncertainties are considered for the derived NN kinematic corrections. To account for the uncertainties in the cross-sections of the subtracted non-$t\bar{t}$+jets background processes, their cross-sections are varied by ±50% simultaneously and the NN is retrained. The resulting uncertainties have a 2–6% effect on the fitted distributions. In addition, the influence of the finite training data sample is evaluated using the MC dropout method [103]. The NN is retrained 1000 times, each time with randomly dropped-out neurons. The standard deviation of the NN outputs from the 1000 sets of training output are propagated to the fitted distributions. The resulting uncertainties range from about 5% in the CRs up to 12% in the SRs.

### 8.3 Other uncertainties

Other small uncertainties arise from the modelling of the minor backgrounds, and the uncertainties due to the finite size of the simulated samples, referred to as 'simulation statistical uncertainties'. The latter are treated as independent for each analysis bin, and separately for the total background and any particular signal sample considered in the fit. The cross-section uncertainties for the minor background are assigned taking into account the high jet multiplicity regime. For $t\bar{t}W$, $t\bar{t}Z$ and $t\bar{t}H$ production, uncertainties of 60% [104], 15% [105] and 20% [106] are assigned to the inclusive production cross-sections. Additional uncertainties of 10%, 20% and 30% are assigned to $t\bar{t}W/Z/H$ events with nine (seven), ten (eight), ≥ 11 (≥ 9) jets in the 1L (2LOS) channel, based on the discrepancies observed between data and $t\bar{t}$+jets simulations in the 2b regions before applying the data-driven corrections. For the $V$+jets backgrounds, an uncertainty of 60% is assigned, estimated by adding in quadrature a 24% uncer-

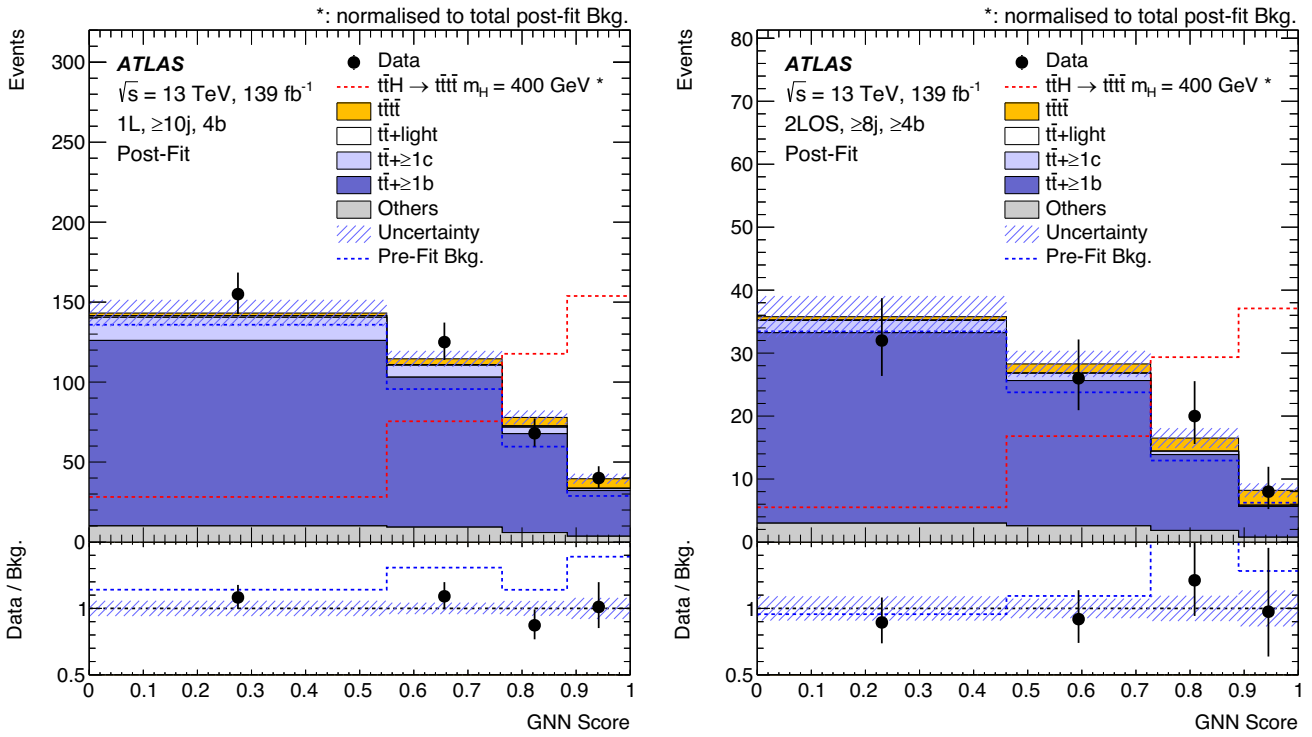


**Fig. 6** Post-fit distribution of the GNN score evaluated with $m_{H/A} = 400$ GeV **a** in the 1L region with $\geq$ 10 jets and four $b$-tagged jets and **b** in the 2LOS region with $\geq$ 8 jets and $\geq$ 4 $b$-tagged jets. The fit is performed under the background-only hypothesis. The hashed area represents the total uncertainty in the background. The distribution of the signal (red dashed line) is shown normalised to the total post-fit background for illustration purposes. The pre-fit background prediction is illustrated using a blue dashed line

tainty for each additional jet based on a comparison of different algorithms for merging LO ME and PS generators [107]. Uncertainties of 30% and 35% are assigned to the single-top-quark and $t\bar{t}t$ production cross-sections [28]. For $t\bar{t}W/Z/H$ and single-top-quark production, uncertainties due to missing higher-order QCD corrections are estimated by using the same method used for the signals. The alternative samples described in Sect. 4 are compared with the nominal samples to evaluate effects from the ME-PS matching or the modelling of the PS, hadronisation and fragmentation. For single-top-quark production, an additional uncertainty is evaluated by comparing the nominal prediction with the one simulated using the diagram subtraction scheme.

## 9 Results and interpretation

### 9.1 Statistical analysis

The $H_{\mathrm{T}}$ distributions in the CRs and the GNN output distributions in the SRs are used to search for the presence of a signal. The simulation is fit to data, using a profile likelihood function $\mathcal{L}(\mu, \boldsymbol{\theta})$ that is constructed as a product of Poisson and Gaussian probability density terms over all bins in the distributions of the CRs and SRs:

$$\mathcal{L}(\boldsymbol{n}|\mu, \boldsymbol{\theta}) = \prod_{r \in \text{region}} \prod_{i \in \text{bin}} \text{Pois}\left(n_{i,r}|\mu S_{i,r}(\boldsymbol{\theta}) + B_{i,r}(\boldsymbol{\theta})\right) \times \prod_{j \in \text{NP}} G\left(\theta_j\right). \quad (4)$$

Here $\mathbf{n}$ represents the data vector, with $n_{i,r}$ representing data yields in the bin $i$ and region $r$. The vector $\boldsymbol{\theta}$ denotes the nuisance parameters (NPs), each representing a systematic uncertainty, that affect the number of signal events $S_{i,r}$ as well as the number of background events $B_{i,r}$ in the bin $i$ and region $r$. The quantity $\mu$ is the signal strength, which is the parameter of interest in the likelihood and it represents the ratio of the measured cross-section to a reference cross-section used to normalise the signal samples. This cross-section is arbitrary and does not change the cross-section upper limit. The terms 'Pois' and 'G' represent the Poisson and Gaussian probability distributions respectively. The Gaussian distribution terms adjust the expectations for signal and background according to their systematic uncertainties.

For limit setting, a test statistic $q(\mu)$ is defined for use with the $\mathrm{CL}_s$ method [108,109]. The profile likelihood ratio

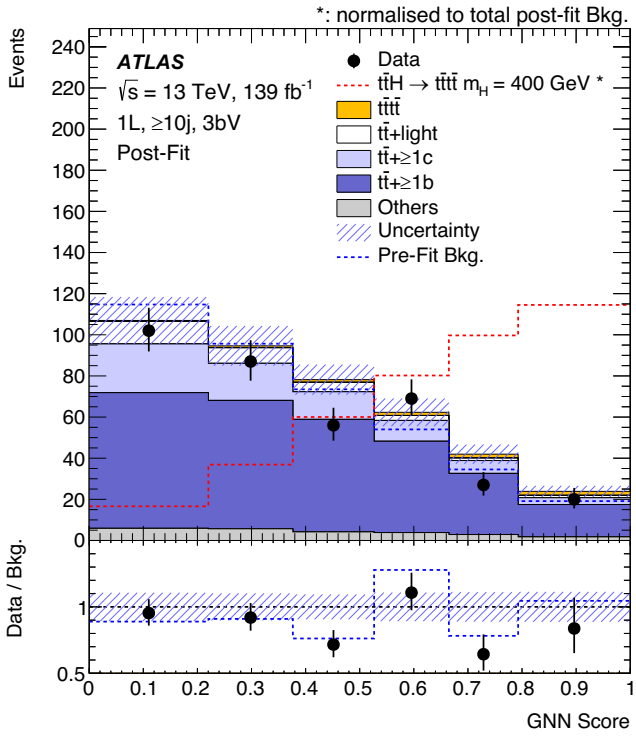


(a)

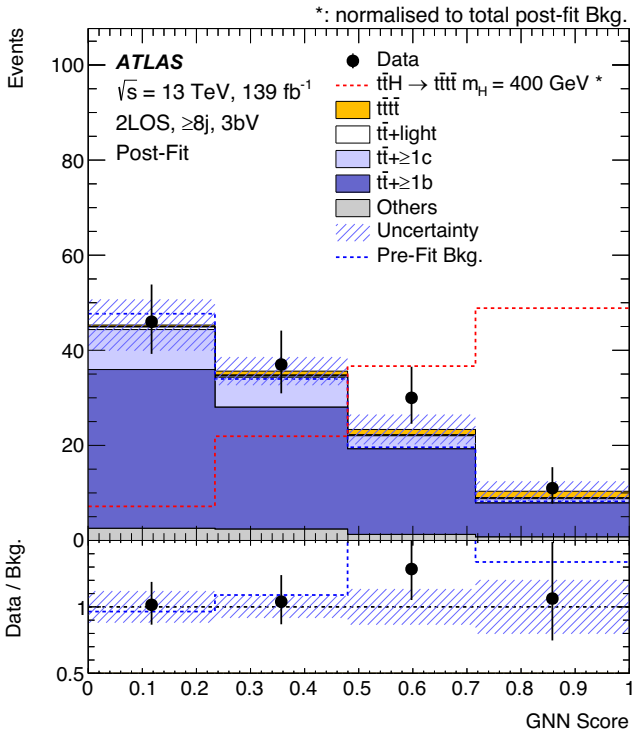


(b)

**Fig. 7** Post-fit distribution of the GNN score evaluated with $m_{H/A} = 400$ GeV in the VRs **a** in the 1L region with $\geq 10$ jets and **b** in the 2LOS region with $\geq 8$ jets. These regions do not enter the fit. The post-fit background prediction is obtained using the post-fit nuisance parameters from the background-only fit in the CRs and SRs. The hashed area represents the total uncertainty in the background. The distribution of the signal (red dashed line) is shown normalised to the total post-fit background for illustration purposes. The pre-fit background prediction is illustrated using a blue dashed line

used is: $q(\mu) = -2\ln(\mathcal{L}(\mu, \hat{\hat{\boldsymbol{\theta}}}_\mu)/\mathcal{L}(\hat{\mu}, \hat{\boldsymbol{\theta}}))$, where $\hat{\mu}$ and $\hat{\boldsymbol{\theta}}$ are the values of the parameters that maximise the likelihood function (with the constraint $0 \leq \hat{\mu} \leq \mu$), and $\hat{\hat{\boldsymbol{\theta}}}_\mu$ are the values of the NPs that maximise the likelihood function for a given value of $\mu$. No significant excess above the background expectation is observed and therefore upper limits on $\mu$ for each of the signal scenarios considered are derived. For a given signal scenario, values of $\mu$ yielding $\mathrm{CL}_s < 0.05$, where $\mathrm{CL}_s$ is computed using the asymptotic approximation [110], are excluded at $\geq 95\%$ confidence level (CL). All the statistical analyses have used the RooStats framework [111–113].

For each $m_H$ scenario, a profile likelihood fit is performed using all CRs and SRs in both the 1L and 2LOS channels simultaneously. The post-fit distributions of the GNN output for the most sensitive regions in the 1L and 2LOS channels are shown in Fig. 6. The GNN scores are evaluated with $m_{H/A} = 400$ GeV. The same distributions in the VRs that are the closest to the SRs in the 1L and 2LOS channels are shown in Fig. 7, illustrating a good agreement between data and post-fit background prediction.

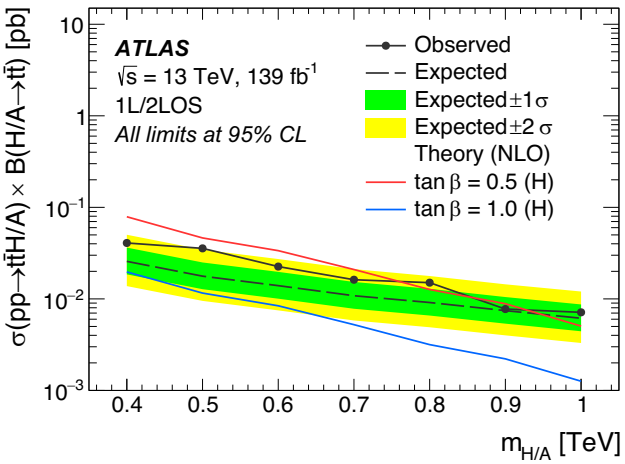


**Fig. 8** Observed (solid line) and expected (dashed line) 95% CL upper limits on the cross-section times branching ratio, $\sigma(pp \to t\bar{t}H/A) \times B(H/A \to t\bar{t})$, as a function of $m_{H/A}$. The green (yellow) band illustrates the $\pm 1\sigma$ ($\pm 2\sigma$) interval around the expected limit. Theoretical predictions for two values of $\tan\beta$ are shown for an $H$ boson. The predicted values for $A$ differ by less than 3‰ for all mass points for the two $\tan\beta$ values shown

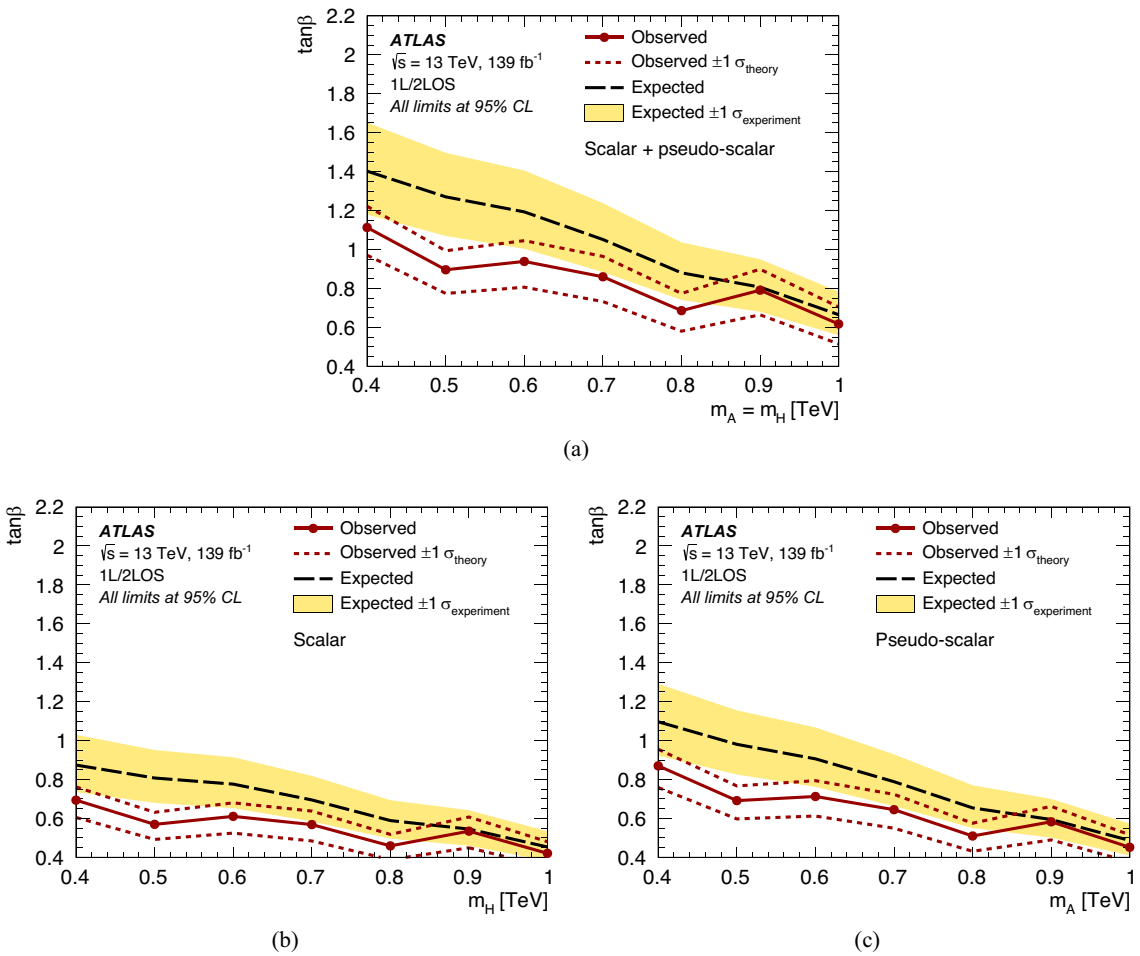


**Fig. 9** Observed (red solid line) and expected (black dashed line) 95% CL lower limits on $\tan\beta$ as a function of the $m_{H/A}$ mass obtained using the 1L/2LOS final states, assuming a Type-II 2HDM in the alignment limit. Values of $\tan\beta$ below the observed limit are excluded. The scenario where both the scalar $H$ and pseudo-scalar $A$ contribute with $m_H = m_A$ is shown in **a**. The scenarios with the contribution from $H$ and $A$ only are shown in **b** and **c**, respectively. The yellow bands illustrate the $\pm 1\sigma$ intervals around the expected limits. The two red dashed lines correspond to the observed limits when the theory cross-sections are varied by $\pm 1\sigma$. Values of $\tan\beta < 0.4$ are not considered so that the top-quark Yukawa coupling remains in the perturbative regime [5]

The search in the 1L/2LOS final states is combined with the previous analysis in the 2LSS/ML final states [21]. The combination is performed via a simultaneous profile likelihood fit including all SRs and CRs of both the final states, with all systematic uncertainties included. The events in the two analyses are statistically independent given the lepton selection criteria. The experimental uncertainties are treated as fully correlated between the two analyses since both the analyses use the same reconstructed objects and data set. Theoretical modelling uncertainties in the non-$t\bar{t}$+jets backgrounds and the signals are also correlated if they have identical definition in both the 1L/2LOS and 2LSS/ML final states. The $t\bar{t}W$ and $t\bar{t}$+jets backgrounds are treated differently in the two analyses. The $t\bar{t}$+jets background is the dominant irreducible background in the 1L/2LOS final state and data-based corrections are applied. In the 2LSS/ML final state this background is a much smaller contribution and arises from prompt leptons with mis-identified charges or from mis-reconstructed or non-prompt leptons, therefore different data-based corrections are applied. The $t\bar{t}W$ background is the most important background in the 2LSS/ML channel, and a detailed model of systematic uncertainties was used, while in the 1L/2LOS channel it is a small background. Uncertainties in $t\bar{t}W$ and $t\bar{t}$+jets backgrounds are thus uncorrelated.

The following sections present the results from the 1L/2LOS final states only and those from the combination of the 1L/2LOS and 2LSS/ML final states.

### 9.2 Limits on $t\bar{t}H/A \to t\bar{t}t\bar{t}$ production in a 2HDM

The expected and observed 95% CL upper limits on the $t\bar{t}H/A \to t\bar{t}t\bar{t}$ production cross-sections as a function of

$m_{H/A}$ mass are shown in Fig. 8. The theoretical predictions at NLO in QCD for two different values of $\tan\beta$ are also shown [114–119]. Overall, the observed limits are consistent with the expected ones. Similar to the results in the 2LSS/ML final states [21], there is a small excess in the observed limits compared with the expected ones. The mass point with the largest deviation is $m_{H/A} = 500$ GeV. The local significance of the fitted signal at this point is evaluated to be 2.1 standard deviations. All other mass points have a local significance of less than 1.5 standard deviations. The goodness-of-fit under the background-only hypothesis is evaluated for all the mass points, using a likelihood-ratio test in which the nominal fit is compared with that of a saturated model [120]. The smallest goodness-of-fit value of 49% is observed for $m_{H/A} = 800$ GeV, whilst for $m_{H/A} = 500$ GeV the value is 64%. Other mass points have a goodness-of-fit value of greater than 81%.

The upper limits on the cross-sections are interpreted as exclusion limits on $\tan\beta$ in the context of a 2HDM Type-II model in the alignment limit. As described in Sect. 4, the signal kinematics is the same at different $\tan\beta$ values and for $H$ and $A$. Therefore, the limits on $\tan\beta$ are obtained by comparing the cross-section upper limits in Fig. 8 with the predicted signal cross-section for $t\bar{t}H \to t\bar{t}t\bar{t}$ and $t\bar{t}A \to t\bar{t}t\bar{t}$ at different values of $\tan\beta$. The uncertainty in the theory cross-sections arises from variations of the PDFs and the renormalisation and factorisation scales. The expected and observed 95% CL lower limits for $\tan\beta$ as a function of the $m_{H/A}$ mass for different scenarios are shown in Fig. 9. Three scenarios are shown where (a) both the scalar $H$ and pseudo-scalar $A$ bosons contribute to the $t\bar{t}t\bar{t}$ cross-section with equal masses, (b) only an $H$ boson contributes, and (c) only an $A$ boson contributes.

The impacts of the systematic and statistical uncertainties in the fitted $t\bar{t}H/A \to t\bar{t}t\bar{t}$ cross-sections are given in Table 3 for three illustrative $m_{H/A}$ values. The impacts are evaluated using the post-fit uncertainties in the $t\bar{t}H/A \to t\bar{t}t\bar{t}$ cross-sections from the fit to data under the signal-plus-background hypothesis, and can be compared with the cross-section upper limits shown in Fig. 8. The impacts are grouped into categories according to their origin. As mentioned in Sect. 8 the largest sources of systematic errors arise from the group of uncertainties in the modelling of the $t\bar{t}$+jets background. The leading individual uncertainties include those from: the comparison between the 4FS and 5FS predictions and the PS, hadronisation and fragmentation modelling in $t\bar{t}+b\bar{b}$ and $t\bar{t}+\geq 3b$ background components; the generator comparison of SM $t\bar{t}t\bar{t}$ production; the normalisation of $t\bar{t}+\geq 1c$ and $t\bar{t}+\geq 1b$; and the NN kinematic corrections in the 2LOS channel.

Figure 10 shows the observed and expected 95% CL upper limits on the $t\bar{t}H/A \to t\bar{t}t\bar{t}$ production cross-section from the combined fit to all SRs and CRs in the 1L/2LOS and 2LSS/ML analyses. The observed (expected) upper limits range from 14 (9.4) fb for $m_{H/A} = 400$ GeV to 5.0 (3.8) fb for $m_{H/A} = 1000$ GeV. The figure also compares the expected upper limits from the 1L/2LOS and 2LSS/ML with the one from the combination. The sensitivity in the low mass regime is dominated by the 2LSS/ML final states. The combination improves the sensitivity relative to using only the 2LSS/ML final states in the high mass regime. The largest improvement in the observed upper limit is 19% for $m_{H/A} = 900$ GeV, with the expected upper limits across the full mass range improving by up to 18%.

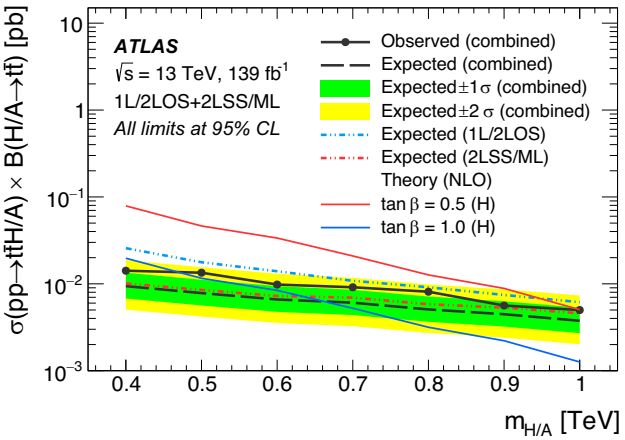


**Fig. 10** Expected and observed 95% CL upper limits on the cross-section times branching ratio, $\sigma(pp \to t\bar{t}H/A) \times B(H/A \to t\bar{t})$, as a function of $m_{H/A}$, obtained from the combination of the 1L/2LOS and 2LSS/ML final states. The green (yellow) band illustrates the $\pm 1\sigma$ ($\pm 2\sigma$) interval around the expected limit from the combination. The expected limits from the individual 1L/2LOS and 2LSS/ML analyses are also shown. Theoretical predictions for two values of $\tan\beta$ are shown for an $H$ boson. The predicted values for $A$ differ by less than 3‰ for all mass points for the two $\tan\beta$ values shown

The resulting 95% CL lower limits for $\tan\beta$ from the combination are shown in Fig. 11. For the case where $m_A = m_H$, at low masses, this result is less restrictive than that from the $gg \to A/H \to t\bar{t}$ search [19]. At high masses, the expected sensitivity is comparable.

### 9.3 Limits on $S_8S_8 \to t\bar{t}t\bar{t}$ production

The same analysis strategy is used to derive upper limits on the $S_8S_8 \to t\bar{t}t\bar{t}$ production cross-section. The 1L/2LOS and 2LSS/ML final states are combined to determine the final limits. For the mass points with $m_{S_8} \leq 1$ TeV, the $m_{H/A}$-parameterised classifiers (GNN for 1L/2LOS and BDT for 2LSS/ML) are evaluated at $m_{S_8} = m_{H/A}$. At each mass point, the binning of the fitted distributions is the same as the one used for $H/A$. For $m_{S_8} > 1$ TeV, the GNN/BDT and binning for $m_{H/A} = 1$ TeV are adopted. The resulting 95% CL upper limits on the $S_8S_8 \to t\bar{t}t\bar{t}$ production cross-section are illustrated in Fig. 12. The observed and expected upper

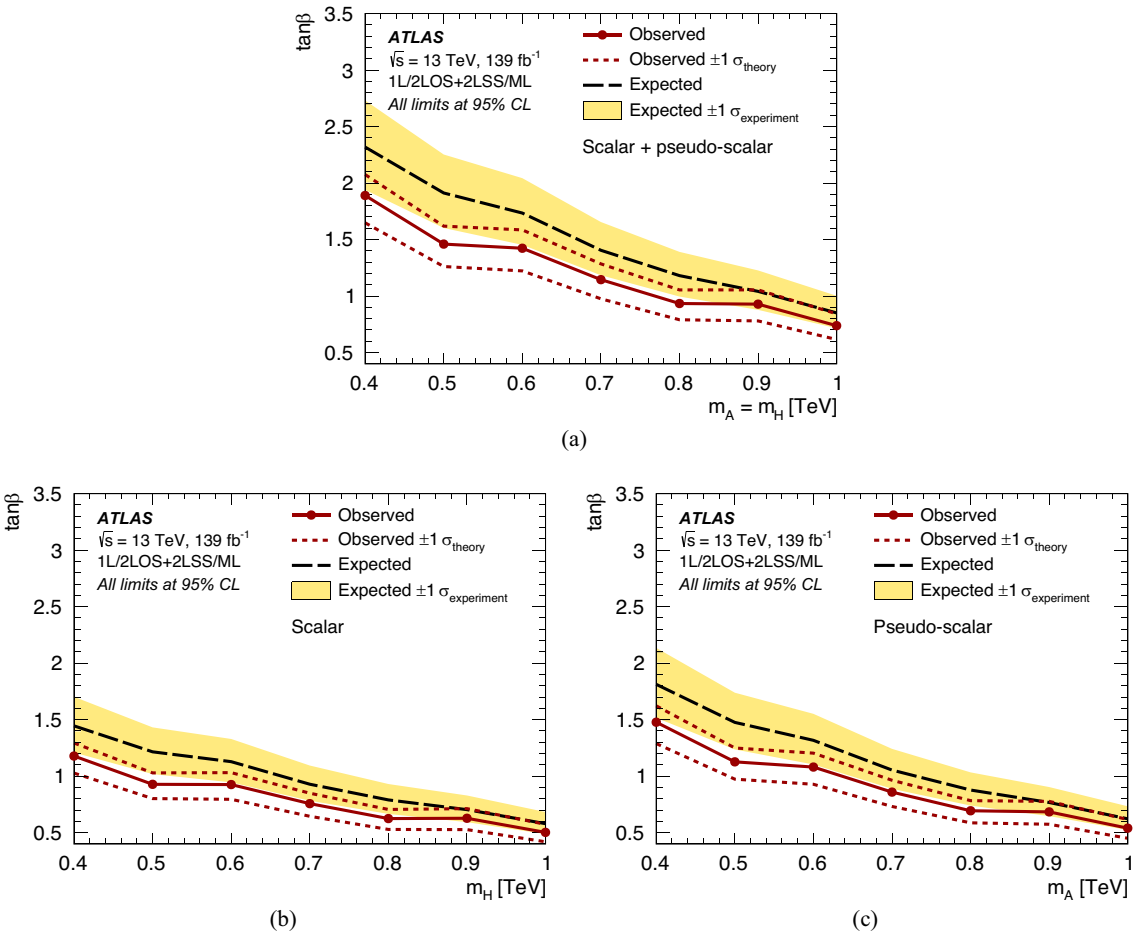


**Fig. 11** Expected (black dashed line) and observed (red solid line) 95% CL limits on $\tan\beta$ as a function of the $m_{H/A}$ mass obtained using the combination of 1L/2LOS and 2LSS/ML final states, assuming type-II 2HDM in the alignment limit. Values of $\tan\beta$ below the observed limit are excluded. The scenario where both the scalar $H$ and pseudo-scalar $A$ contribute with $m_H = m_A$ is shown in **a**. The scenarios with the contribution from $H$ and $A$ only are shown in **b** and **c**, respectively. The yellow bands illustrate the $\pm 1\sigma$ bands of the expected limits. The two red dashed lines correspond to the observed limits when the theory cross-sections are varied by $\pm 1\sigma$. Values of $\tan\beta < 0.4$ are not considered so that the top-quark Yukawa coupling remains in the perturbative regime [5]

limits from the combination of 1L/2LOS and 2LSS/ML final states are shown, compared with the expected limits from using only the 1L/2LOS or the 2LSS/ML final states. The behaviour of the limits for $m_{S_8} \leq 1$ TeV is similar to that for $t\bar{t}H/A \to t\bar{t}t\bar{t}$ production, with an improvement of up to 26% when using the combination relative to using the 2LSS/ML final states only. The limits slightly weaken for $m_{S_8} > 1$ TeV given that the classifiers are optimised for $m_{H/A} = 1$ TeV. For the sgluon signals under consideration as described in Sect. 4, $m_{S_8} \leq 1.3$ TeV are excluded at 95% CL.

## 10 Conclusions

A search for $t\bar{t}H/A \to t\bar{t}t\bar{t}$ production is presented using the full LHC Run 2 data sample collected by the ATLAS experiment during 2015–2018, corresponding to an integrated luminosity of 139 fb$^{-1}$ of $pp$ collisions at $\sqrt{s} = 13$ TeV. Events with one lepton or two leptons with opposite-sign charges and high jet multiplicities are selected. The dominant background in all selected regions is $t\bar{t}$+jets. Data-driven corrections are applied to the normalisation of the $t\bar{t}$+light, $t\bar{t}+\geq 1c$ and $t\bar{t}+\geq 1b$ background components, and their kinematics. The kinematic corrections are derived based on NNs and improve the modelling of the $t\bar{t}$+jets background in multiple dimensions. A $m_{H/A}$-parameterised GNN is used to optimise the signal-to-background discrimination.

Upper limits at 95% CL are set on the production cross-section times branching ratio, $\sigma(pp \to t\bar{t}H/A) \times B(H/A \to t\bar{t})$, for $H/A$ masses between 400 GeV and 1000 GeV. These results are combined with a previous search from ATLAS using multilepton final states. The combined upper limits range from 14 fb at 400 GeV to 5.0 fb at

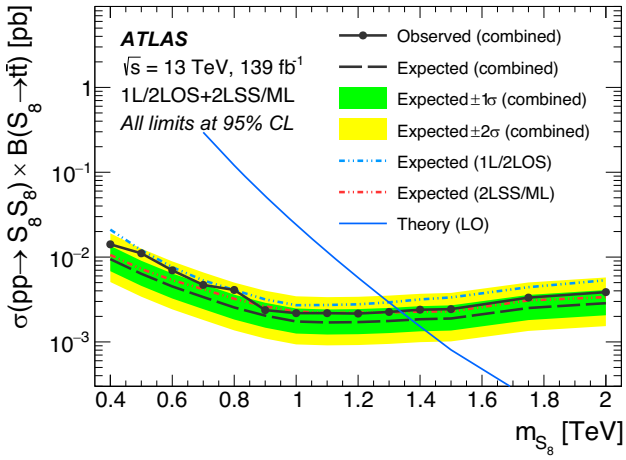


**Fig. 12** Expected and observed 95% CL upper limits on the $S_8S_8 \to t\bar{t}t\bar{t}$ production cross-section as a function of $m_{S_8}$, obtained from the combination of the 1L/2LOS and 2LSS/ML final states. The expected limits from the individual 1L/2LOS and 2LSS/ML analyses are also shown. The predicted production cross-section from Ref. [34] is shown with the solid blue curve

1000 GeV, with an improvement of up to 19% relative to using only the multilepton final states. These results are interpreted in the context of a 2HDM Type-II model in the alignment limit to set limits on the values of $\tan\beta$. Assuming only the scalar $H$ (pseudo-scalar $A$) boson contributes to the cross-section, values of $\tan\beta$ below 1.2 (1.5) and 0.5 (0.5) are excluded at the low and high mass $H/A$ mass values. In case both the particles contribute, the exclusion range is below 1.9 and 0.7 at masses of 400 GeV and 1000 GeV. When considering the sgluon pair production signals with $m_{S_8}$ from 400 GeV to 2 TeV, the observed 95% CL upper limits on the $S_8S_8 \to t\bar{t}t\bar{t}$ cross-section range from 14 fb (400 GeV) to 2.2 fb (1 TeV). Sgluon masses $m_{S_8} \leq 1.3$ TeV are excluded.

**Acknowledgements** We thank CERN for the very successful operation of the LHC and its injectors, as well as the support staff at CERN and at our institutions worldwide without whom ATLAS could not be operated efficiently. The crucial computing support from all WLCG partners is acknowledged gratefully, in particular from CERN, the ATLAS Tier-1 facilities at TRIUMF/SFU (Canada), NDGF (Denmark, Norway, Sweden), CC-IN2P3 (France), KIT/GridKA (Germany), INFN-CNAF (Italy), NL-T1 (Netherlands), PIC (Spain), RAL (UK) and BNL (USA), the Tier-2 facilities worldwide and large non-WLCG resource providers. Major contributors of computing resources are listed in Ref. [121]. We gratefully acknowledge the support of ANPCyT, Argentina; YerPhI, Armenia; ARC, Australia; BMWFW and FWF, Austria; ANAS, Azerbaijan; CNPq and FAPESP, Brazil; NSERC, NRC and CFI, Canada; CERN; ANID, Chile; CAS, MOST and NSFC, China; Minciencias, Colombia; MEYS CR, Czech Republic; DNRF and DNSRC, Denmark; IN2P3-CNRS and CEA-DRF/IRFU, France; SRNSFG, Georgia; BMBF, HGF and MPG, Germany; GSRI, Greece; RGC and Hong Kong SAR, China; ISF and Benoziyo Center, Israel; INFN, Italy; MEXT and JSPS, Japan; CNRST, Morocco; NWO, Netherlands; RCN, Norway; MNiSW, Poland; FCT, Portugal; MNE/IFA, Romania; MESTD, Serbia; MSSR, Slovakia; ARIS and MVZI, Slovenia; DSI/NRF, South Africa; MICIU/AEI, Spain; SRC and Wallenberg Foundation, Sweden; SERI, SNSF and Cantons of Bern and Geneva, Switzerland; NSTC, Taipei; TENMAK, Türkiye; STFC/UKRI, United Kingdom; DOE and NSF, United States of America. Individual groups and members have received support from BCKDF, CANARIE, CRC and DRAC, Canada; PRIMUS 21/SCI/017, CERN-CZ and FORTE, Czech Republic; COST, ERC, ERDF, Horizon 2020, ICSC-NextGenerationEU and Marie Skłodowska-Curie Actions, European Union; Investissements d'Avenir Labex, Investissements d'Avenir Idex and ANR, France; DFG and AvH Foundation, Germany; Herakleitos, Thales and Aristeia programmes co-financed by EU-ESF and the Greek NSRF, Greece; BSF-NSF and MINERVA, Israel; Norwegian Financial Mechanism 2014-2021, Norway; NCN and NAWA, Poland; La Caixa Banking Foundation, CERCA Programme Generalitat de Catalunya and PROMETEO and GenT Programmes Generalitat Valenciana, Spain; Göran Gustafssons Stiftelse, Sweden; The Royal Society and Leverhulme Trust, United Kingdom. In addition, individual members wish to acknowledge support from CERN: European Organization for Nuclear Research (CERN PJAS); Chile: Agencia Nacional de Investigación y Desarrollo (FONDECYT 1190886, FONDECYT 1210400, FONDECYT 1230812, FONDECYT 1230987); China: Chinese Ministry of Science and Technology (MOST-2023YFA1605700, MOST-2023YFA1609300), National Natural Science Foundation of China (NSFC - 12175119, NSFC 12275265, NSFC-12075060); Czech Republic: Czech Science Foundation (GACR - 24-11373S), Ministry of Education Youth and Sports (FORTE CZ.02.01.01/00/22_008/0004632), PRIMUS Research Programme (PRIMUS/21/SCI/017); EU: H2020 European Research Council (ERC - 101002463); European Union: European Research Council (ERC - 948254, ERC 101089007), Horizon 2020 Framework Programme (MUCCA - CHIST-ERA-19-XAI-00), European Union, Future Artificial Intelligence Research (FAIR-NextGenerationEU PE00000013), Italian Center for High Performance Computing, Big Data and Quantum Computing (ICSC, NextGenerationEU); France: Agence Nationale de la Recherche (ANR-20-CE31-0013, ANR-21-CE31-0013, ANR-21-CE31-0022, ANR-22-EDIR-00-02), Investissements d'Avenir Labex (ANR-11-LABX-0012); Germany: Baden-Württemberg Stiftung (BW Stiftung-Postdoc Eliteprogramme), Deutsche Forschungsgemeinschaft (DFG - 469666862, DFG - CR 312/5-2); Italy: Istituto Nazionale di Fisica Nucleare (ICSC, NextGenerationEU), Ministero dell'Università e della Ricerca (PRIN - 20223N7F8K - PNRR M4.C2.1.1); Japan: Japan Society for the Promotion of Science (JSPS KAKENHI JP21H05085, JSPS KAKENHI JP22H01227, JSPS KAKENHI JP22H04944, JSPS KAKENHI JP22KK0227); Netherlands: Netherlands Organisation for Scientific Research (NWO Veni 2020 - VI.Veni.202.179); Norway: Research Council of Norway (RCN-314472); Poland: Ministry of Science and Higher Education (IDUB AGH, POB8, D4 no 9722), Polish National Agency for Academic Exchange (PPN/PPO/2020/1/00002/U/00001), Polish National Science Centre (NCN 2021/42/E/ST2/00350, NCN OPUS nr 2022/47/B/ST2/03059, NCN UMO-2019/34/E/ST2/00393, NCN and H2020 MSCA 945339, UMO-2020/37/B/ST2/01043, UMO-2021/40/C/ST2/00187, UMO-2022/47/O/ST2/00148, UMO-2023/49/B/ST2/04085); Slovenia: Slovenian Research Agency (ARIS grant J1-3010); Spain: Generalitat Valenciana (Artemisa, FEDER, IDIFEDER/2018/048), Ministry of Science and Innovation (MCIN and NextGenEU PCI2022-135018-2, MICIN and FEDER PID2021-125273NB, RYC2019-028510-I, RYC2020-030254-I, RYC2021-031273-I, RYC2022-038164-I), PROMETEO and GenT Programmes Generalitat Valenciana (CIDEGENT/2019/023, CIDEGENT/2019/027); Sweden: Carl Trygger Foundation (Carl Trygger Foundation CTS 22:2312), Swedish Research Council (Swedish Research Council 2023-04654, VR 2018-00482, VR 2022-03845, VR 2022-04683, VR 2023-03403, VR grant 2021-03651), Knut and Alice Wallenberg Foundation (KAW 2018.0157, KAW 2018.0458, KAW 2019.0447, KAW 2022.0358); Switzerland: Swiss National Science Foundation (SNSF - PCEFP2_194658); United Kingdom: Leverhulme Trust (Leverhulme Trust RPG-2020-004), Royal

Society (NIF-R1-231091); United States of America: U.S. Department of Energy (ECA DE-AC02-76SF00515), Neubauer Family Foundation.

**Data Availability Statement** This manuscript has no associated data. [Author's comment: All ATLAS scientific output is published in journals, and preliminary results are made available in Conference Notes. All are openly available, without restriction on use by external parties beyond copyright law and the standard conditions agreed by CERN. Data associated with journal publications are also made available: tables and data from plots (e.g. cross section values, likelihood profiles, selection efficiencies, cross section limits, ...) are stored in appropriate repositories such as HEPDATA (http://hepdata.cedar.ac.uk/). ATLAS also strives to make additional material related to the paper available that allows a reinterpretation of the data in the context of new theoretical models. For example, an extended encapsulation of the analysis is often provided for measurements in the framework of RIVET (http://rivet.hepforge.org/). This information is taken from the ATLAS Data Access Policy, which is a public document that can be downloaded from http://opendata.cern.ch/record/413 [opendata.cern.ch].]

**Code Availability Statement** This manuscript has no associated code/software. [Author's comment: ATLAS collaboration software is open source, and all code necessary to recreate an analysis is publicly available. The Athena (http://gitlab.cern.ch/atlas/athena) software repository provides all code needed for calibration and uncertainty application, with configuration files that are also publicly available via Docker containers and cvmfs. The specific code and configurations written in support of this analysis are not public; however, these are internally preserved.]

## References


1. ATLAS Collaboration, Observation of a new particle in the search for the Standard Model Higgs boson with the ATLAS detector at the LHC. Phys. Lett. B **716**, 1 (2012). https://doi.org/10.1016/j.physletb.2012.08.020. arXiv:1207.7214 [hep-ex]
2. CMS Collaboration, Observation of a new boson at a mass of 125 GeV with the CMS experiment at the LHC. Phys. Lett. B **716**, 30 (2012). https://doi.org/10.1016/j.physletb.2012.08.021. arXiv:1207.7235 [hep-ex]
3. L. Susskind, Dynamics of spontaneous symmetry breaking in the Weinberg–Salam theory. Phys. Rev. D **20**, 2619 (1979). https://doi.org/10.1103/PhysRevD.20.2619
4. G. Bertone, D. Hooper, History of dark matter. Rev. Mod. Phys. **90**, 045002 (2018). https://doi.org/10.1103/RevModPhys.90.045002. arXiv:1605.04909 [astro-ph.CO]
5. G.C. Branco et al., Theory and phenomenology of two-Higgs-doublet models. Phys. Rep. **516**, 1 (2012). https://doi.org/10.1016/j.physrep.2012.02.002. arXiv:1106.0034 [hep-ph]
6. A. Djouadi, L. Maiani, A. Polosa, J. Quevillon, V. Riquer, Fully covering the MSSM Higgs sector at the LHC. JHEP **06**, 168 (2015). https://doi.org/10.1007/JHEP06(2015)168. arXiv:1502.05653 [hep-ph]
7. L. Maiani, A.D. Polosa, V. Riquer, Bounds to the Higgs sector masses in minimal supersymmetry from LHC data. Phys. Lett. B **724**, 274 (2013). https://doi.org/10.1016/j.physletb.2013.06.026. arXiv:1305.2172 [hep-ph]
8. A. Djouadi et al., The post-Higgs MSSM scenario: Habemus MSSM? Eur. Phys. J. C **73**, 2650 (2013). https://doi.org/10.1140/epjc/s10052-013-2650-0. arXiv:1307.5205 [hep-ph]
9. T.D. Lee, A theory of spontaneous $T$ violation. Phys. Rev. D **8**, 1226 (1973). https://doi.org/10.1103/PhysRevD.8.1226, ed. by G. Feinberg
10. T.P. Cheng, L.-F. Li, Neutrino masses, mixings and oscillations in SU(2) x U(1) models of electroweak interactions. Phys. Rev. D **22**, 2860 (1980). https://doi.org/10.1103/PhysRevD.22.2860
11. J. Schechter, J.W.F. Valle, Neutrino masses in SU(2) $\otimes$ U(1) theories. Phys. Rev. D **22**, 2227 (1980). https://doi.org/10.1103/PhysRevD.22.2227
12. G. Lazarides, Q. Shafi, C. Wetterich, Proton lifetime and fermion masses in an SO(10) model. Nucl. Phys. B **181**, 287 (1981). https://doi.org/10.1016/0550-3213(81)90354-0
13. R.N. Mohapatra, G. Senjanović, Neutrino masses and mixings in gauge models with spontaneous parity violation. Phys. Rev. D **23**, 165 (1981). https://doi.org/10.1103/PhysRevD.23.165
14. M. Magg, C. Wetterich, Neutrino mass problem and gauge hierarchy. Phys. Lett. B **94**, 61 (1980). https://doi.org/10.1016/0370-2693(80)90825-4
15. ATLAS Collaboration, Search for heavy Higgs bosons decaying into two tau leptons with the ATLAS detector using $pp$ collisions at $\sqrt{s} = 13$ TeV. Phys. Rev. Lett. **125**, 051801 (2020). https://doi.org/10.1103/PhysRevLett.125.051801. arXiv:2002.12223 [hep-ex]
16. CMS Collaboration, Search for additional neutral MSSM Higgs bosons in the $\tau\tau$ final state in proton–proton collisions at $\sqrt{s} = 13$ TeV. JHEP **09**, 007 (2018). https://doi.org/10.1007/JHEP09(2018)007. arXiv:1803.06553 [hep-ex]
17. ATLAS Collaboration, Combination of searches for Higgs boson pairs in $pp$ collisions at $\sqrt{s} = 13$ TeV with the ATLAS detector. Phys. Lett. B **800**, 135103 (2020). https://doi.org/10.1016/j.physletb.2019.135103. arXiv:1906.02025 [hep-ex]
18. CMS Collaboration, Search for a heavy Higgs boson decaying into two lighter Higgs bosons in the $\tau\tau bb$ final state at 13 TeV. JHEP **11**, 057 (2021). https://doi.org/10.1007/JHEP11(2021)057. arXiv:2106.10361 [hep-ex]
19. ATLAS Collaboration, Search for heavy neutral Higgs bosons decaying into a top quark pair in 140 fb$^{-1}$ of proton–proton collision data at $\sqrt{s} = 13$ TeV with the ATLAS detector. JHEP **08**, 013 (2024). https://doi.org/10.1007/JHEP08(2024)013. arXiv:2404.18986 [hep-ex]
20. CMS Collaboration, Search for heavy Higgs bosons decaying to a top quark pair in proton–proton collisions at $\sqrt{s} = 13$ TeV. JHEP **04**, 171 (2020). https://doi.org/10.1007/JHEP04(2020)171. arXiv:1908.01115 [hep-ex]
21. ATLAS Collaboration, Search for $t\bar{t}H/A \to t\bar{t}t\bar{t}$ production in the multilepton final state in proton–proton collisions at $\sqrt{s} = 13$ TeV with the ATLAS detector. JHEP **07**, 203 (2023). https://doi.org/10.1007/JHEP07(2023)203. arXiv:2211.01136 [hep-ex]
22. CMS Collaboration, Search for production of four top quarks in final states with same-sign or multiple leptons in proton–proton collisions at $\sqrt{s} = 13$ TeV. Eur. Phys. J. C **80**, 75 (2020). https://doi.org/10.1140/epjc/s10052-019-7593-7. arXiv:1908.06463 [hep-ex]
23. ATLAS Collaboration, Constraints on new phenomena via Higgs boson couplings and invisible decays with the ATLAS detector. JHEP **11**, 206 (2015). https://doi.org/10.1007/JHEP11(2015)206. arXiv:1509.00672 [hep-ex]
24. ATLAS Collaboration, Interpretations of the ATLAS measurements of Higgs boson production and decay rates and differential cross-sections in pp collisions at $\sqrt{s}$=13 TeV. JHEP 11, 097 (2024). https://doi.org/10.1007/JHEP11%282024%29097. arXiv: 2402.05742 [hep-ex]
25. J. Hajer, Y.-Y. Li, T. Liu, J.F.H. Shiu, Heavy Higgs bosons at 14 TeV and 100 TeV. JHEP **11**, 124 (2015). https://doi.org/10.1007/JHEP11(2015)124. arXiv:1504.07617 [hep-ph]

26. K.J.F. Gaemers, F. Hoogeveen, Higgs production and decay into heavy flavours with the gluon fusion mechanism. Phys. Lett. B **146**, 347 (1984). https://doi.org/10.1016/0370-2693(84)91711-8
27. ATLAS Collaboration, Search for heavy Higgs bosons $A/H$ decaying to a top quark pair in $pp$ collisions at $\sqrt{s} = 8$ TeV with the ATLAS detector. Phys. Rev. Lett. **119**, 191803 (2017). https://doi.org/10.1103/PhysRevLett.119.191803. arXiv:1707.06025 [hep-ex]
28. ATLAS Collaboration, Observation of four-top-quark production in the multilepton final state with the ATLAS detector. Eur. Phys. J. C **83**, 496 (2023). https://doi.org/10.1140/epjc/s10052-023-11573-0. arXiv:2303.15061 [hep-ex]
29. CMS Collaboration, Observation of four top quark production in proton–proton collisions at $\sqrt{s} = 13$ TeV. Phys. Lett. B **847**, 138290 (2023). https://doi.org/10.1016/j.physletb.2023.138290. arXiv:2305.13439 [hep-ex]
30. M. van Beekveld, A. Kulesza, L. Moreno Valero, Threshold resummation for the production of four top quarks at the LHC. Phys. Rev. Lett. **131**, 211901 (2023). https://doi.org/10.1103/PhysRevLett.131.211901. arXiv:2212.03259 [hep-ph]
31. ATLAS Collaboration, Search for new phenomena in events with same-charge leptons and $b$-jets in $pp$ collisions at $\sqrt{s} = 13$ TeV with the ATLAS detector. JHEP **12**, 039 (2018). https://doi.org/10.1007/JHEP12(2018)039. arXiv:1807.11883 [hep-ex]
32. CMS Collaboration, Search for physics beyond the standard model in events with two leptons of same sign, missing transverse momentum, and jets in proton–proton collisions at $\sqrt{s} = 13$ TeV. Eur. Phys. J. C **77**, 578 (2017). https://doi.org/10.1140/epjc/s10052-017-5079-z. arXiv:1704.07323 [hep-ex]
33. ATLAS Collaboration, Measurement of the $t\bar{t}t\bar{t}$ production cross section in $pp$ collisions at $\sqrt{s} = 13$ TeV with the ATLAS detector. JHEP **11**, 118 (2021). https://doi.org/10.1007/JHEP11(2021)118. arXiv:2106.11683 [hep-ex]
34. L. Darmé, B. Fuks, F. Maltoni, Top-philic heavy resonances in four-top final states and their EFT interpretation. JHEP **09**, 143 (2021). https://doi.org/10.1007/JHEP09(2021)143. arXiv:2104.09512 [hep-ph]
35. ATLAS Collaboration, The ATLAS experiment at the CERN large hadron collider. JINST **3**, S08003 (2008). https://doi.org/10.1088/1748-0221/3/08/S08003
36. ATLAS Collaboration, ATLAS Insertable B-layer: technical design report. ATLAS-TDR-19; CERN-LHCC-2010-013 (2010). https://cds.cern.ch/record/1291633. [Addendum: ATLAS-TDR-19-ADD-1; CERN-LHCC-2012-009 (2012). https://cds.cern.ch/record/1451888]
37. B. Abbott et al., Production and integration of the ATLAS Insertable B-Layer. JINST **13**, T05008 (2018). https://doi.org/10.1088/1748-0221/13/05/T05008. arXiv:1803.00844 [physics.ins-det]
38. G. Avoni et al., The new LUCID-2 detector for luminosity measurement and monitoring in ATLAS. JINST **13**, P07017 (2018). https://doi.org/10.1088/1748-0221/13/07/P07017
39. ATLAS Collaboration, Performance of the ATLAS trigger system in 2015. Eur. Phys. J. C **77**, 317 (2017). https://doi.org/10.1140/epjc/s10052-017-4852-3. arXiv:1611.09661 [hep-ex]
40. ATLAS Collaboration, Software and computing for Run3 of the ATLAS experiment at the LHC. Eur. Phys. J. C **85**, 234 (2025). https://doi.org/10.1140/epjc/s10052-024-13701-w arXiv:2404.06335 [hep-ex]
41. ATLAS Collaboration, Luminosity determination in $pp$ collisions at $\sqrt{s} = 13$ TeV using the ATLAS detector at the LHC. ATLAS-CONF-2019-021 (2019). https://cds.cern.ch/record/2677054
42. ATLAS Collaboration, ATLAS data quality operations and performance for 2015–2018 data-taking. JINST **15**, P04003 (2020). https://doi.org/10.1088/1748-0221/15/04/P04003. arXiv:1911.04632 [physics.ins-det]
43. ATLAS Collaboration, Performance of electron and photon triggers in ATLAS during LHC Run 2. Eur. Phys. J. C **80**, 47 (2020). https://doi.org/10.1140/epjc/s10052-019-7500-2. arXiv:1909.00761 [hep-ex]
44. ATLAS Collaboration, Performance of the ATLAS muon triggers in Run 2. JINST **15**, P09015 (2020). https://doi.org/10.1088/1748-0221/15/09/p09015. arXiv:2004.13447 [physics.ins-det]
45. ATLAS Collaboration, Vertex reconstruction performance of the ATLAS detector at $\sqrt{s} = 13$ TeV. ATL-PHYS-PUB-2015-026 (2015). https://cds.cern.ch/record/2037717
46. ATLAS Collaboration, Electron and photon performance measurements with the ATLAS detector using the 2015–2017 LHC proton–proton collision data. JINST **14**, P12006 (2019). https://doi.org/10.1088/1748-0221/14/12/P12006. arXiv:1908.00005 [hep-ex]
47. ATLAS Collaboration, Muon reconstruction and identification efficiency in ATLAS using the full Run 2 $pp$ collision data set at $\sqrt{s} = 13$ TeV. Eur. Phys. J. C **81**, 578 (2021). https://doi.org/10.1140/epjc/s10052-021-09233-2. arXiv:2012.00578 [hep-ex]
48. ATLAS Collaboration, Jet reconstruction and performance using particle flow with the ATLAS Detector. Eur. Phys. J. C **77**, 466 (2017). https://doi.org/10.1140/epjc/s10052-017-5031-2. arXiv:1703.10485 [hep-ex]
49. M. Cacciari, G.P. Salam, G. Soyez, The anti-$k_t$ jet clustering algorithm. JHEP **04**, 063 (2008). https://doi.org/10.1088/1126-6708/2008/04/063. arXiv:0802.1189 [hep-ph]
50. M. Cacciari, G.P. Salam, G. Soyez, FastJet user manual. Eur. Phys. J. C **72**, 1896 (2012). https://doi.org/10.1140/epjc/s10052-012-1896-2. arXiv:1111.6097 [hep-ph]
51. ATLAS Collaboration, Jet energy scale and resolution measured in proton–proton collisions at $\sqrt{s} = 13$ TeV with the ATLAS detector. Eur. Phys. J. C **81**, 689 (2021). https://doi.org/10.1140/epjc/s10052-021-09402-3. arXiv:2007.02645 [hep-ex]
52. ATLAS Collaboration, Performance of pile-up mitigation techniques for jets in $pp$ collisions at $\sqrt{s} = 8$ TeV using the ATLAS detector. Eur. Phys. J. C **76**, 581 (2016). https://doi.org/10.1140/epjc/s10052-016-4395-z. arXiv:1510.03823 [hep-ex]
53. ATLAS Collaboration, Selection of jets produced in 13 TeV proton–proton collisions with the ATLAS detector. ATLAS-CONF-2015-029 (2015). https://cds.cern.ch/record/2037702
54. ATLAS Collaboration, ATLAS flavour-tagging algorithms for the LHC Run 2 $pp$ collision dataset. Eur. Phys. J. C **83**, 681 (2023). https://doi.org/10.1140/epjc/s10052-023-11699-1. arXiv:2211.16345 [physics.data-an]
55. ATLAS Collaboration, Jet reclustering and close-by effects in ATLAS Run 2. ATLAS-CONF-2017-062 (2017). https://cds.cern.ch/record/2275649
56. ATLAS Collaboration, The performance of missing transverse momentum reconstruction and its significance with the ATLAS detector using 140 fb$^{-1}$ of $\sqrt{s} = 13$ TeV $pp$ collisions (2024). arXiv:2402.05858 [hep-ex]
57. ATLAS Collaboration, The ATLAS simulation infrastructure. Eur. Phys. J. C **70**, 823 (2010). https://doi.org/10.1140/epjc/s10052-010-1429-9. arXiv:1005.4568 [physics.ins-det]
58. P. Nason, A new method for combining NLO QCD with shower Monte Carlo algorithms. JHEP **11**, 040 (2004). https://doi.org/10.1088/1126-6708/2004/11/040. arXiv:hep-ph/0409146
59. S. Frixione, G. Ridolfi, P. Nason, A positive-weight next-to-leading-order Monte Carlo for heavy flavour hadroproduction. JHEP **09**, 126 (2007). https://doi.org/10.1088/1126-6708/2007/09/126. arXiv:0707.3088 [hep-ph]
60. S. Frixione, P. Nason, C. Oleari, Matching NLO QCD computations with parton shower simulations: the POWHEG method. JHEP **11**, 070 (2007). https://doi.org/10.1088/1126-6708/2007/11/070. arXiv:0709.2092 [hep-ph]

61. S. Alioli, P. Nason, C. Oleari, E. Re, A general framework for implementing NLO calculations in shower Monte Carlo programs: the POWHEG BOX. JHEP **06**, 043 (2010). https://doi.org/10.1007/JHEP06(2010)043. arXiv:1002.2581 [hep-ph]
62. J. Alwall et al., The automated computation of tree-level and next-to-leading order differential cross sections, and their matching to parton shower simulations. JHEP **07**, 079 (2014). https://doi.org/10.1007/JHEP07(2014)079. arXiv:1405.0301 [hep-ph]
63. T. Sjöstrand et al., An introduction to PYTHIA 8.2. Comput. Phys. Commun. **191**, 159 (2015). https://doi.org/10.1016/j.cpc.2015.01.024. arXiv:1410.3012 [hep-ph]
64. M. Bähr et al., Herwig++ physics and manual. Eur. Phys. J. C **58**, 639 (2008). https://doi.org/10.1140/epjc/s10052-008-0798-9. arXiv:0803.0883 [hep-ph]
65. J. Bellm et al., Herwig 7.0/Herwig++ 3.0 release note. Eur. Phys. J. C **76**, 196 (2016). https://doi.org/10.1140/epjc/s10052-016-4018-8. arXiv:1512.01178 [hep-ph]
66. E. Bothmann et al., Event generation with Sherpa 2.2. SciPost Phys. **7**, 034 (2019). https://doi.org/10.21468/SciPostPhys.7.3.034. arXiv:1905.09127 [hep-ph]
67. S. Catani, F. Krauss, B.R. Webber, R. Kuhn, QCD matrix elements + parton showers. JHEP **11**, 063 (2001). https://doi.org/10.1088/1126-6708/2001/11/063. arXiv:hep-ph/0109231
68. S. Schumann, F. Krauss, A parton shower algorithm based on Catani–Seymour dipole factorisation. JHEP **03**, 038 (2008). https://doi.org/10.1088/1126-6708/2008/03/038. arXiv:0709.1027 [hep-ph]
69. S. Höche, F. Krauss, S. Schumann, F. Siegert, QCD matrix elements and truncated showers. JHEP **05**, 053 (2009). https://doi.org/10.1088/1126-6708/2009/05/053. arXiv:0903.1219 [hep-ph]
70. S. Höche, F. Krauss, M. Schönherr, F. Siegert, A critical appraisal of NLO+PS matching methods. JHEP **09**, 049 (2012). https://doi.org/10.1007/JHEP09(2012)049. arXiv:1111.1220 [hep-ph]
71. S. Höche, F. Krauss, M. Schönherr, F. Siegert, QCD matrix elements + parton showers. The NLO case. JHEP **04**, 027 (2013). https://doi.org/10.1007/JHEP04(2013)027. arXiv:1207.5030 [hep-ph]
72. ATLAS Collaboration, ATLAS Pythia 8 tunes to 7 TeV data. ATL-PHYS-PUB-2014-021 (2014). https://cds.cern.ch/record/1966419
73. NNPDF Collaboration, R.D. Ball et al., Parton distributions with LHC data. Nucl. Phys. B **867**, 244 (2013). https://doi.org/10.1016/j.nuclphysb.2012.10.003. arXiv:1207.1303 [hep-ph]
74. NNPDF Collaboration, R.D. Ball et al., Parton distributions for the LHC run II. JHEP **04**, 040 (2015). https://doi.org/10.1007/JHEP04(2015)040. arXiv:1410.8849 [hep-ph]
75. T. Sjöstrand, S. Mrenna, P. Skands, A brief introduction to PYTHIA 8.1. Comput. Phys. Commun. **178**, 852 (2008). https://doi.org/10.1016/j.cpc.2008.01.036. arXiv:0710.3820 [hep-ph]
76. ATLAS Collaboration, The Pythia 8 A3 tune description of ATLAS minimum bias and inelastic measurements incorporating the Donnachie–Landshoff diffractive model. ATL-PHYS-PUB-2016-017 (2016). https://cds.cern.ch/record/2206965
77. D.J. Lange, The EvtGen particle decay simulation package. Nucl. Instrum. Methods A **462**, 152 (2001). https://doi.org/10.1016/S0168-9002(01)00089-4
78. S. Agostinelli et al., Geant4—a simulation toolkit. Nucl. Instrum. Methods A **506**, 250 (2003). https://doi.org/10.1016/S0168-9002(03)01368-8
79. ATLAS Collaboration, The simulation principle and performance of the ATLAS fast calorimeter simulation FastCaloSim. ATL-PHYS-PUB-2010-013 (2010). https://cds.cern.ch/record/1300517
80. S. Frixione, E. Laenen, P. Motylinski, B.R. Webber, Angular correlations of lepton pairs from vector boson and top quark decays in Monte Carlo simulations. JHEP **04**, 081 (2007). https://doi.org/10.1088/1126-6708/2007/04/081. arXiv:hep-ph/0702198
81. P. Artoisenet, R. Frederix, O. Mattelaer, R. Rietkerk, Automatic spin-entangled decays of heavy resonances in Monte Carlo simulations. JHEP **03**, 015 (2013). https://doi.org/10.1007/JHEP03(2013)015. arXiv:1212.3460 [hep-ph]
82. T. Ježo, J.M. Lindert, N. Moretti, S. Pozzorini, New NLOPS predictions for $t\bar{t}+b$-jet production at the LHC. Eur. Phys. J. C **78**, 502 (2018). https://doi.org/10.1140/epjc/s10052-018-5956-0. arXiv:1802.00426 [hep-ph]
83. T. Ježo, Powheg-Box-Res ttbb source code (2019). https://gitlab.cern.ch/tjezo/powheg-box-res_ttbb/
84. F. Cascioli, P. Maierhöfer, S. Pozzorini, Scattering amplitudes with open loops. Phys. Rev. Lett. **108**, 111601 (2012). https://doi.org/10.1103/PhysRevLett.108.111601. arXiv:1111.5206 [hep-ph]
85. F. Buccioni, S. Pozzorini, M. Zoller, On-the-fly reduction of open loops. Eur. Phys. J. C **78**, 70 (2018). https://doi.org/10.1140/epjc/s10052-018-5562-1. arXiv:1710.11452 [hep-ph]
86. A. Denner, S. Dittmaier, L. Hofer, Collier: a Fortran-based complex one-loop library in extended regularizations. Comput. Phys. Commun. **212**, 220 (2017). https://doi.org/10.1016/j.cpc.2016.10.013. arXiv:1604.06792 [hep-ph]
87. ATLAS Collaboration, Study of $ttbb$ and $ttW$ background modelling for $ttH$ analyses. ATL-PHYS-PUB-2022-026 (2022). https://cds.cern.ch/record/2810864
88. R. Frederix, D. Pagani, M. Zaro, Large NLO corrections in $t\bar{t}W^{\pm}$ and $t\bar{t}t\bar{t}$ hadroproduction from supposedly subleading EW contributions. JHEP **02**, 031 (2018). https://doi.org/10.1007/JHEP02(2018)031. arXiv:1711.02116 [hep-ph]
89. E. Re, Single-top $Wt$-channel production matched with parton showers using the POWHEG method. Eur. Phys. J. C **71**, 1547 (2011). https://doi.org/10.1140/epjc/s10052-011-1547-z. arXiv:1009.2450 [hep-ph]
90. ATLAS Collaboration, Measurements of top-quark pair differential and double-differential cross-sections in the $\ell$+jets channel with $pp$ collisions at $\sqrt{s}=13$ TeV using the ATLAS detector. Eur. Phys. J. C **79**, 1028 (2019). https://doi.org/10.1140/epjc/s10052-019-7525-6. arXiv:1908.07305 [hep-ex]. [Erratum: Eur. Phys. J. C **80**, 1092 (2020). https://doi.org/10.1140/epjc/s10052-020-08541-3]
91. ATLAS Collaboration, Measurement of tt production in association with additional b-jets in the $e\mu$ final state in proton-proton collisions at $\sqrt{s}=13$ TeV with the ATLAS detector. JHEP **1**, 068 (2025). https://doi.org/10.1007/JHEP01%282025%29068. arXiv: 2407.13473 [hep-ex]
92. CMS Collaboration, Inclusive and differential cross section measurements of ttbb production in the lepton+jets channel at $\sqrt{s}$=13 TeV. JHEP **5**, 042 (2023). https://doi.org/10.1007/JHEP05%282024%29042. arXiv: 2309.14442 [hep-ex]
93. ATLAS Collaboration, ATLAS $b$-jet identification performance and efficiency measurement with $t\bar{t}$ events in $pp$ collisions at $\sqrt{s}=13$ TeV. Eur. Phys. J. C **79**, 970 (2019). https://doi.org/10.1140/epjc/s10052-019-7450-8. arXiv:1907.05120 [hep-ex]
94. ATLAS Collaboration, Measurement of the $c$-jet mistagging efficiency in $t\bar{t}$ events using $pp$ collision data at $\sqrt{s}=13$ TeV collected with the ATLAS detector. Eur. Phys. J. C **82**, 95 (2022). https://doi.org/10.1140/epjc/s10052-021-09843-w. arXiv:2109.10627 [hep-ex]
95. ATLAS Collaboration, Calibration of the light-flavour jet mistagging efficiency of the $b$-tagging algorithms with $Z$+jets events using 139 fb$^{-1}$ of ATLAS proton–proton collision data at $\sqrt{s}=13$ TeV. Eur. Phys. J. C **83**, 728 (2023). https://doi.org/10.1140/epjc/s10052-023-11736-z. arXiv:2301.06319 [hep-ex]
96. L. Garrido, A. Juste, On the determination of probability density functions by using Neural Networks. Com-

put. Phys. Commun. **115**, 25 (1998). https://doi.org/10.1016/S0010-4655(98)00107-6. arXiv:physics/9807018 [physics.data-an]
97. G.V. Moustakides, K. Basioti, Training neural networks for likelihood/density ratio estimation (2019). arXiv:1911.00405 [eess.SP]
98. P.W. Battaglia et al., Relational inductive biases, deep learning, and graph networks (2018). https://doi.org/10.48550/ARXIV.1806.01261. arXiv:1806.01261 [cs.LG]
99. P. Baldi, K. Cranmer, T. Faucett, P. Sadowski, D. Whiteson, Parameterized neural networks for high-energy physics. Eur. Phys. J. C **76** (2016). https://doi.org/10.1140/epjc/s10052-016-4099-4. arXiv:1601.07913 [hep-ex]
100. A. Paszke et al., PyTorch: an imperative style, high-performance deep learning library (2019). arXiv:1912.01703 [cs.LG]
101. ATLAS Collaboration, Performance of missing transverse momentum reconstruction with the ATLAS detector using proton–proton collisions at $\sqrt{s} = 13$ TeV. Eur. Phys. J. C **78**, 903 (2018). https://doi.org/10.1140/epjc/s10052-018-6288-9. arXiv:1802.08168 [hep-ex]
102. J. Butterworth et al., PDF4LHC recommendations for LHC Run II. J. Phys. G **43**, 023001 (2016). https://doi.org/10.1088/0954-3899/43/2/023001. arXiv:1510.03865 [hep-ph]
103. Y. Gal, Z. Ghahramani, Dropout as a Bayesian approximation: representing model uncertainty in deep learning (2016). arXiv:1506.02142 [stat.ML]
104. ATLAS Collaboration, Evidence for $t\bar{t}t\bar{t}$ production in the multilepton final state in proton–proton collisions at $\sqrt{s} = 13$ TeV with the ATLAS detector. Eur. Phys. J. C **80**, 1085 (2020). https://doi.org/10.1140/epjc/s10052-020-08509-3. arXiv:2007.14858 [hep-ex]
105. D. de Florian et al., Handbook of LHC Higgs cross sections: 4. Deciphering the nature of the Higgs sector (2017). https://doi.org/10.23731/CYRM-2017-002. arXiv:1610.07922 [hep-ph]
106. ATLAS Collaboration, Combined measurements of Higgs boson production and decay using up to 80 fb$^{-1}$ of proton–proton collision data at $\sqrt{s} = 13$ TeV collected with the ATLAS experiment. Phys. Rev. D **101**, 012002 (2020). https://doi.org/10.1103/PhysRevD.101.012002. arXiv:1909.02845 [hep-ex]
107. J. Alwall et al., Comparative study of various algorithms for the merging of parton showers and matrix elements in hadronic collisions. Eur. Phys. J. C **53**, 473 (2008). https://doi.org/10.1140/epjc/s10052-007-0490-5. arXiv:0706.2569 [hep-ph]
108. T. Junk, Confidence level computation for combining searches with small statistics. Nucl. Instrum. Methods A **434**, 435 (1999). https://doi.org/10.1016/S0168-9002(99)00498-2. arXiv:hep-ex/9902006
109. A.L. Read, Presentation of search results: the $CL_S$ technique. J. Phys. G **28**, 2693 (2002). https://doi.org/10.1088/0954-3899/28/10/313
110. G. Cowan, K. Cranmer, E. Gross, O. Vitells, Asymptotic formulae for likelihood-based tests of new physics. Eur. Phys. J. C **71**, 1554 (2011). https://doi.org/10.1140/epjc/s10052-011-1554-0. arXiv:1007.1727 [physics.data-an]. [Erratum: Eur. Phys. J. C **73**, 2501 (2013). https://doi.org/10.1140/epjc/s10052-013-2501-z]
111. K. Cranmer, G. Lewis, L. Moneta, A. Shibata, W. Verkerke, HistFactory: a tool for creating statistical models for use with RooFit and RooStats. CERN-OPEN-2012-016 (2012). https://cds.cern.ch/record/1456844
112. W. Verkerke, D. Kirkby, The RooFit toolkit for data modeling (2003). arXiv:physics/0306116 [physics.data-an]
113. L. Moneta et al., The RooStats project (2011). arXiv:1009.1003 [physics.data-an]
114. R.V. Harlander, S. Liebler, H. Mantler, SusHi: a program for the calculation of Higgs production in gluon fusion and bottom-quark annihilation in the Standard Model and the MSSM. Comput. Phys. Commun. **184**, 1605 (2013). https://doi.org/10.1016/j.cpc.2013.02.006. arXiv:1212.3249 [hep-ph]
115. R.V. Harlander, W.B. Kilgore, Next-to-next-to-leading order Higgs production at hadron colliders. Phys. Rev. Lett. **88**, 201801 (2002). https://doi.org/10.1103/PhysRevLett.88.201801. arXiv:hep-ph/0201206
116. R.V. Harlander, W.B. Kilgore, Higgs boson production in bottom quark fusion at next-to-next-to-leading order. Phys. Rev. D **68**, 013001 (2003). https://doi.org/10.1103/PhysRevD.68.013001. arXiv:hep-ph/0304035
117. U. Aglietti, R. Bonciani, G. Degrassi, A. Vicini, Two-loop light fermion contribution to Higgs production and decays. Phys. Lett. B **595**, 432 (2004). https://doi.org/10.1016/j.physletb.2004.06.063. arXiv:hep-ph/0404071
118. R. Bonciani, G. Degrassi, A. Vicini, On the generalized harmonic polylogarithms of one complex variable. Comput. Phys. Commun. **182**, 1253 (2011). https://doi.org/10.1016/j.cpc.2011.02.011. arXiv:1007.1891 [hep-ph]
119. R.V. Harlander, P. Kant, Higgs production and decay: analytic results at next-to-leading order QCD. JHEP **12**, 015 (2005). https://doi.org/10.1088/1126-6708/2005/12/015. arXiv:hep-ph/0509189
120. R.D. Cousins, Generalization of Chisquare goodness-of-fit test for binned data using saturated models, with application to histograms (2013). http://www.physics.ucla.edu/~cousins/stats/cousins_saturated.pdf (visited on 12/07/2024)
121. ATLAS Collaboration, ATLAS computing acknowledgements. ATL-SOFT-PUB-2023-001 (2023). https://cds.cern.ch/record/2869272

## ATLAS Collaboration*

G. Aad[104], E. Aakvaag[17], B. Abbott[123], S. Abdelhameed[119a], K. Abeling[56], N. J. Abicht[50], S. H. Abidi[30], M. Aboelela[45], A. Aboulhorma[36e], H. Abramowicz[155], H. Abreu[154], Y. Abulaiti[120], B. S. Acharya[70a,70b,l], A. Ackermann[64a], C. Adam Bourdarios[4], L. Adamczyk[87a], S. V. Addepalli[27], M. J. Addison[103], J. Adelman[118], A. Adiguzel[22c], T. Adye[137], A. A. Affolder[139], Y. Afik[40], M. N. Agaras[13], J. Agarwala[74a,74b], A. Aggarwal[102], C. Agheorghiesei[28c], A. Ahmad[37], F. Ahmadov[39,z], W. S. Ahmed[106], S. Ahuja[97], X. Ai[63e], G. Aielli[77a,77b], A. Aikot[166], M. Ait Tamlihat[36e], B. Aitbenchikh[36a], M. Akbiyik[102], T. P. A. Åkesson[100], A. V. Akimov[38], D. Akiyama[171], N. N. Akolkar[25], S. Aktas[22a], K. Al Khoury[42], G. L. Alberghi[24b], J. Albert[168], P. Albicocco[54], G. L. Albouy[61], S. Alderweireldt[53], Z. L. Alegria[124], M. Aleksa[37], I. N. Aleksandrov[39], C. Alexa[28b], T. Alexopoulos[10], F. Alfonsi[24b], M. Algren[57], M. Alhroob[170], B. Ali[135], H. M. J. Ali[93], S. Ali[32], S. W. Alibocus[94], M. Aliev[34c], G. Alimonti[72a], W. Alkakhi[56], C. Allaire[67], B. M. M. Allbrooke[150], J. F. Allen[53], C. A. Allendes Flores[140f], P. P. Allport[21], A. Aloisio[73a,73b], F. Alonso[92], C. Alpigiani[142], Z. M. K. Alsolami[93], M. Alvarez Estevez[101], A. Alvarez Fernandez[102], M. Alves Cardoso[57], M. G. Alviggi[73a,73b], M. Aly[103], Y. Amaral Coutinho[84b], A. Ambler[106], C. Amelung[37], M. Amerl[103], C. G. Ames[111], D. Amidei[108], K. Amirie[158], S. P. Amor Dos Santos[133a], K. R. Amos[166], S. An[85], V. Ananiev[128], C. Anastopoulos[143], T. Andeen[11], J. K. Anders[37], A. C. Anderson[60], S. Y. Andrean[48a,48b], A. Andreazza[72a,72b], S. Angelidakis[9], A. Angerami[42,ab], A. V. Anisenkov[38], A. Annovi[75a], C. Antel[57], E. Antipov[149], M. Antonelli[54], F. Anulli[76a], M. Aoki[85], T. Aoki[157], M. A. Aparo[150], L. Aperio Bella[49], C. Appelt[19], A. Apyan[27], S. J. Arbiol Val[88], C. Arcangeletti[54], A. T. H. Arce[52], E. Arena[94], J.-F. Arguin[110], S. Argyropoulos[55], J.-H. Arling[49], O. Arnaez[4], H. Arnold[149], G. Artoni[76a,76b], H. Asada[113], K. Asai[121], S. Asai[157], N. A. Asbah[37], R. A. Ashby Pickering[170], K. Assamagan[30], R. Astalos[29a], K. S. V. Astrand[100], S. Atashi[162], R. J. Atkin[34a], M. Atkinson[165], H. Atmani[36f], P. A. Atmasiddha[131], K. Augsten[135], S. Auricchio[73a,73b], A. D. Auriol[21], V. A. Austrup[103], G. Avolio[37], K. Axiotis[57], G. Azuelos[110,af], D. Babal[29b], H. Bachacou[138], K. Bachas[156,p], A. Bachiu[35], F. Backman[48a,48b], A. Badea[40], T. M. Baer[108], P. Bagnaia[76a,76b], M. Bahmani[19], D. Bahner[55], K. Bai[126], J. T. Baines[137], L. Baines[96], O. K. Baker[175], E. Bakos[16], D. Bakshi Gupta[8], L. E. Balabram Filho[84b], V. Balakrishnan[123], R. Balasubramanian[117], E. M. Baldin[38], P. Balek[87a], E. Ballabene[24a,24b], F. Balli[138], L. M. Baltes[64a], W. K. Balunas[33], J. Balz[102], I. Bamwidhi[119b], E. Banas[88], M. Bandieramonte[132], A. Bandyopadhyay[25], S. Bansal[25], L. Barak[155], M. Barakat[49], E. L. Barberio[107], D. Barberis[58a,58b], M. Barbero[104], M. Z. Barel[117], K. N. Barends[34a], T. Barillari[112], M.-S. Barisits[37], T. Barklow[147], P. Baron[125], D. A. Baron Moreno[103], A. Baroncelli[63a], G. Barone[30], A. J. Barr[129], J. D. Barr[98], F. Barreiro[101], J. Barreiro Guimarães da Costa[14], U. Barron[155], M. G. Barros Teixeira[133a], S. Barsov[38], F. Bartels[64a], R. Bartoldus[147], A. E. Barton[93], P. Bartos[29a], A. Basan[102], M. Baselga[50], A. Bassalat[67,b], M. J. Basso[159a], S. Bataju[45], R. Bate[167], R. L. Bates[60], S. Batlamous[101], B. Batool[145], M. Battaglia[139], D. Battulga[19], M. Bauce[76a,76b], M. Bauer[37], P. Bauer[25], L. T. Bazzano Hurrell[31], J. B. Beacham[52], T. Beau[130], J. Y. Beaucamp[92], P. H. Beauchemin[161], P. Bechtle[25], H. P. Beck[20,o], K. Becker[170], A. J. Beddall[83], V. A. Bednyakov[39], C. P. Bee[149], L. J. Beemster[16], T. A. Beermann[37], M. Begalli[84d], M. Begel[30], A. Behera[149], J. K. Behr[49], J. F. Beirer[37], F. Beisiegel[25], M. Belfkir[119b], G. Bella[155], L. Bellagamba[24b], A. Bellerive[35], P. Bellos[21], K. Beloborodov[38], D. Benchekroun[36a], F. Bendebba[36a], Y. Benhammou[155], K. C. Benkendorfer[62], L. Beresford[49], M. Beretta[54], E. Bergeaas Kuutmann[164], N. Berger[4], B. Bergmann[135], J. Beringer[18a], G. Bernardi[5], C. Bernius[147], F. U. Bernlochner[25], F. Bernon[37,104], A. Berrocal Guardia[13], T. Berry[97], P. Berta[136], A. Berthold[51], S. Bethke[112], A. Betti[76a,76b], A. J. Bevan[96], N. K. Bhalla[55], S. Bhatta[149], D. S. Bhattacharya[169], P. Bhattarai[147], K. D. Bhide[55], V. S. Bhopatkar[124], R. M. Bianchi[132], G. Bianco[24a,24b], O. Biebel[111], R. Bielski[126], M. Biglietti[78a], C. S. Billingsley[45], M. Bindi[56], A. Bingul[22b], C. Bini[76a,76b], A. Biondini[94], G. A. Bird[33], M. Birman[172], M. Biros[136], S. Biryukov[150], T. Bisanz[50], E. Bisceglie[44a,44b], J. P. Biswal[137], D. Biswas[145], I. Bloch[49], A. Blue[60], U. Blumenschein[96], J. Blumenthal[102], V. S. Bobrovnikov[38], M. Boehler[55], B. Boehm[169], D. Bogavac[37], A. G. Bogdanchikov[38], C. Bohm[48a], V. Boisvert[97], P. Bokan[37], T. Bold[87a], M. Bomben[5], M. Bona[96], M. Boonekamp[138], C. D. Booth[97], A. G. Borbély[60], I. S. Bordulev[38], H. M. Borecka-Bielska[110], G. Borissov[93], D. Bortoletto[129], D. Boscherini[24b], M. Bosman[13], J. D. Bossio Sola[37], K. Bouaouda[36a], N. Bouchhar[166], L. Boudet[4], J. Boudreau[132], E. V. Bouhova-Thacker[93], D. Boumediene[41], R. Bouquet[58a,58b], A. Boveia[122], J. Boyd[37], D. Boye[30], I. R. Boyko[39], L. Bozianu[57], J. Bracinik[21], N. Brahimi[4],

G. Brandt[174], O. Brandt[33], F. Braren[49], B. Brau[105], J. E. Brau[126], R. Brener[172], L. Brenner[117], R. Brenner[164], S. Bressler[172], D. Britton[60], D. Britzger[112], I. Brock[25], R. Brock[109], G. Brooijmans[42], E. Brost[30], L. M. Brown[168], L. E. Bruce[62], T. L. Bruckler[129], P. A. Bruckman de Renstrom[88], B. Brüers[49], A. Bruni[24b], G. Bruni[24b], M. Bruschi[24b], N. Bruscino[76a,76b], T. Buanes[17], Q. Buat[142], D. Buchin[112], A. G. Buckley[60], O. Bulekov[38], B. A. Bullard[147], S. Burdin[94], C. D. Burgard[50], A. M. Burger[37], B. Burghgrave[8], O. Burlayenko[55], J. T. P. Burr[33], J. C. Burzynski[146], E. L. Busch[42], V. Büscher[102], P. J. Bussey[60], J. M. Butler[26], C. M. Buttar[60], J. M. Butterworth[98], W. Buttinger[137], C. J. Buxo Vazquez[109], A. R. Buzykaev[38], S. Cabrera Urbán[166], L. Cadamuro[67], D. Caforio[59], H. Cai[132], Y. Cai[14,114c], Y. Cai[114a], V. M. M. Cairo[37], O. Cakir[3a], N. Calace[37], P. Calafiura[18a], G. Calderini[130], P. Calfayan[69], G. Callea[60], L. P. Caloba[84b], D. Calvet[41], S. Calvet[41], M. Calvetti[75a,75b], R. Camacho Toro[130], S. Camarda[37], D. Camarero Munoz[27], P. Camarri[77a,77b], M. T. Camerlingo[73a,73b], D. Cameron[37], C. Camincher[168], M. Campanelli[98], A. Camplani[43], V. Canale[73a,73b], A. C. Canbay[3a], E. Canonero[97], J. Cantero[166], Y. Cao[165], F. Capocasa[27], M. Capua[44a,44b], A. Carbone[72a,72b], R. Cardarelli[77a], J. C. J. Cardenas[8], G. Carducci[44a,44b], T. Carli[37], G. Carlino[73a], J. I. Carlotto[13], B. T. Carlson[132,q], E. M. Carlson[159a,168], J. Carmignani[94], L. Carminati[72a,72b], A. Carnelli[138], M. Carnesale[76a,76b], S. Caron[116], E. Carquin[140f], S. Carrá[72a], G. Carratta[24a,24b], A. M. Carroll[126], T. M. Carter[53], M. P. Casado[13,i], M. Caspar[49], F. L. Castillo[4], L. Castillo Garcia[13], V. Castillo Gimenez[166], N. F. Castro[133a,133e], A. Catinaccio[37], J. R. Catmore[128], T. Cavaliere[4], V. Cavaliere[30], N. Cavalli[24a,24b], L. J. Caviedes Betancourt[23b], Y. C. Cekmecelioglu[49], E. Celebi[22a], S. Cella[37], F. Celli[129], M. S. Centonze[71a,71b], V. Cepaitis[57], K. Cerny[125], A. S. Cerqueira[84a], A. Cerri[150], L. Cerrito[77a,77b], F. Cerutti[18a], B. Cervato[145], A. Cervelli[24b], G. Cesarini[54], S. A. Cetin[83], D. Chakraborty[118], J. Chan[18a], W. Y. Chan[157], J. D. Chapman[33], E. Chapon[138], B. Chargeishvili[153b], D. G. Charlton[21], M. Chatterjee[20], C. Chauhan[136], Y. Che[114a], S. Chekanov[6], S. V. Chekulaev[159a], G. A. Chelkov[39,a], A. Chen[108], B. Chen[155], B. Chen[168], H. Chen[114a], H. Chen[30], J. Chen[63c], J. Chen[146], M. Chen[129], S. Chen[157], S. J. Chen[114a], X. Chen[63c,138], X. Chen[15,ae], Y. Chen[63a], C. L. Cheng[173], H. C. Cheng[65a], S. Cheong[147], A. Cheplakov[39], E. Cheremushkina[49], E. Cherepanova[117], R. Cherkaoui El Moursli[36e], E. Cheu[7], K. Cheung[66], L. Chevalier[138], V. Chiarella[54], G. Chiarelli[75a], N. Chiedde[104], G. Chiodini[71a], A. S. Chisholm[21], A. Chitan[28b], M. Chitishvili[166], M. V. Chizhov[39,r], K. Choi[11], Y. Chou[142], E. Y. S. Chow[116], K. L. Chu[172], M. C. Chu[65a], X. Chu[14,114c], Z. Chubinidze[54], J. Chudoba[134], J. J. Chwastowski[88], D. Cieri[112], K. M. Ciesla[87a], V. Cindro[95], A. Ciocio[18a], F. Cirotto[73a,73b], Z. H. Citron[172], M. Citterio[72a], D. A. Ciubotaru[28b], A. Clark[57], P. J. Clark[53], N. Clarke Hall[98], C. Clarry[158], J. M. Clavijo Columbie[49], S. E. Clawson[49], C. Clement[48a,48b], J. Clercx[49], Y. Coadou[104], M. Cobal[70a,70c], A. Coccaro[58b], R. F. Coelho Barrue[133a], R. Coelho Lopes De Sa[105], S. Coelli[72a], B. Cole[42], J. Collot[61], P. Conde Muiño[133a,133g], M. P. Connell[34c], S. H. Connell[34c], E. I. Conroy[129], F. Conventi[73a,ag], H. G. Cooke[21], A. M. Cooper-Sarkar[129], F. A. Corchia[24a,24b], A. Cordeiro Oudot Choi[130], L. D. Corpe[41], M. Corradi[76a,76b], F. Corriveau[106,x], A. Cortes-Gonzalez[19], M. J. Costa[166], F. Costanza[4], D. Costanzo[143], B. M. Cote[122], J. Couthures[4], G. Cowan[97], K. Cranmer[173], D. Cremonini[24a,24b], S. Crépé-Renaudin[61], F. Crescioli[130], M. Cristinziani[145], M. Cristoforetti[79a,79b], V. Croft[117], J. E. Crosby[124], G. Crosetti[44a,44b], A. Cueto[101], Z. Cui[7], W. R. Cunningham[60], F. Curcio[166], J. R. Curran[53], P. Czodrowski[37], M. M. Czurylo[37], M. J. Da Cunha Sargedas De Sousa[58a,58b], J. V. Da Fonseca Pinto[84b], C. Da Via[103], W. Dabrowski[87a], T. Dado[50], S. Dahbi[152], T. Dai[108], D. Dal Santo[20], C. Dallapiccola[105], M. Dam[43], G. D'amen[30], V. D'Amico[111], J. Damp[102], J. R. Dandoy[35], D. Dannheim[37], M. Danninger[146], V. Dao[149], G. Darbo[58b], S. J. Das[30,ah], F. Dattola[49], S. D'Auria[72a,72b], A. D'Avanzo[73a,73b], C. David[34a], T. Davidek[136], I. Dawson[96], H. A. Day-hall[135], K. De[8], R. De Asmundis[73a], N. De Biase[49], S. De Castro[24a,24b], N. De Groot[116], P. de Jong[117], H. De la Torre[118], A. De Maria[114a], A. De Salvo[76a], U. De Sanctis[77a,77b], F. De Santis[71a,71b], A. De Santo[150], J. B. De Vivie De Regie[61], D. V. Dedovich[39], J. Degens[94], A. M. Deiana[45], F. Del Corso[24a,24b], J. Del Peso[101], F. Del Rio[64a], L. Delagrange[130], F. Deliot[138], C. M. Delitzsch[50], M. Della Pietra[73a,73b], D. Della Volpe[57], A. Dell'Acqua[37], L. Dell'Asta[72a,72b], M. Delmastro[4], P. A. Delsart[61], S. Demers[175], M. Demichev[39], S. P. Denisov[38], L. D'Eramo[41], D. Derendarz[88], F. Derue[130], P. Dervan[94], K. Desch[25], C. Deutsch[25], F. A. Di Bello[58a,58b], A. Di Ciaccio[77a,77b], L. Di Ciaccio[4], A. Di Domenico[76a,76b], C. Di Donato[73a,73b], A. Di Girolamo[37], G. Di Gregorio[37], A. Di Luca[79a,79b], B. Di Micco[78a,78b], R. Di Nardo[78a,78b], K. F. Di Petrillo[40], M. Diamantopoulou[35], F. A. Dias[117], T. Dias Do Vale[146], M. A. Diaz[140a,140b], F. G. Diaz Capriles[25], M. Didenko[166], E. B. Diehl[108], S. Díez Cornell[49], C. Diez Pardos[145], C. Dimitriadi[25,164], A. Dimitrievska[21], J. Dingfelder[25], I.-M. Dinu[28b],

S. J. Dittmeier[64b], F. Dittus[37], M. Divisek[136], F. Djama[104], T. Djobava[153b], C. Doglioni[100,103], A. Dohnalova[29a], J. Dolejsi[136], Z. Dolezal[136], K. Domijan[87a], K. M. Dona[40], M. Donadelli[84d], B. Dong[109], J. Donini[41], A. D'Onofrio[73a,73b], M. D'Onofrio[94], J. Dopke[137], A. Doria[73a], N. Dos Santos Fernandes[133a], P. Dougan[103], M. T. Dova[92], A. T. Doyle[60], M. A. Draguet[129], E. Dreyer[172], I. Drivas-koulouris[10], M. Drnevich[120], M. Drozdova[57], D. Du[63a], T. A. du Pree[117], F. Dubinin[38], M. Dubovsky[29a], E. Duchovni[172], G. Duckeck[111], O. A. Ducu[28b], D. Duda[53], A. Dudarev[37], E. R. Duden[27], M. D'uffizi[103], L. Duflot[67], M. Dührssen[37], I. Duminica[28g], A. E. Dumitriu[28b], M. Dunford[64a], S. Dungs[50], K. Dunne[48a,48b], A. Duperrin[104], H. Duran Yildiz[3a], M. Düren[59], A. Durglishvili[153b], B. L. Dwyer[118], G. I. Dyckes[18a], M. Dyndal[87a], B. S. Dziedzic[37], Z. O. Earnshaw[150], G. H. Eberwein[129], B. Eckerova[29a], S. Eggebrecht[56], E. Egidio Purcino De Souza[130], L. F. Ehrke[57], G. Eigen[17], K. Einsweiler[18a], T. Ekelof[164], P. A. Ekman[100], S. El Farkh[36b], Y. El Ghazali[36b], H. El Jarrari[37], A. El Moussaouy[36a], V. Ellajosyula[164], M. Ellert[164], F. Ellinghaus[174], N. Ellis[37], J. Elmsheuser[30], M. Elsawy[119a], M. Elsing[37], D. Emeliyanov[137], Y. Enari[157], I. Ene[18a], S. Epari[13], P. A. Erland[88], D. Ernani Martins Neto[88], M. Errenst[174], M. Escalier[67], C. Escobar[166], E. Etzion[155], G. Evans[133a,133b], H. Evans[69], L. S. Evans[97], A. Ezhilov[38], S. Ezzarqtouni[36a], F. Fabbri[24a,24b], L. Fabbri[24a,24b], G. Facini[98], V. Fadeyev[139], R. M. Fakhrutdinov[38], D. Fakoudis[102], S. Falciano[76a], L. F. Falda Ulhoa Coelho[37], F. Fallavollita[112], G. Falsetti[44a,44b], J. Faltova[136], C. Fan[165], Y. Fan[14], Y. Fang[14,114c], M. Fanti[72a,72b], M. Faraj[70a,70b], Z. Farazpay[99], A. Farbin[8], A. Farilla[78a], T. Farooque[109], S. M. Farrington[53], F. Fassi[36e], D. Fassouliotis[9], M. Faucci Giannelli[77a,77b], W. J. Fawcett[33], L. Fayard[67], P. Federic[136], P. Federicova[134], O. L. Fedin[38,a], M. Feickert[173], L. Feligioni[104], D. E. Fellers[126], C. Feng[63b], M. Feng[15], Z. Feng[117], M. J. Fenton[162], L. Ferencz[49], R. A. M. Ferguson[93], S. I. Fernandez Luengo[140f], P. Fernandez Martinez[13], M. J. V. Fernoux[104], J. Ferrando[93], A. Ferrari[164], P. Ferrari[116,117], R. Ferrari[74a], D. Ferrere[57], C. Ferretti[108], D. Fiacco[76a,76b], F. Fiedler[102], P. Fiedler[135], A. Filipčič[95], E. K. Filmer[1], F. Filthaut[116], M. C. N. Fiolhais[133a,133c,c], L. Fiorini[166], W. C. Fisher[109], T. Fitschen[103], P. M. Fitzhugh[138], I. Fleck[145], P. Fleischmann[108], T. Flick[174], M. Flores[34d,ac], L. R. Flores Castillo[65a], L. Flores Sanz De Acedo[37], F. M. Follega[79a,79b], N. Fomin[17], J. H. Foo[158], A. Formica[138], A. C. Forti[103], E. Fortin[37], A. W. Fortman[18a], M. G. Foti[18a], L. Fountas[9,j], D. Fournier[67], H. Fox[93], P. Francavilla[75a,75b], S. Francescato[62], S. Franchellucci[57], M. Franchini[24a,24b], S. Franchino[64a], D. Francis[37], L. Franco[116], V. Franco Lima[37], L. Franconi[49], M. Franklin[62], G. Frattari[27], Y. Y. Frid[155], J. Friend[60], N. Fritzsche[51], A. Froch[55], D. Froidevaux[37], J. A. Frost[129], Y. Fu[63a], S. Fuenzalida Garrido[140f], M. Fujimoto[104], K. Y. Fung[65a], E. Furtado De Simas Filho[84e], M. Furukawa[157], J. Fuster[166], A. Gaa[56], A. Gabrielli[24a,24b], A. Gabrielli[158], P. Gadow[37], G. Gagliardi[58a,58b], L. G. Gagnon[18a], S. Gaid[163], S. Galantzan[155], E. J. Gallas[129], B. J. Gallop[137], K. K. Gan[122], S. Ganguly[157], Y. Gao[53], F. M. Garay Walls[140a,140b], B. Garcia[30], C. García[166], A. Garcia Alonso[117], A. G. Garcia Caffaro[175], J. E. García Navarro[166], M. Garcia-Sciveres[18a], G. L. Gardner[131], R. W. Gardner[40], N. Garelli[161], D. Garg[81], R. B. Garg[147], J. M. Gargan[53], C. A. Garner[158], C. M. Garvey[34a], V. K. Gassmann[161], G. Gaudio[74a], V. Gautam[13], P. Gauzzi[76a,76b], J. Gavranovic[95], I. L. Gavrilenko[38], A. Gavrilyuk[38], C. Gay[167], G. Gaycken[49], E. N. Gazis[10], A. A. Geanta[28b], C. M. Gee[139], A. Gekow[122], C. Gemme[58b], M. H. Genest[61], A. D. Gentry[115], S. George[97], W. F. George[21], T. Geralis[47], P. Gessinger-Befurt[37], M. E. Geyik[174], M. Ghani[170], K. Ghorbanian[96], A. Ghosal[145], A. Ghosh[162], A. Ghosh[7], B. Giacobbe[24b], S. Giagu[76a,76b], T. Giani[117], P. Giannetti[75a], A. Giannini[63a], S. M. Gibson[97], M. Gignac[139], D. T. Gil[87b], A. K. Gilbert[87a], B. J. Gilbert[42], D. Gillberg[35], G. Gilles[117], L. Ginabat[130], D. M. Gingrich[2,af], M. P. Giordani[70a,70c], P. F. Giraud[138], G. Giugliarelli[70a,70c], D. Giugni[72a], F. Giuli[37], I. Gkialas[9,j], L. K. Gladilin[38], C. Glasman[101], G. R. Gledhill[126], G. Glemža[49], M. Glisic[126], I. Gnesi[44b,f], Y. Go[30], M. Goblirsch-Kolb[37], B. Gocke[50], D. Godin[110], B. Gokturk[22a], S. Goldfarb[107], T. Golling[57], M. G. D. Gololo[34g], D. Golubkov[38], J. P. Gombas[109], A. Gomes[133a,133b], G. Gomes Da Silva[145], A. J. Gomez Delegido[166], R. Gonçalo[133a], L. Gonella[21], A. Gongadze[153c], F. Gonnella[21], J. L. Gonski[147], R. Y. González Andana[53], S. González de la Hoz[166], R. Gonzalez Lopez[94], C. Gonzalez Renteria[18a], M. V. Gonzalez Rodrigues[49], R. Gonzalez Suarez[164], S. Gonzalez-Sevilla[57], L. Goossens[37], B. Gorini[37], E. Gorini[71a,71b], A. Gorišek[95], T. C. Gosart[131], A. T. Goshaw[52], M. I. Gostkin[39], S. Goswami[124], C. A. Gottardo[37], S. A. Gotz[111], M. Gouighri[36b], V. Goumarre[49], A. G. Goussiou[142], N. Govender[34c], I. Grabowska-Bold[87a], K. Graham[35], E. Gramstad[128], S. Grancagnolo[71a,71b], C. M. Grant[1,138], P. M. Gravila[28f], F. G. Gravili[71a,71b], H. M. Gray[18a], M. Greco[71a,71b], M. J. Green[1], C. Grefe[25], A. S. Grefsrud[17], I. M. Gregor[49], K. T. Greif[162], P. Grenier[147], S. G. Grewe[112], A. A. Grillo[139], K. Grimm[32], S. Grinstein[13,t], J.-F. Grivaz[67], E. Gross[172], J. Grosse-Knetter[56],

J. C. Grundy[129], L. Guan[108], J. G. R. Guerrero Rojas[166], G. Guerrieri[70a,70c], R. Gugel[102], J. A. M. Guhit[108], A. Guida[19], E. Guilloton[170], S. Guindon[37], F. Guo[14,114c], J. Guo[63c], L. Guo[49], Y. Guo[108], R. Gupta[132], S. Gurbuz[25], S. S. Gurdasani[55], G. Gustavino[76a,76b], M. Guth[57], P. Gutierrez[123], L. F. Gutierrez Zagazeta[131], M. Gutsche[51], C. Gutschow[98], C. Gwenlan[129], C. B. Gwilliam[94], E. S. Haaland[128], A. Haas[120], M. Habedank[49], C. Haber[18a], H. K. Hadavand[8], A. Hadef[51], S. Hadzic[112], A. I. Hagan[93], J. J. Hahn[145], E. H. Haines[98], M. Haleem[169], J. Haley[124], J. J. Hall[143], G. D. Hallewell[104], L. Halser[20], K. Hamano[168], M. Hamer[25], G. N. Hamity[53], E. J. Hampshire[97], J. Han[63b], K. Han[63a], L. Han[114a], L. Han[63a], S. Han[18a], Y. F. Han[158], K. Hanagaki[85], M. Hance[139], D. A. Hangal[42], H. Hanif[146], M. D. Hank[131], J. B. Hansen[43], P. H. Hansen[43], K. Hara[160], D. Harada[57], T. Harenberg[174], S. Harkusha[38], M. L. Harris[105], Y. T. Harris[129], J. Harrison[13], N. M. Harrison[122], P. F. Harrison[170], N. M. Hartman[112], N. M. Hartmann[111], R. Z. Hasan[97,137], Y. Hasegawa[144], S. Hassan[17], R. Hauser[109], C. M. Hawkes[21], R. J. Hawkings[37], Y. Hayashi[157], S. Hayashida[113], D. Hayden[109], C. Hayes[108], R. L. Hayes[117], C. P. Hays[129], J. M. Hays[96], H. S. Hayward[94], F. He[63a], M. He[14,114c], Y. He[141], Y. He[49], Y. He[98], N. B. Heatley[96], V. Hedberg[100], A. L. Heggelund[128], N. D. Hehir[96,*], C. Heidegger[55], K. K. Heidegger[55], J. Heilman[35], S. Heim[49], T. Heim[18a], J. G. Heinlein[131], J. J. Heinrich[126], L. Heinrich[112,ad], J. Hejbal[134], A. Held[173], S. Hellesund[17], C. M. Helling[167], S. Hellman[48a,48b], R. C. W. Henderson[93], L. Henkelmann[33], A. M. Henriques Correia[37], H. Herde[100], Y. Hernández Jiménez[149], L. M. Herrmann[25], T. Herrmann[51], G. Herten[55], R. Hertenberger[111], L. Hervas[37], M. E. Hesping[102], N. P. Hessey[159a], M. Hidaoui[36b], N. Hidic[136], E. Hill[158], S. J. Hillier[21], J. R. Hinds[109], F. Hinterkeuser[25], M. Hirose[127], S. Hirose[160], D. Hirschbuehl[174], T. G. Hitchings[103], B. Hiti[95], J. Hobbs[149], R. Hobincu[28e], N. Hod[172], M. C. Hodgkinson[143], B. H. Hodkinson[129], A. Hoecker[37], D. D. Hofer[108], J. Hofer[49], T. Holm[25], M. Holzbock[112], L. B. A. H. Hommels[33], B. P. Honan[103], J. J. Hong[69], J. Hong[63c], T. M. Hong[132], B. H. Hooberman[165], W. H. Hopkins[6], M. C. Hoppesch[165], Y. Horii[113], S. Hou[152], A. S. Howard[95], J. Howarth[60], J. Hoya[6], M. Hrabovsky[125], A. Hrynevich[49], T. Hryn'ova[4], P. J. Hsu[66], S.-C. Hsu[142], T. Hsu[67], M. Hu[18a], Q. Hu[63a], S. Huang[65b], X. Huang[14,114c], Y. Huang[143], Y. Huang[102], Y. Huang[14], Z. Huang[103], Z. Hubacek[135], M. Huebner[25], F. Huegging[25], T. B. Huffman[129], C. A. Hugli[49], M. Huhtinen[37], S. K. Huiberts[17], R. Hulsken[106], N. Huseynov[12], J. Huston[109], J. Huth[62], R. Hyneman[147], G. Iacobucci[57], G. Iakovidis[30], L. Iconomidou-Fayard[67], J. P. Iddon[37], P. Iengo[73a,73b], R. Iguchi[157], Y. Iiyama[157], T. Iizawa[129], Y. Ikegami[85], N. Ilic[158], H. Imam[36a], M. Ince Lezki[57], T. Ingebretsen Carlson[48a,48b], J. M. Inglis[96], G. Introzzi[74a,74b], M. Iodice[78a], V. Ippolito[76a,76b], R. K. Irwin[94], M. Ishino[157], W. Islam[173], C. Issever[19,49], S. Istin[22a,aj], H. Ito[171], R. Iuppa[79a,79b], A. Ivina[172], J. M. Izen[46], V. Izzo[73a], P. Jacka[134], P. Jackson[1], C. S. Jagfeld[111], G. Jain[159a], P. Jain[49], K. Jakobs[55], T. Jakoubek[172], J. Jamieson[60], W. Jang[157], M. Javurkova[105], L. Jeanty[126], J. Jejelava[153a,aa], P. Jenni[55,g], C. E. Jessiman[35], C. Jia[63b], J. Jia[149], X. Jia[62], X. Jia[14,114c], Z. Jia[114a], C. Jiang[53], S. Jiggins[49], J. Jimenez Pena[13], S. Jin[114a], A. Jinaru[28b], O. Jinnouchi[141], P. Johansson[143], K. A. Johns[7], J. W. Johnson[139], D. M. Jones[150], E. Jones[49], P. Jones[33], R. W. L. Jones[93], T. J. Jones[94], H. L. Joos[37,56], R. Joshi[122], J. Jovicevic[16], X. Ju[18a], J. J. Junggeburth[105], T. Junkermann[64a], A. Juste Rozas[13,t], M. K. Juzek[88], S. Kabana[140e], A. Kaczmarska[88], M. Kado[112], H. Kagan[122], M. Kagan[147], A. Kahn[131], C. Kahra[102], T. Kaji[157], E. Kajomovitz[154], N. Kakati[172], I. Kalaitzidou[55], C. W. Kalderon[30], N. J. Kang[139], D. Kar[34g], K. Karava[129], M. J. Kareem[159b], E. Karentzos[55], O. Karkout[117], S. N. Karpov[39], Z. M. Karpova[39], V. Kartvelishvili[93], A. N. Karyukhin[38], E. Kasimi[156], J. Katzy[49], S. Kaur[35], K. Kawade[144], M. P. Kawale[123], C. Kawamoto[89], T. Kawamoto[63a], E. F. Kay[37], F. I. Kaya[161], S. Kazakos[109], V. F. Kazanin[38], Y. Ke[149], J. M. Keaveney[34a], R. Keeler[168], G. V. Kehris[62], J. S. Keller[35], A. S. Kelly[98], J. J. Kempster[150], P. D. Kennedy[102], O. Kepka[134], B. P. Kerridge[137], S. Kersten[174], B. P. Kerševan[95], L. Keszeghova[29a], S. Ketabchi Haghighat[158], R. A. Khan[132], A. Khanov[124], A. G. Kharlamov[38], T. Kharlamova[38], E. E. Khoda[142], M. Kholodenko[38], T. J. Khoo[19], G. Khoriauli[169], J. Khubua[153b,*], Y. A. R. Khwaira[130], B. Kibirige[34g], D. W. Kim[48a,48b], Y. K. Kim[40], N. Kimura[98], M. K. Kingston[56], A. Kirchhoff[56], C. Kirfel[25], F. Kirfel[25], J. Kirk[137], A. E. Kiryunin[112], C. Kitsaki[10], O. Kivernyk[25], M. Klassen[161], C. Klein[35], L. Klein[169], M. H. Klein[45], S. B. Klein[57], U. Klein[94], P. Klimek[37], A. Klimentov[30], T. Klioutchnikova[37], P. Kluit[117], S. Kluth[112], E. Kneringer[80], T. M. Knight[158], A. Knue[50], R. Kobayashi[89], D. Kobylianskii[172], S. F. Koch[129], M. Kocian[147], P. Kodyš[136], D. M. Koeck[126], P. T. Koenig[25], T. Koffas[35], O. Kolay[51], I. Koletsou[4], T. Komarek[125], K. Köneke[55], A. X. Y. Kong[1], T. Kono[121], N. Konstantinidis[98], P. Kontaxakis[57], B. Konya[100], R. Kopeliansky[42], S. Koperny[87a], K. Korcyl[88], K. Kordas[156,e], A. Korn[98], S. Korn[56], I. Korolkov[13], N. Korotkova[38], B. Kortman[117],

O. Kortner[112], S. Kortner[112], W. H. Kostecka[118], V. V. Kostyukhin[145], A. Kotsokechagia[138], A. Kotwal[52], A. Koulouris[37], A. Kourkoumeli-Charalampidi[74a,74b], C. Kourkoumelis[9], E. Kourlitis[112], O. Kovanda[126], R. Kowalewski[168], W. Kozanecki[138], A. S. Kozhin[38], V. A. Kramarenko[38], G. Kramberger[95], P. Kramer[102], M. W. Krasny[130], A. Krasznahorkay[37], A. C. Kraus[118], J. W. Kraus[174], J. A. Kremer[49], T. Kresse[51], J. Kretzschmar[94], K. Kreul[19], P. Krieger[158], S. Krishnamurthy[105], M. Krivos[136], K. Krizka[21], K. Kroeninger[50], H. Kroha[112], J. Kroll[134], J. Kroll[131], K. S. Krowpman[109], U. Kruchonak[39], H. Krüger[25], N. Krumnack[82], M. C. Kruse[52], O. Kuchinskaia[38], S. Kuday[3a], S. Kuehn[37], R. Kuesters[55], T. Kuhl[49], V. Kukhtin[39], Y. Kulchitsky[38,a], S. Kuleshov[140b,140d], M. Kumar[34g], N. Kumari[49], P. Kumari[159b], A. Kupco[134], T. Kupfer[50], A. Kupich[38], O. Kuprash[55], H. Kurashige[86], L. L. Kurchaninov[159a], O. Kurdysh[67], Y. A. Kurochkin[38], A. Kurova[38], M. Kuze[141], A. K. Kvam[105], J. Kvita[125], T. Kwan[106], N. G. Kyriacou[108], L. A. O. Laatu[104], C. Lacasta[166], F. Lacava[76a,76b], H. Lacker[19], D. Lacour[130], N. N. Lad[98], E. Ladygin[39], A. Lafarge[41], B. Laforge[130], T. Lagouri[175], F. Z. Lahbabi[36a], S. Lai[56], J. E. Lambert[168], S. Lammers[69], W. Lampl[7], C. Lampoudis[156,e], G. Lamprinoudis[102], A. N. Lancaster[118], E. Lançon[30], U. Landgraf[55], M. P. J. Landon[96], V. S. Lang[55], O. K. B. Langrekken[128], A. J. Lankford[162], F. Lanni[37], K. Lantzsch[25], A. Lanza[74a], J. F. Laporte[138], T. Lari[72a], F. Lasagni Manghi[24b], M. Lassnig[37], V. Latonova[134], A. Laudrain[102], A. Laurier[154], S. D. Lawlor[143], Z. Lawrence[103], R. Lazaridou[170], M. Lazzaroni[72a,72b], B. Le[103], E. M. Le Boulicaut[52], L. T. Le Pottier[18a], B. Leban[24a,24b], A. Lebedev[82], M. LeBlanc[103], F. Ledroit-Guillon[61], S. C. Lee[152], S. Lee[48a,48b], T. F. Lee[94], L. L. Leeuw[34c], H. P. Lefebvre[97], M. Lefebvre[168], C. Leggett[18a], G. Lehmann Miotto[37], M. Leigh[57], W. A. Leight[105], W. Leinonen[116], A. Leisos[156,s], M. A. L. Leite[84c], C. E. Leitgeb[19], R. Leitner[136], K. J. C. Leney[45], T. Lenz[25], S. Leone[75a], C. Leonidopoulos[53], A. Leopold[148], C. Leroy[110], R. Les[109], C. G. Lester[33], M. Levchenko[38], J. Levêque[4], L. J. Levinson[172], G. Levrini[24a,24b], M. P. Lewicki[88], C. Lewis[142], D. J. Lewis[4], A. Li[5], B. Li[63b], C. Li[63a], C.-Q. Li[112], H. Li[63a], H. Li[63b], H. Li[114a], H. Li[15], H. Li[63b], J. Li[63c], K. Li[142], L. Li[63c], M. Li[14,114c], S. Li[14,114c], S. Li[63c,63d,d], T. Li[5], X. Li[106], Z. Li[129], Z. Li[157], Z. Li[14,114c], S. Liang[14,114c], Z. Liang[14], M. Liberatore[138], B. Liberti[77a], K. Lie[65c], J. Lieber Marin[84e], H. Lien[69], H. Lin[108], K. Lin[109], R. E. Lindley[7], J. H. Lindon[2], J. Ling[62], E. Lipeles[131], A. Lipniacka[17], A. Lister[167], J. D. Little[69], B. Liu[14], B. X. Liu[114b], D. Liu[63c,63d], E. H. L. Liu[21], J. B. Liu[63a], J. K. K. Liu[33], K. Liu[63d], K. Liu[63c,63d], M. Liu[63a], M. Y. Liu[63a], P. Liu[14], Q. Liu[63c,63d,142], X. Liu[63a], X. Liu[63b], Y. Liu[114b,114c], Y. L. Liu[63b], Y. W. Liu[63a], J. Llorente Merino[146], S. L. Lloyd[96], E. M. Lobodzinska[49], P. Loch[7], T. Lohse[19], K. Lohwasser[143], E. Loiacono[49], M. Lokajicek[134,*], J. D. Lomas[21], J. D. Long[165], I. Longarini[162], R. Longo[165], I. Lopez Paz[68], A. Lopez Solis[49], N. Lorenzo Martinez[4], A. M. Lory[111], M. Losada[119a], G. Löschcke Centeno[150], O. Loseva[38], X. Lou[48a,48b], X. Lou[14,114c], A. Lounis[67], P. A. Love[93], G. Lu[14,114c], M. Lu[67], S. Lu[131], Y. J. Lu[66], H. J. Lubatti[142], C. Luci[76a,76b], F. L. Lucio Alves[114a], F. Luehring[69], I. Luise[149], O. Lukianchuk[67], O. Lundberg[148], B. Lund-Jensen[148,*], N. A. Luongo[6], M. S. Lutz[37], A. B. Lux[26], D. Lynn[30], R. Lysak[134], E. Lytken[100], V. Lyubushkin[39], T. Lyubushkina[39], M. M. Lyukova[149], M. Firdaus M. Soberi[53], H. Ma[30], K. Ma[63a], L. L. Ma[63b], W. Ma[63a], Y. Ma[124], J. C. MacDonald[102], P. C. Machado De Abreu Farias[84e], R. Madar[41], T. Madula[98], J. Maeda[86], T. Maeno[30], H. Maguire[143], V. Maiboroda[138], A. Maio[133a,133b,133d], K. Maj[87a], O. Majersky[49], S. Majewski[126], N. Makovec[67], V. Maksimovic[16], B. Malaescu[130], Pa. Malecki[88], V. P. Maleev[38], F. Malek[61,n], M. Mali[95], D. Malito[97], U. Mallik[81,*], S. Maltezos[10], S. Malyukov[39], J. Mamuzic[13], G. Mancini[54], M. N. Mancini[27], G. Manco[74a,74b], J. P. Mandalia[96], S. S. Mandarry[150], I. Mandić[95], L. Manhaes de Andrade Filho[84a], I. M. Maniatis[172], J. Manjarres Ramos[91], D. C. Mankad[172], A. Mann[111], S. Manzoni[37], L. Mao[63c], X. Mapekula[34c], A. Marantis[156,s], G. Marchiori[5], M. Marcisovsky[134], C. Marcon[72a], M. Marinescu[21], S. Marium[49], M. Marjanovic[123], A. Markhoos[55], M. Markovitch[67], E. J. Marshall[93], Z. Marshall[18a], S. Marti-Garcia[166], J. Martin[98], T. A. Martin[137], V. J. Martin[53], B. Martin dit Latour[17], L. Martinelli[76a,76b], M. Martinez[13,t], P. Martinez Agullo[166], V. I. Martinez Outschoorn[105], P. Martinez Suarez[13], S. Martin-Haugh[137], G. Martinovicova[136], V. S. Martoiu[28b], A. C. Martyniuk[98], A. Marzin[37], D. Mascione[79a,79b], L. Masetti[102], T. Mashimo[157], J. Masik[103], A. L. Maslennikov[38], P. Massarotti[73a,73b], P. Mastrandrea[75a,75b], A. Mastroberardino[44a,44b], T. Masubuchi[157], T. Mathisen[164], J. Matousek[136], N. Matsuzawa[157], J. Maurer[28b], A. J. Maury[67], B. Maček[95], D. A. Maximov[38], A. E. May[103], R. Mazini[152], I. Maznas[118], M. Mazza[109], S. M. Mazza[139], E. Mazzeo[72a,72b], C. Mc Ginn[30], J. P. Mc Gowan[168], S. P. Mc Kee[108], C. C. McCracken[167], E. F. McDonald[107], A. E. McDougall[117], J. A. Mcfayden[150], R. P. McGovern[131], R. P. Mckenzie[34g], T. C. Mclachlan[49], D. J. Mclaughlin[98], S. J. McMahon[137], C. M. Mcpartland[94], R. A. McPherson[168,x],

S. Mehlhase[111], A. Mehta[94], D. Melini[166], B. R. Mellado Garcia[34g], A. H. Melo[56], F. Meloni[49], A. M. Mendes Jacques Da Costa[103], H. Y. Meng[158], L. Meng[93], S. Menke[112], M. Mentink[37], E. Meoni[44a,44b], G. Mercado[118], S. Merianos[156], C. Merlassino[70a,70c], L. Merola[73a,73b], C. Meroni[72a,72b], J. Metcalfe[6], A. S. Mete[6], E. Meuser[102], C. Meyer[69], J.-P. Meyer[138], R. P. Middleton[137], L. Mijović[53], G. Mikenberg[172], M. Mikestikova[134], M. Mikuž[95], H. Mildner[102], A. Milic[37], D. W. Miller[40], E. H. Miller[147], L. S. Miller[35], A. Milov[172], D. A. Milstead[48a,48b], T. Min[114a], A. A. Minaenko[38], I. A. Minashvili[153b], L. Mince[60], A. I. Mincer[120], B. Mindur[87a], M. Mineev[39], Y. Mino[89], L. M. Mir[13], M. Miralles Lopez[60], M. Mironova[18a], A. Mishima[157], M. C. Missio[116], A. Mitra[170], V. A. Mitsou[166], Y. Mitsumori[113], O. Miu[158], P. S. Miyagawa[96], T. Mkrtchyan[64a], M. Mlinarevic[98], T. Mlinarevic[98], M. Mlynarikova[37], S. Mobius[20], P. Mogg[111], M. H. Mohamed Farook[115], A. F. Mohammed[14,114c], S. Mohapatra[42], G. Mokgatitswane[34g], L. Moleri[172], B. Mondal[145], S. Mondal[135], K. Mönig[49], E. Monnier[104], L. Monsonis Romero[166], J. Montejo Berlingen[13], M. Montella[122], F. Montereali[78a,78b], F. Monticelli[92], S. Monzani[70a,70c], N. Morange[67], A. L. Moreira De Carvalho[49], M. Moreno Llácer[166], C. Moreno Martinez[57], P. Morettini[58b], S. Morgenstern[37], M. Morii[62], M. Morinaga[157], F. Morodei[76a,76b], L. Morvaj[37], P. Moschovakos[37], B. Moser[37], M. Mosidze[153b], T. Moskalets[45], P. Moskvitina[116], J. Moss[32,k], P. Moszkowicz[87a], A. Moussa[36d], E. J. W. Moyse[105], O. Mtintsilana[34g], S. Muanza[104], J. Mueller[132], D. Muenstermann[93], R. Müller[20], G. A. Mullier[164], A. J. Mullin[33], J. J. Mullin[131], D. P. Mungo[158], D. Munoz Perez[166], F. J. Munoz Sanchez[103], M. Murin[103], W. J. Murray[137,170], M. Muškinja[95], C. Mwewa[30], A. G. Myagkov[38,a], A. J. Myers[8], G. Myers[108], M. Myska[135], B. P. Nachman[18a], O. Nackenhorst[50], K. Nagai[129], K. Nagano[85], J. L. Nagle[30,ah], E. Nagy[104], A. M. Nairz[37], Y. Nakahama[85], K. Nakamura[85], K. Nakkalil[5], H. Nanjo[127], E. A. Narayanan[115], I. Naryshkin[38], L. Nasella[72a,72b], M. Naseri[35], S. Nasri[119b], C. Nass[25], G. Navarro[23a], J. Navarro-Gonzalez[166], R. Nayak[155], A. Nayaz[19], P. Y. Nechaeva[38], S. Nechaeva[24a,24b], F. Nechansky[49], L. Nedic[129], T. J. Neep[21], A. Negri[74a,74b], M. Negrini[24b], C. Nellist[117], C. Nelson[106], K. Nelson[108], S. Nemecek[134], M. Nessi[37,h], M. S. Neubauer[165], F. Neuhaus[102], J. Neundorf[49], P. R. Newman[21], C. W. Ng[132], Y. W. Y. Ng[49], B. Ngair[119a], H. D. N. Nguyen[110], R. B. Nickerson[129], R. Nicolaidou[138], J. Nielsen[139], M. Niemeyer[56], J. Niermann[56], N. Nikiforou[37], V. Nikolaenko[38,a], I. Nikolic-Audit[130], K. Nikolopoulos[21], P. Nilsson[30], I. Ninca[49], G. Ninio[155], A. Nisati[76a], N. Nishu[2], R. Nisius[112], J.-E. Nitschke[51], E. K. Nkadimeng[34g], T. Nobe[157], T. Nommensen[151], M. B. Norfolk[143], B. J. Norman[35], M. Noury[36a], J. Novak[95], T. Novak[95], L. Novotny[135], R. Novotny[115], L. Nozka[125], K. Ntekas[162], N. M. J. Nunes De Moura Junior[84b], J. Ocariz[130], A. Ochi[86], I. Ochoa[133a], S. Oerdek[49,u], J. T. Offermann[40], A. Ogrodnik[136], A. Oh[103], C. C. Ohm[148], H. Oide[85], R. Oishi[157], M. L. Ojeda[49], Y. Okumura[157], L. F. Oleiro Seabra[133a], I. Oleksiyuk[57], S. A. Olivares Pino[140d], G. Oliveira Correa[13], D. Oliveira Damazio[30], D. Oliveira Goncalves[84a], J. L. Oliver[162], Ö. O. Öncel[55], A. P. O'Neill[20], A. Onofre[133a,133e], P. U. E. Onyisi[11], M. J. Oreglia[40], G. E. Orellana[92], D. Orestano[78a,78b], N. Orlando[13], R. S. Orr[158], L. M. Osojnak[131], R. Ospanov[63a], G. Otero y Garzon[31], H. Otono[90], P. S. Ott[64a], G. J. Ottino[18a], M. Ouchrif[36d], F. Ould-Saada[128], T. Ovsiannikova[142], M. Owen[60], R. E. Owen[137], V. E. Ozcan[22a], F. Ozturk[88], N. Ozturk[8], S. Ozturk[83], H. A. Pacey[129], A. Pacheco Pages[13], C. Padilla Aranda[13], G. Padovano[76a,76b], S. Pagan Griso[18a], G. Palacino[69], A. Palazzo[71a,71b], J. Pampel[25], J. Pan[175], T. Pan[65a], D. K. Panchal[11], C. E. Pandini[117], J. G. Panduro Vazquez[137], H. D. Pandya[1], H. Pang[15], P. Pani[49], G. Panizzo[70a,70c], L. Panwar[130], L. Paolozzi[57], S. Parajuli[165], A. Paramonov[6], C. Paraskevopoulos[54], D. Paredes Hernandez[65b], A. Pareti[74a,74b], K. R. Park[42], T. H. Park[158], M. A. Parker[33], F. Parodi[58a,58b], E. W. Parrish[118], V. A. Parrish[53], J. A. Parsons[42], U. Parzefall[55], B. Pascual Dias[110], L. Pascual Dominguez[101], E. Pasqualucci[76a], S. Passaggio[58b], F. Pastore[97], P. Patel[88], U. M. Patel[52], J. R. Pater[103], T. Pauly[37], C. I. Pazos[161], J. Pearkes[147], M. Pedersen[128], R. Pedro[133a], S. V. Peleganchuk[38], O. Penc[37], E. A. Pender[53], G. D. Penn[175], K. E. Penski[111], M. Penzin[38], B. S. Peralva[84d], A. P. Pereira Peixoto[142], L. Pereira Sanchez[147], D. V. Perepelitsa[30,ah], G. Perera[105], E. Perez Codina[159a], M. Perganti[10], H. Pernegger[37], S. Perrella[76a,76b], O. Perrin[41], K. Peters[49], R. F. Y. Peters[103], B. A. Petersen[37], T. C. Petersen[43], E. Petit[104], V. Petousis[135], C. Petridou[156,e], T. Petru[136], A. Petrukhin[145], M. Pettee[18a], A. Petukhov[38], K. Petukhova[136], R. Pezoa[140f], L. Pezzotti[37], G. Pezzullo[175], T. M. Pham[173], T. Pham[107], P. W. Phillips[137], G. Piacquadio[149], E. Pianori[18a], F. Piazza[126], R. Piegaia[31], D. Pietreanu[28b], A. D. Pilkington[103], M. Pinamonti[70a,70c], J. L. Pinfold[2], B. C. Pinheiro Pereira[133a], A. E. Pinto Pinoargote[138], L. Pintucci[70a,70c], K. M. Piper[150], A. Pirttikoski[57], D. A. Pizzi[35], L. Pizzimento[65b], A. Pizzini[117], M.-A. Pleier[30], V. Pleskot[136], E. Plotnikova[39], G. Poddar[96], R. Poettgen[100], L. Poggioli[130], I. Pokharel[56], S. Polacek[136], G. Polesello[74a], A. Poley[146,159a], A. Polini[24b],

C. S. Pollard[170], Z. B. Pollock[122], E. Pompa Pacchi[76a,76b], N. I. Pond[98], D. Ponomarenko[116], L. Pontecorvo[37], S. Popa[28a], G. A. Popeneciu[28d], A. Poreba[37], D. M. Portillo Quintero[159a], S. Pospisil[135], M. A. Postill[143], P. Postolache[28c], K. Potamianos[170], P. A. Potepa[87a], I. N. Potrap[39], C. J. Potter[33], H. Potti[151], J. Poveda[166], M. E. Pozo Astigarraga[37], A. Prades Ibanez[166], J. Pretel[55], D. Price[103], M. Primavera[71a], M. A. Principe Martin[101], R. Privara[125], T. Procter[60], M. L. Proffitt[142], N. Proklova[131], K. Prokofiev[65c], G. Proto[112], J. Proudfoot[6], M. Przybycien[87a], W. W. Przygoda[87b], A. Psallidas[47], J. E. Puddefoot[143], D. Pudzha[38], D. Pyatiizbyantseva[38], J. Qian[108], D. Qichen[103], Y. Qin[13], T. Qiu[53], A. Quadt[56], M. Queitsch-Maitland[103], G. Quetant[57], R. P. Quinn[167], G. Rabanal Bolanos[62], D. Rafanoharana[55], F. Raffaeli[77a,77b], F. Ragusa[72a,72b], J. L. Rainbolt[40], J. A. Raine[57], S. Rajagopalan[30], E. Ramakoti[38], I. A. Ramirez-Berend[35], K. Ran[49,114c], N. P. Rapheeha[34g], H. Rasheed[28b], V. Raskina[130], D. F. Rassloff[64a], A. Rastogi[18a], S. Rave[102], S. Ravera[58a,58b], B. Ravina[56], I. Ravinovich[172], M. Raymond[37], A. L. Read[128], N. P. Readioff[143], D. M. Rebuzzi[74a,74b], G. Redlinger[30], A. S. Reed[112], K. Reeves[27], J. A. Reidelsturz[174], D. Reikher[155], A. Rej[50], C. Rembser[37], M. Renda[28b], M. B. Rendel[112], F. Renner[49], A. G. Rennie[162], A. L. Rescia[49], S. Resconi[72a], M. Ressegotti[58a,58b], S. Rettie[37], J. G. Reyes Rivera[109], E. Reynolds[18a], O. L. Rezanova[38], P. Reznicek[136], H. Riani[36d], N. Ribaric[93], E. Ricci[79a,79b], R. Richter[112], S. Richter[48a,48b], E. Richter-Was[87b], M. Ridel[130], S. Ridouani[36d], P. Rieck[120], P. Riedler[37], E. M. Riefel[48a,48b], J. O. Rieger[117], M. Rijssenbeek[149], M. Rimoldi[37], L. Rinaldi[24a,24b], P. Rincke[56,164], T. T. Rinn[30], M. P. Rinnagel[111], G. Ripellino[164], I. Riu[13], J. C. Rivera Vergara[168], F. Rizatdinova[124], E. Rizvi[96], B. R. Roberts[18a], S. H. Robertson[106,x], D. Robinson[33], C. M. Robles Gajardo[140f], M. Robles Manzano[102], A. Robson[60], A. Rocchi[77a,77b], C. Roda[75a,75b], S. Rodriguez Bosca[37], Y. Rodriguez Garcia[23a], A. Rodriguez Rodriguez[55], A. M. Rodríguez Vera[118], S. Roe[37], J. T. Roemer[162], A. R. Roepe-Gier[139], J. Roggel[174], O. Røhne[128], R. A. Rojas[105], C. P. A. Roland[130], J. Roloff[30], A. Romaniouk[38], E. Romano[74a,74b], M. Romano[24b], A. C. Romero Hernandez[165], N. Rompotis[94], L. Roos[130], S. Rosati[76a], B. J. Rosser[40], E. Rossi[129], E. Rossi[73a,73b], L. P. Rossi[62], L. Rossini[55], R. Rosten[122], M. Rotaru[28b], B. Rottler[55], C. Rougier[91], D. Rousseau[67], D. Rousso[49], A. Roy[165], S. Roy-Garand[158], A. Rozanov[104], Z. M. A. Rozario[60], Y. Rozen[154], A. Rubio Jimenez[166], A. J. Ruby[94], V. H. Ruelas Rivera[19], T. A. Ruggeri[1], A. Ruggiero[129], A. Ruiz-Martinez[166], A. Rummler[37], Z. Rurikova[55], N. A. Rusakovich[39], H. L. Russell[168], G. Russo[76a,76b], J. P. Rutherfoord[7], S. Rutherford Colmenares[33], M. Rybar[136], E. B. Rye[128], A. Ryzhov[45], J. A. Sabater Iglesias[57], P. Sabatini[166], H. F.-W. Sadrozinski[139], F. Safai Tehrani[76a], B. Safarzadeh Samani[137], S. Saha[1], M. Sahinsoy[112], A. Saibel[166], M. Saimpert[138], M. Saito[157], T. Saito[157], A. Sala[72a,72b], D. Salamani[37], A. Salnikov[147], J. Salt[166], A. Salvador Salas[155], D. Salvatore[44a,44b], F. Salvatore[150], A. Salzburger[37], D. Sammel[55], E. Sampson[93], D. Sampsonidis[156,e], D. Sampsonidou[126], J. Sánchez[166], V. Sanchez Sebastian[166], H. Sandaker[128], C. O. Sander[49], J. A. Sandesara[105], M. Sandhoff[174], C. Sandoval[23b], L. Sanfilippo[64a], D. P. C. Sankey[137], T. Sano[89], A. Sansoni[54], L. Santi[37,76b], C. Santoni[41], H. Santos[133a,133b], A. Santra[172], E. Sanzani[24a,24b], K. A. Saoucha[163], J. G. Saraiva[133a,133d], J. Sardain[7], O. Sasaki[85], K. Sato[160], C. Sauer[64b], E. Sauvan[4], P. Savard[158,af], R. Sawada[157], C. Sawyer[137], L. Sawyer[99], C. Sbarra[24b], A. Sbrizzi[24a,24b], T. Scanlon[98], J. Schaarschmidt[142], U. Schäfer[102], A. C. Schaffer[45,67], D. Schaile[111], R. D. Schamberger[149], C. Scharf[19], M. M. Schefer[20], V. A. Schegelsky[38], D. Scheirich[136], M. Schernau[162], C. Scheulen[56], C. Schiavi[58a,58b], M. Schioppa[44a,44b], B. Schlag[147], K. E. Schleicher[55], S. Schlenker[37], J. Schmeing[174], M. A. Schmidt[174], K. Schmieden[102], C. Schmitt[102], N. Schmitt[102], S. Schmitt[49], L. Schoeffel[138], A. Schoening[64b], P. G. Scholer[35], E. Schopf[129], M. Schott[25], J. Schovancova[37], S. Schramm[57], T. Schroer[57], H.-C. Schultz-Coulon[64a], M. Schumacher[55], B. A. Schumm[139], Ph. Schune[138], A. J. Schuy[142], H. R. Schwartz[139], A. Schwartzman[147], T. A. Schwarz[108], Ph. Schwemling[138], R. Schwienhorst[109], F. G. Sciacca[20], A. Sciandra[30], G. Sciolla[27], F. Scuri[75a], C. D. Sebastiani[94], K. Sedlaczek[118], S. C. Seidel[115], A. Seiden[139], B. D. Seidlitz[42], C. Seitz[49], J. M. Seixas[84b], G. Sekhniaidze[73a], L. Selem[61], N. Semprini-Cesari[24a,24b], D. Sengupta[57], V. Senthilkumar[166], L. Serin[67], M. Sessa[77a,77b], H. Severini[123], F. Sforza[58a,58b], A. Sfyrla[57], Q. Sha[14], E. Shabalina[56], A. H. Shah[33], R. Shaheen[148], J. D. Shahinian[131], D. Shaked Renous[172], L. Y. Shan[14], M. Shapiro[18a], A. Sharma[37], A. S. Sharma[167], P. Sharma[81], P. B. Shatalov[38], K. Shaw[150], S. M. Shaw[103], Q. Shen[5,63c], D. J. Sheppard[146], P. Sherwood[98], L. Shi[98], X. Shi[14], C. O. Shimmin[175], J. D. Shinner[97], I. P. J. Shipsey[129,*], S. Shirabe[90], M. Shiyakova[39,v], M. J. Shochet[40], J. Shojaii[107], D. R. Shope[128], B. Shrestha[123], S. Shrestha[122,ai], M. J. Shroff[168], P. Sicho[134], A. M. Sickles[165], E. Sideras Haddad[34g], A. C. Sidley[117], A. Sidoti[24b], F. Siegert[51], Dj. Sijacki[16], F. Sili[92], J. M. Silva[53], I. Silva Ferreira[84b], M. V. Silva Oliveira[30],

S. B. Silverstein[48a], S. Simion[67], R. Simoniello[37], E. L. Simpson[103], H. Simpson[150], L. R. Simpson[108], N. D. Simpson[100], S. Simsek[83], S. Sindhu[56], P. Sinervo[158], S. Singh[158], S. Sinha[49], S. Sinha[103], M. Sioli[24a,24b], I. Siral[37], E. Sitnikova[49], J. Sjölin[48a,48b], A. Skaf[56], E. Skorda[21], P. Skubic[123], M. Slawinska[88], V. Smakhtin[172], B. H. Smart[137], S. Yu. Smirnov[38], Y. Smirnov[38], L. N. Smirnova[38,a], O. Smirnova[100], A. C. Smith[42], D. R. Smith[162], E. A. Smith[40], H. A. Smith[129], J. L. Smith[103], R. Smith[147], M. Smizanska[93], K. Smolek[135], A. A. Snesarev[38], S. R. Snider[158], H. L. Snoek[117], S. Snyder[30], R. Sobie[168,x], A. Soffer[155], C. A. Solans Sanchez[37], E. Yu. Soldatov[38], U. Soldevila[166], A. A. Solodkov[38], S. Solomon[27], A. Soloshenko[39], K. Solovieva[55], O. V. Solovyanov[41], P. Sommer[37], A. Sonay[13], W. Y. Song[159b], A. Sopczak[135], A. L. Sopio[98], F. Sopkova[29b], J. D. Sorenson[115], I. R. Sotarriva Alvarez[141], V. Sothilingam[64a], O. J. Soto Sandoval[140b,140c], S. Sottocornola[69], R. Soualah[163], Z. Soumaimi[36e], D. South[49], N. Soybelman[172], S. Spagnolo[71a,71b], M. Spalla[112], D. Sperlich[55], G. Spigo[37], S. Spinali[93], D. P. Spiteri[60], M. Spousta[136], E. J. Staats[35], R. Stamen[64a], A. Stampekis[21], M. Standke[25], E. Stanecka[88], W. Stanek-Maslouska[49], M. V. Stange[51], B. Stanislaus[18a], M. M. Stanitzki[49], B. Stapf[49], E. A. Starchenko[38], G. H. Stark[139], J. Stark[91], P. Staroba[134], P. Starovoitov[64a], S. Stärz[106], R. Staszewski[88], G. Stavropoulos[47], J. Steentoft[164], P. Steinberg[30], B. Stelzer[146,159a], H. J. Stelzer[132], O. Stelzer-Chilton[159a], H. Stenzel[59], T. J. Stevenson[150], G. A. Stewart[37], J. R. Stewart[124], M. C. Stockton[37], G. Stoicea[28b], M. Stolarski[133a], S. Stonjek[112], A. Straessner[51], J. Strandberg[148], S. Strandberg[48a,48b], M. Stratmann[174], M. Strauss[123], T. Strebler[104], P. Strizenec[29b], R. Ströhmer[169], D. M. Strom[126], R. Stroynowski[45], A. Strubig[48a,48b], S. A. Stucci[30], B. Stugu[17], J. Stupak[123], N. A. Styles[49], D. Su[147], S. Su[63a], W. Su[63d], X. Su[63a], D. Suchy[29a], K. Sugizaki[157], V. V. Sulin[38], M. J. Sullivan[94], D. M. S. Sultan[129], L. Sultanaliyeva[38], S. Sultansoy[3b], T. Sumida[89], S. Sun[173], O. Sunneborn Gudnadottir[164], N. Sur[104], M. R. Sutton[150], H. Suzuki[160], M. Svatos[134], M. Swiatlowski[159a], T. Swirski[169], I. Sykora[29a], M. Sykora[136], T. Sykora[136], D. Ta[102], K. Tackmann[49,u], A. Taffard[162], R. Tafirout[159a], J. S. Tafoya Vargas[67], Y. Takubo[85], M. Talby[104], A. A. Talyshev[38], K. C. Tam[65b], N. M. Tamir[155], A. Tanaka[157], J. Tanaka[157], R. Tanaka[67], M. Tanasini[149], Z. Tao[167], S. Tapia Araya[140f], S. Tapprogge[102], A. Tarek Abouelfadl Mohamed[109], S. Tarem[154], K. Tariq[14], G. Tarna[28b], G. F. Tartarelli[72a], M. J. Tartarin[91], P. Tas[136], M. Tasevsky[134], E. Tassi[44a,44b], A. C. Tate[165], G. Tateno[157], Y. Tayalati[36e,w], G. N. Taylor[107], W. Taylor[159b], R. Teixeira De Lima[147], P. Teixeira-Dias[97], J. J. Teoh[158], K. Terashi[157], J. Terron[101], S. Terzo[13], M. Testa[54], R. J. Teuscher[158,x], A. Thaler[80], O. Theiner[57], N. Themistokleous[53], T. Theveneaux-Pelzer[104], O. Thielmann[174], D. W. Thomas[97], J. P. Thomas[21], E. A. Thompson[18a], P. D. Thompson[21], E. Thomson[131], R. E. Thornberry[45], C. Tian[63a], Y. Tian[56], V. Tikhomirov[38,a], Yu. A. Tikhonov[38], S. Timoshenko[38], D. Timoshyn[136], E. X. L. Ting[1], P. Tipton[175], A. Tishelman-Charny[30], S. H. Tlou[34g], K. Todome[141], S. Todorova-Nova[136], S. Todt[51], L. Toffolin[70a,70c], M. Togawa[85], J. Tojo[90], S. Tokár[29a], K. Tokushuku[85], O. Toldaiev[69], R. Tombs[33], M. Tomoto[85,113], L. Tompkins[147,m], K. W. Topolnicki[87b], E. Torrence[126], H. Torres[91], E. Torró Pastor[166], M. Toscani[31], C. Tosciri[40], M. Tost[11], D. R. Tovey[143], I. S. Trandafir[28b], T. Trefzger[169], A. Tricoli[30], I. M. Trigger[159a], S. Trincaz-Duvoid[130], D. A. Trischuk[27], B. Trocmé[61], L. Truong[34c], M. Trzebinski[88], A. Trzupek[88], F. Tsai[149], M. Tsai[108], A. Tsiamis[156,e], P. V. Tsiareshka[38], S. Tsigaridas[159a], A. Tsirigotis[156,s], V. Tsiskaridze[158], E. G. Tskhadadze[153a], M. Tsopoulou[156], Y. Tsujikawa[89], I. I. Tsukerman[38], V. Tsulaia[18a], S. Tsuno[85], K. Tsuri[121], D. Tsybychev[149], Y. Tu[65b], A. Tudorache[28b], V. Tudorache[28b], A. N. Tuna[62], S. Turchikhin[58a,58b], I. Turk Cakir[3a], R. Turra[72a], T. Turtuvshin[39,y], P. M. Tuts[42], S. Tzamarias[156,e], E. Tzovara[102], F. Ukegawa[160], P. A. Ulloa Poblete[140b,140c], E. N. Umaka[30], G. Unal[37], A. Undrus[30], G. Unel[162], J. Urban[29b], P. Urrejola[140a], G. Usai[8], R. Ushioda[141], M. Usman[110], Z. Uysal[83], V. Vacek[135], B. Vachon[106], T. Vafeiadis[37], A. Vaitkus[98], C. Valderanis[111], E. Valdes Santurio[48a,48b], M. Valente[159a], S. Valentinetti[24a,24b], A. Valero[166], E. Valiente Moreno[166], A. Vallier[91], J. A. Valls Ferrer[166], D. R. Van Arneman[117], T. R. Van Daalen[142], A. Van Der Graaf[50], P. Van Gemmeren[6], M. Van Rijnbach[37], S. Van Stroud[98], I. Van Vulpen[117], P. Vana[136], M. Vanadia[77a,77b], W. Vandelli[37], E. R. Vandewall[124], D. Vannicola[155], L. Vannoli[54], R. Vari[76a], E. W. Varnes[7], C. Varni[18b], T. Varol[152], D. Varouchas[67], L. Varriale[166], K. E. Varvell[151], M. E. Vasile[28b], L. Vaslin[85], G. A. Vasquez[168], A. Vasyukov[39], L. M. Vaughan[124], R. Vavricka[102], T. Vazquez Schroeder[37], J. Veatch[32], V. Vecchio[103], M. J. Veen[105], I. Veliscek[30], L. M. Veloce[158], F. Veloso[133a,133c], S. Veneziano[76a], A. Ventura[71a,71b], S. Ventura Gonzalez[138], A. Verbytskyi[112], M. Verducci[75a,75b], C. Vergis[96], M. Verissimo De Araujo[84b], W. Verkerke[117], J. C. Vermeulen[117], C. Vernieri[147], M. Vessella[105], M. C. Vetterli[146,af], A. Vgenopoulos[156,e], N. Viaux Maira[140f], T. Vickey[143], O. E. Vickey Boeriu[143], G. H. A. Viehhauser[129], L. Vigani[64b],

M. Villa[24a,24b], M. Villaplana Perez[166], E. M. Villhauer[53], E. Vilucchi[54], M. G. Vincter[35], A. Visibile[117], C. Vittori[37], I. Vivarelli[24a,24b], E. Voevodina[112], F. Vogel[111], J. C. Voigt[51], P. Vokac[135], Yu. Volkotrub[87b], J. Von Ahnen[49], E. Von Toerne[25], B. Vormwald[37], V. Vorobel[136], K. Vorobev[38], M. Vos[166], K. Voss[145], M. Vozak[117], L. Vozdecky[123], N. Vranjes[16], M. Vranjes Milosavljevic[16], M. Vreeswijk[117], N. K. Vu[63c,63d], R. Vuillermet[37], O. Vujinovic[102], I. Vukotic[40], S. Wada[160], C. Wagner[105], J. M. Wagner[18a], W. Wagner[174], S. Wahdan[174], H. Wahlberg[92], M. Wakida[113], J. Walder[137], R. Walker[111], W. Walkowiak[145], A. Wall[131], E. J. Wallin[100], T. Wamorkar[6], A. Z. Wang[139], C. Wang[102], C. Wang[11], H. Wang[18a], J. Wang[65c], P. Wang[98], R. Wang[62], R. Wang[6], S. M. Wang[152], S. Wang[63b], S. Wang[14], T. Wang[63a], W. T. Wang[81], W. Wang[14], X. Wang[114a], X. Wang[165], X. Wang[63c], Y. Wang[63d], Y. Wang[114a], Z. Wang[108], Z. Wang[52,63c,63d], Z. Wang[108], A. Warburton[106], R. J. Ward[21], N. Warrack[60], S. Waterhouse[97], A. T. Watson[21], H. Watson[60], M. F. Watson[21], E. Watton[60,137], G. Watts[142], B. M. Waugh[98], J. M. Webb[55], C. Weber[30], H. A. Weber[19], M. S. Weber[20], S. M. Weber[64a], C. Wei[63a], Y. Wei[55], A. R. Weidberg[129], E. J. Weik[120], J. Weingarten[50], C. Weiser[55], C. J. Wells[49], T. Wenaus[30], B. Wendland[50], T. Wengler[37], N. S. Wenke[112], N. Wermes[25], M. Wessels[64a], A. M. Wharton[93], A. S. White[62], A. White[8], M. J. White[1], D. Whiteson[162], L. Wickremasinghe[127], W. Wiedenmann[173], M. Wielers[137], C. Wiglesworth[43], D. J. Wilbern[123], H. G. Wilkens[37], J. J. H. Wilkinson[33], D. M. Williams[42], H. H. Williams[131], S. Williams[33], S. Willocq[105], B. J. Wilson[103], P. J. Windischhofer[40], F. I. Winkel[31], F. Winklmeier[126], B. T. Winter[55], J. K. Winter[103], M. Wittgen[147], M. Wobisch[99], T. Wojtkowski[61], Z. Wolffs[117], J. Wollrath[162], M. W. Wolter[88], H. Wolters[133a,133c], M. C. Wong[139], E. L. Woodward[42], S. D. Worm[49], B. K. Wosiek[88], K. W. Woźniak[88], S. Wozniewski[56], K. Wraight[60], C. Wu[21], M. Wu[114b], M. Wu[116], S. L. Wu[173], X. Wu[57], Y. Wu[63a], Z. Wu[4], J. Wuerzinger[112,ad], T. R. Wyatt[103], B. M. Wynne[53], S. Xella[43], L. Xia[114a], M. Xia[15], J. Xiang[65c], M. Xie[63a], S. Xin[14,114c], A. Xiong[126], J. Xiong[18a], D. Xu[14], H. Xu[63a], L. Xu[63a], R. Xu[131], T. Xu[108], Y. Xu[15], Z. Xu[53], Z. Xu[114a], B. Yabsley[151], S. Yacoob[34a], Y. Yamaguchi[141], E. Yamashita[157], H. Yamauchi[160], T. Yamazaki[18a], Y. Yamazaki[86], J. Yan[63c], S. Yan[60], Z. Yan[105], H. J. Yang[63c,63d], H. T. Yang[63a], S. Yang[63a], T. Yang[65c], X. Yang[37], X. Yang[14], Y. Yang[45], Y. Yang[63a], Z. Yang[63a], W.-M. Yao[18a], H. Ye[114a], H. Ye[56], J. Ye[14], S. Ye[30], X. Ye[63a], Y. Yeh[98], I. Yeletskikh[39], B. Yeo[18b], M. R. Yexley[98], T. P. Yildirim[129], P. Yin[42], K. Yorita[171], S. Younas[28b], C. J. S. Young[37], C. Young[147], C. Yu[14,114c], Y. Yu[63a], J. Yuan[14,114c], M. Yuan[108], R. Yuan[63c,63d], L. Yue[98], M. Zaazoua[63a], B. Zabinski[88], E. Zaid[53], Z. K. Zak[88], T. Zakareishvili[166], N. Zakharchuk[35], S. Zambito[57], J. A. Zamora Saa[140b,140d], J. Zang[157], D. Zanzi[55], O. Zaplatilek[135], C. Zeitnitz[174], H. Zeng[14], J. C. Zeng[165], D. T. Zenger Jr.[27], O. Zenin[38], T. Ženiš[29a], S. Zenz[96], S. Zerradi[36a], D. Zerwas[67], M. Zhai[14,114c], D. F. Zhang[143], J. Zhang[63b], J. Zhang[6], K. Zhang[14,114c], L. Zhang[63a], L. Zhang[114a], P. Zhang[14,114c], R. Zhang[173], S. Zhang[108], S. Zhang[91], T. Zhang[157], X. Zhang[63c], X. Zhang[63b], Y. Zhang[63c], Y. Zhang[98], Y. Zhang[114a], Z. Zhang[18a], Z. Zhang[63b], Z. Zhang[67], H. Zhao[142], T. Zhao[63b], Y. Zhao[139], Z. Zhao[63a], Z. Zhao[63a], A. Zhemchugov[39], J. Zheng[114a], K. Zheng[165], X. Zheng[63a], Z. Zheng[147], D. Zhong[165], B. Zhou[108], H. Zhou[7], N. Zhou[63c], Y. Zhou[15], Y. Zhou[114a], Y. Zhou[7], C. G. Zhu[63b], J. Zhu[108], X. Zhu[63d], Y. Zhu[63c], Y. Zhu[63a], X. Zhuang[14], K. Zhukov[38], N. I. Zimine[39], J. Zinsser[64b], M. Ziolkowski[145], L. Živković[16], A. Zoccoli[24a,24b], K. Zoch[62], T. G. Zorbas[143], O. Zormpa[47], W. Zou[42], L. Zwalinski[37]

[1] Department of Physics, University of Adelaide, Adelaide, Australia
[2] Department of Physics, University of Alberta, Edmonton, AB, Canada
[3] [(a)]Department of Physics, Ankara University, Ankara, Turkey; [(b)]Division of Physics, TOBB University of Economics and Technology, Ankara, Turkey
[4] LAPP, Université Savoie Mont Blanc, CNRS/IN2P3, Annecy, France
[5] APC, Université Paris Cité, CNRS/IN2P3, Paris, France
[6] High Energy Physics Division, Argonne National Laboratory, Argonne, IL, USA
[7] Department of Physics, University of Arizona, Tucson, AZ, USA
[8] Department of Physics, University of Texas at Arlington, Arlington, TX, USA
[9] Physics Department, National and Kapodistrian University of Athens, Athens, Greece
[10] Physics Department, National Technical University of Athens, Zografou, Greece
[11] Department of Physics, University of Texas at Austin, Austin, TX, USA
[12] Institute of Physics, Azerbaijan Academy of Sciences, Baku, Azerbaijan
[13] Institut de Física d'Altes Energies (IFAE), Barcelona Institute of Science and Technology, Barcelona, Spain

[14] Institute of High Energy Physics, Chinese Academy of Sciences, Beijing, China
[15] Physics Department, Tsinghua University, Beijing, China
[16] Institute of Physics, University of Belgrade, Belgrade, Serbia
[17] Department for Physics and Technology, University of Bergen, Bergen, Norway
[18] [(a)]Physics Division, Lawrence Berkeley National Laboratory, Berkeley, CA, USA; [(b)]University of California, Berkeley, CA, USA
[19] Institut für Physik, Humboldt Universität zu Berlin, Berlin, Germany
[20] Albert Einstein Center for Fundamental Physics and Laboratory for High Energy Physics, University of Bern, Bern, Switzerland
[21] School of Physics and Astronomy, University of Birmingham, Birmingham, UK
[22] [(a)]Department of Physics, Bogazici University, Istanbul, Turkey; [(b)]Department of Physics Engineering, Gaziantep University, Gaziantep, Turkey; [(c)]Department of Physics, Istanbul University, Istanbul, Turkey
[23] [(a)]Facultad de Ciencias y Centro de Investigaciónes, Universidad Antonio Nariño, Bogotá, Colombia; [(b)]Departamento de Física, Universidad Nacional de Colombia, Bogotá, Colombia
[24] [(a)]Dipartimento di Fisica e Astronomia A. Righi, Università di Bologna, Bologna, Italy; [(b)]INFN Sezione di Bologna, Bologna, Italy
[25] Physikalisches Institut, Universität Bonn, Bonn, Germany
[26] Department of Physics, Boston University, Boston, MA, USA
[27] Department of Physics, Brandeis University, Waltham, MA, USA
[28] [(a)]Transilvania University of Brasov, Brasov, Romania; [(b)]Horia Hulubei National Institute of Physics and Nuclear Engineering, Bucharest, Romania; [(c)]Department of Physics, Alexandru Ioan Cuza University of Iasi, Iasi, Romania; [(d)]Physics Department, National Institute for Research and Development of Isotopic and Molecular Technologies, Cluj-Napoca, Romania; [(e)]National University of Science and Technology Politechnica, Bucharest, Romania; [(f)]West University in Timisoara, Timisoara, Romania; [(g)]Faculty of Physics, University of Bucharest, Bucharest, Romania
[29] [(a)]Faculty of Mathematics, Physics and Informatics, Comenius University, Bratislava, Slovak Republic; [(b)]Department of Subnuclear Physics, Institute of Experimental Physics of the Slovak Academy of Sciences, Kosice, Slovak Republic
[30] Physics Department, Brookhaven National Laboratory, Upton, NY, USA
[31] Universidad de Buenos Aires, Facultad de Ciencias Exactas y Naturales, Departamento de Física, y CONICET, Instituto de Física de Buenos Aires (IFIBA), Buenos Aires, Argentina
[32] California State University, Long Beach, CA, USA
[33] Cavendish Laboratory, University of Cambridge, Cambridge, UK
[34] [(a)]Department of Physics, University of Cape Town, Cape Town, South Africa; [(b)]iThemba Labs, Western Cape, South Africa; [(c)]Department of Mechanical Engineering Science, University of Johannesburg, Johannesburg, South Africa; [(d)]National Institute of Physics, University of the Philippines Diliman (Philippines), Quezon City, Philippines; [(e)]Department of Physics, University of South Africa, Pretoria, South Africa; [(f)]University of Zululand, KwaDlangezwa, Empangeni, South Africa; [(g)]School of Physics, University of the Witwatersrand, Johannesburg, South Africa
[35] Department of Physics, Carleton University, Ottawa, ON, Canada
[36] [(a)]Faculté des Sciences Ain Chock, Université Hassan II de Casablanca, Casablanca, Morocco; [(b)]Faculté des Sciences, Université Ibn-Tofail, Kenitra, Morocco; [(c)]Faculté des Sciences Semlalia, Université Cadi Ayyad, LPHEA-Marrakech, Marrakech, Morocco; [(d)]LPMR, Faculté des Sciences, Université Mohamed Premier, Oujda, Morocco; [(e)]Faculté des sciences, Université Mohammed V, Rabat, Morocco; [(f)]Institute of Applied Physics, Mohammed VI Polytechnic University, Ben Guerir, Morocco
[37] CERN, Geneva, Switzerland
[38] Affiliated with an Institute Covered by a Cooperation Agreement with CERN, Geneva, Switzerland
[39] Affiliated with an International Laboratory Covered by a Cooperation Agreement with CERN, Geneva, Switzerland
[40] Enrico Fermi Institute, University of Chicago, Chicago, IL, USA
[41] LPC, Université Clermont Auvergne, CNRS/IN2P3, Clermont-Ferrand, France
[42] Nevis Laboratory, Columbia University, Irvington, NY, USA
[43] Niels Bohr Institute, University of Copenhagen, Copenhagen, Denmark
[44] [(a)]Dipartimento di Fisica, Università della Calabria, Rende, Italy; [(b)]INFN Gruppo Collegato di Cosenza, Laboratori Nazionali di Frascati, Frascati, Italy

[45] Physics Department, Southern Methodist University, Dallas, TX, USA
[46] Physics Department, University of Texas at Dallas, Richardson, TX, USA
[47] National Centre for Scientific Research "Demokritos", Agia Paraskevi, Greece
[48] [(a)]Department of Physics, Stockholm University, Stockholm, Sweden; [(b)]Oskar Klein Centre, Stockholm, Sweden
[49] Deutsches Elektronen-Synchrotron DESY, Hamburg and Zeuthen, Germany
[50] Fakultät Physik, Technische Universität Dortmund, Dortmund, Germany
[51] Institut für Kern- und Teilchenphysik, Technische Universität Dresden, Dresden, Germany
[52] Department of Physics, Duke University, Durham, NC, USA
[53] SUPA-School of Physics and Astronomy, University of Edinburgh, Edinburgh, UK
[54] INFN e Laboratori Nazionali di Frascati, Frascati, Italy
[55] Physikalisches Institut, Albert-Ludwigs-Universität Freiburg, Freiburg, Germany
[56] II. Physikalisches Institut, Georg-August-Universität Göttingen, Göttingen, Germany
[57] Département de Physique Nucléaire et Corpusculaire, Université de Genève, Geneva, Switzerland
[58] [(a)]Dipartimento di Fisica, Università di Genova, Genoa, Italy; [(b)]INFN Sezione di Genova, Genoa, Italy
[59] II. Physikalisches Institut, Justus-Liebig-Universität Giessen, Giessen, Germany
[60] SUPA-School of Physics and Astronomy, University of Glasgow, Glasgow, UK
[61] LPSC, Université Grenoble Alpes, CNRS/IN2P3, Grenoble INP, Grenoble, France
[62] Laboratory for Particle Physics and Cosmology, Harvard University, Cambridge, MA, USA
[63] [(a)]Department of Modern Physics and State Key Laboratory of Particle Detection and Electronics, University of Science and Technology of China, Hefei, China; [(b)]Institute of Frontier and Interdisciplinary Science and Key Laboratory of Particle Physics and Particle Irradiation (MOE), Shandong University, Qingdao, China; [(c)]School of Physics and Astronomy, Key Laboratory for Particle Astrophysics and Cosmology (MOE), SKLPPC, Shanghai Jiao Tong University, Shanghai, China; [(d)]Tsung-Dao Lee Institute, Shanghai, China; [(e)]School of Physics, Zhengzhou University, Zhengzhou, China
[64] [(a)]Kirchhoff-Institut für Physik, Ruprecht-Karls-Universität Heidelberg, Heidelberg, Germany; [(b)]Physikalisches Institut, Ruprecht-Karls-Universität Heidelberg, Heidelberg, Germany
[65] [(a)]Department of Physics, Chinese University of Hong Kong, Shatin, N.T., Hong Kong, China; [(b)]Department of Physics, University of Hong Kong, Hong Kong, China; [(c)]Department of Physics and Institute for Advanced Study, Hong Kong University of Science and Technology, Clear Water Bay, Kowloon, Hong Kong, China
[66] Department of Physics, National Tsing Hua University, Hsinchu, Taiwan
[67] IJCLab, Université Paris-Saclay, CNRS/IN2P3, 91405 Orsay, France
[68] Centro Nacional de Microelectrónica (IMB-CNM-CSIC), Barcelona, Spain
[69] Department of Physics, Indiana University, Bloomington, IN, USA
[70] [(a)]INFN Gruppo Collegato di Udine, Sezione di Trieste, Udine, Italy; [(b)]ICTP, Trieste, Italy; [(c)]Dipartimento Politecnico di Ingegneria e Architettura, Università di Udine, Udine, Italy
[71] [(a)]INFN Sezione di Lecce, Lecce, Italy; [(b)]Dipartimento di Matematica e Fisica, Università del Salento, Lecce, Italy
[72] [(a)]INFN Sezione di Milano, Milan, Italy; [(b)]Dipartimento di Fisica, Università di Milano, Milan, Italy
[73] [(a)]INFN Sezione di Napoli, Naples, Italy; [(b)]Dipartimento di Fisica, Università di Napoli, Naples, Italy
[74] [(a)]INFN Sezione di Pavia, Pavia, Italy; [(b)]Dipartimento di Fisica, Università di Pavia, Pavia, Italy
[75] [(a)]INFN Sezione di Pisa, Pisa, Italy; [(b)]Dipartimento di Fisica E. Fermi, Università di Pisa, Pisa, Italy
[76] [(a)]INFN Sezione di Roma, Rome, Italy; [(b)]Dipartimento di Fisica, Sapienza Università di Roma, Rome, Italy
[77] [(a)]INFN Sezione di Roma Tor Vergata, Rome, Italy; [(b)]Dipartimento di Fisica, Università di Roma Tor Vergata, Rome, Italy
[78] [(a)]INFN Sezione di Roma Tre, Rome, Italy; [(b)]Dipartimento di Matematica e Fisica, Università Roma Tre, Rome, Italy
[79] [(a)]INFN-TIFPA, Povo, Italy; [(b)]Università degli Studi di Trento, Trento, Italy
[80] Department of Astro and Particle Physics, Universität Innsbruck, Innsbruck, Austria
[81] University of Iowa, Iowa City, IA, USA
[82] Department of Physics and Astronomy, Iowa State University, Ames, IA, USA
[83] Istinye University, Sariyer, Istanbul, Turkey
[84] [(a)]Departamento de Engenharia Elétrica, Universidade Federal de Juiz de Fora (UFJF), Juiz de Fora, Brazil; [(b)]Universidade Federal do Rio De Janeiro COPPE/EE/IF, Rio de Janeiro, Brazil; [(c)]Instituto de Física, Universidade de São Paulo, São Paulo, Brazil; [(d)]Rio de Janeiro State University, Rio de Janeiro, Brazil; [(e)]Federal University of Bahia, Bahia, Brazil

[85] KEK, High Energy Accelerator Research Organization, Tsukuba, Japan
[86] Graduate School of Science, Kobe University, Kobe, Japan
[87] [(a)]Faculty of Physics and Applied Computer Science, AGH University of Krakow, Kraków, Poland; [(b)]Marian Smoluchowski Institute of Physics, Jagiellonian University, Kraków, Poland
[88] Institute of Nuclear Physics Polish Academy of Sciences, Kraków, Poland
[89] Faculty of Science, Kyoto University, Kyoto, Japan
[90] Research Center for Advanced Particle Physics and Department of Physics, Kyushu University, Fukuoka, Japan
[91] L2IT, Université de Toulouse, CNRS/IN2P3, UPS, Toulouse, France
[92] Instituto de Física La Plata, Universidad Nacional de La Plata and CONICET, La Plata, Argentina
[93] Physics Department, Lancaster University, Lancaster, UK
[94] Oliver Lodge Laboratory, University of Liverpool, Liverpool, UK
[95] Department of Experimental Particle Physics, Jožef Stefan Institute and Department of Physics, University of Ljubljana, Ljubljana, Slovenia
[96] School of Physics and Astronomy, Queen Mary University of London, London, UK
[97] Department of Physics, Royal Holloway University of London, Egham, UK
[98] Department of Physics and Astronomy, University College London, London, UK
[99] Louisiana Tech University, Ruston, LA, USA
[100] Fysiska institutionen, Lunds universitet, Lund, Sweden
[101] Departamento de Física Teorica C-15 and CIAFF, Universidad Autónoma de Madrid, Madrid, Spain
[102] Institut für Physik, Universität Mainz, Mainz, Germany
[103] School of Physics and Astronomy, University of Manchester, Manchester, UK
[104] CPPM, Aix-Marseille Université, CNRS/IN2P3, Marseille, France
[105] Department of Physics, University of Massachusetts, Amherst, MA, USA
[106] Department of Physics, McGill University, Montreal, QC, Canada
[107] School of Physics, University of Melbourne, Melbourne, VIC, Australia
[108] Department of Physics, University of Michigan, Ann Arbor, MI, USA
[109] Department of Physics and Astronomy, Michigan State University, East Lansing, MI, USA
[110] Group of Particle Physics, University of Montreal, Montreal, QC, Canada
[111] Fakultät für Physik, Ludwig-Maximilians-Universität München, Munich, Germany
[112] Max-Planck-Institut für Physik (Werner-Heisenberg-Institut), Munich, Germany
[113] Graduate School of Science and Kobayashi-Maskawa Institute, Nagoya University, Nagoya, Japan
[114] [(a)]Department of Physics, Nanjing University, Nanjing, China; [(b)]School of Science, Shenzhen Campus of Sun Yat-sen University, Shenzhen, China; [(c)]University of Chinese Academy of Science (UCAS), Beijing, China
[115] Department of Physics and Astronomy, University of New Mexico, Albuquerque, NM, USA
[116] Institute for Mathematics, Astrophysics and Particle Physics, Radboud University/Nikhef, Nijmegen, The Netherlands
[117] Nikhef National Institute for Subatomic Physics and University of Amsterdam, Amsterdam, The Netherlands
[118] Department of Physics, Northern Illinois University, De Kalb, IL, USA
[119] [(a)]New York University Abu Dhabi, Abu Dhabi, United Arab Emirates; [(b)]United Arab Emirates University, Al Ain, United Arab Emirates
[120] Department of Physics, New York University, New York, NY, USA
[121] Ochanomizu University, Otsuka, Bunkyo-ku, Tokyo, Japan
[122] Ohio State University, Columbus, OH, USA
[123] Homer L. Dodge Department of Physics and Astronomy, University of Oklahoma, Norman, OK, USA
[124] Department of Physics, Oklahoma State University, Stillwater, OK, USA
[125] Joint Laboratory of Optics, Palacký University, Olomouc, Czech Republic
[126] Institute for Fundamental Science, University of Oregon, Eugene, OR, USA
[127] Graduate School of Science, Osaka University, Osaka, Japan
[128] Department of Physics, University of Oslo, Oslo, Norway
[129] Department of Physics, Oxford University, Oxford, UK
[130] LPNHE, Sorbonne Université, Université Paris Cité, CNRS/IN2P3, Paris, France
[131] Department of Physics, University of Pennsylvania, Philadelphia, PA, USA
[132] Department of Physics and Astronomy, University of Pittsburgh, Pittsburgh, PA, USA

[133] [(a)]Laboratório de Instrumentação e Física Experimental de Partículas-LIP, Lisbon, Portugal; [(b)]Departamento de Física, Faculdade de Ciências, Universidade de Lisboa, Lisbon, Portugal; [(c)]Departamento de Física, Universidade de Coimbra, Coimbra, Portugal; [(d)]Centro de Física Nuclear da Universidade de Lisboa, Lisbon, Portugal; [(e)]Departamento de Física, Universidade do Minho, Braga, Portugal; [(f)]Departamento de Física Teórica y del Cosmos, Universidad de Granada, Granada, Spain; [(g)]Departamento de Física, Instituto Superior Técnico, Universidade de Lisboa, Lisbon, Portugal
[134] Institute of Physics of the Czech Academy of Sciences, Prague, Czech Republic
[135] Czech Technical University in Prague, Prague, Czech Republic
[136] Faculty of Mathematics and Physics, Charles University, Prague, Czech Republic
[137] Particle Physics Department, Rutherford Appleton Laboratory, Didcot, UK
[138] IRFU, CEA, Université Paris-Saclay, Gif-sur-Yvette, France
[139] Santa Cruz Institute for Particle Physics, University of California Santa Cruz, Santa Cruz, CA, USA
[140] [(a)]Departamento de Física, Pontificia Universidad Católica de Chile, Santiago, Chile; [(b)]Millennium Institute for Subatomic Physics at High Energy Frontier (SAPHIR), Santiago, Chile; [(c)]Instituto de Investigación Multidisciplinario en Ciencia y Tecnología, y Departamento de Física, Universidad de La Serena, La Serena, Chile; [(d)]Department of Physics, Universidad Andres Bello, Santiago, Chile; [(e)]Instituto de Alta Investigación, Universidad de Tarapacá, Arica, Chile; [(f)]Departamento de Física, Universidad Técnica Federico Santa María, Valparaíso, Chile
[141] Department of Physics, Institute of Science, Tokyo, Japan
[142] Department of Physics, University of Washington, Seattle, WA, USA
[143] Department of Physics and Astronomy, University of Sheffield, Sheffield, UK
[144] Department of Physics, Shinshu University, Nagano, Japan
[145] Department Physik, Universität Siegen, Siegen, Germany
[146] Department of Physics, Simon Fraser University, Burnaby, BC, Canada
[147] SLAC National Accelerator Laboratory, Stanford, CA, USA
[148] Department of Physics, Royal Institute of Technology, Stockholm, Sweden
[149] Departments of Physics and Astronomy, Stony Brook University, Stony Brook, NY, USA
[150] Department of Physics and Astronomy, University of Sussex, Brighton, UK
[151] School of Physics, University of Sydney, Sydney, Australia
[152] Institute of Physics, Academia Sinica, Taipei, Taiwan
[153] [(a)]E. Andronikashvili Institute of Physics, Iv. Javakhishvili Tbilisi State University, Tbilisi, Georgia; [(b)]High Energy Physics Institute, Tbilisi State University, Tbilisi, Georgia; [(c)]University of Georgia, Tbilisi, Georgia
[154] Department of Physics, Technion, Israel Institute of Technology, Haifa, Israel
[155] Raymond and Beverly Sackler School of Physics and Astronomy, Tel Aviv University, Tel Aviv, Israel
[156] Department of Physics, Aristotle University of Thessaloniki, Thessaloníki, Greece
[157] International Center for Elementary Particle Physics and Department of Physics, University of Tokyo, Tokyo, Japan
[158] Department of Physics, University of Toronto, Toronto, ON, Canada
[159] [(a)]TRIUMF, Vancouver, BC, Canada; [(b)]Department of Physics and Astronomy, York University, Toronto, ON, Canada
[160] Division of Physics and Tomonaga Center for the History of the Universe, Faculty of Pure and Applied Sciences, University of Tsukuba, Tsukuba, Japan
[161] Department of Physics and Astronomy, Tufts University, Medford, MA, USA
[162] Department of Physics and Astronomy, University of California Irvine, Irvine, CA, USA
[163] University of Sharjah, Sharjah, United Arab Emirates
[164] Department of Physics and Astronomy, University of Uppsala, Uppsala, Sweden
[165] Department of Physics, University of Illinois, Urbana, IL, USA
[166] Instituto de Física Corpuscular (IFIC), Centro Mixto Universidad de Valencia-CSIC, Valencia, Spain
[167] Department of Physics, University of British Columbia, Vancouver, BC, Canada
[168] Department of Physics and Astronomy, University of Victoria, Victoria, BC, Canada
[169] Fakultät für Physik und Astronomie, Julius-Maximilians-Universität Würzburg, Würzburg, Germany
[170] Department of Physics, University of Warwick, Coventry, UK
[171] Waseda University, Tokyo, Japan
[172] Department of Particle Physics and Astrophysics, Weizmann Institute of Science, Rehovot, Israel
[173] Department of Physics, University of Wisconsin, Madison, WI, USA
[174] Fakultät für Mathematik und Naturwissenschaften, Fachgruppe Physik, Bergische Universität Wuppertal, Wuppertal, Germany

[175] Department of Physics, Yale University, New Haven, CT, USA

[a] Also Affiliated with an Institute Covered by a Cooperation Agreement with CERN, Geneva, Switzerland
[b] Also at An-Najah National University, Nablus, Palestine
[c] Also at Borough of Manhattan Community College, City University of New York, New York, NY, USA
[d] Also at Center for High Energy Physics, Peking University, Beijing, China
[e] Also at Center for Interdisciplinary Research and Innovation (CIRI-AUTH), Thessaloníki, Greece
[f] Also at Centro Studi e Ricerche Enrico Fermi, Rome, Italy
[g] Also at CERN, Geneva, Switzerland
[h] Also at Département de Physique Nucléaire et Corpusculaire, Université de Genève, Geneva, Switzerland
[i] Also at Departament de Fisica de la Universitat Autonoma de Barcelona, Barcelona, Spain
[j] Also at Department of Financial and Management Engineering, University of the Aegean, Chios, Greece
[k] Also at Department of Physics, California State University, Sacramento, USA
[l] Also at Department of Physics, King's College London, London, UK
[m] Also at Department of Physics, Stanford University, Stanford, CA, USA
[n] Also at Department of Physics, Stellenbosch University, Stellenbosch, South Africa
[o] Also at Department of Physics, University of Fribourg, Fribourg, Switzerland
[p] Also at Department of Physics, University of Thessaly, Vólos, Greece
[q] Also at Department of Physics, Westmont College, Santa Barbara, USA
[r] Also at Faculty of Physics, Sofia University, 'St. Kliment Ohridski', Sofia, Bulgaria
[s] Also at Hellenic Open University, Patras, Greece
[t] Also at Institucio Catalana de Recerca i Estudis Avancats, ICREA, Barcelona, Spain
[u] Also at Institut für Experimentalphysik, Universität Hamburg, Hamburg, Germany
[v] Also at Institute for Nuclear Research and Nuclear Energy (INRNE) of the Bulgarian Academy of Sciences, Sofia, Bulgaria
[w] Also at Institute of Applied Physics, Mohammed VI Polytechnic University, Ben Guerir, Morocco
[x] Also at Institute of Particle Physics (IPP), Victoria, Canada
[y] Also at Institute of Physics and Technology, Mongolian Academy of Sciences, Ulaanbaatar, Mongolia
[z] Also at Institute of Physics, Azerbaijan Academy of Sciences, Baku, Azerbaijan
[aa] Also at Institute of Theoretical Physics, Ilia State University, Tbilisi, Georgia
[ab] Also at Lawrence Livermore National Laboratory, Livermore, USA
[ac] Also at National Institute of Physics, University of the Philippines Diliman (Philippines), Quezon City, Philippines
[ad] Also at Technical University of Munich, Munich, Germany
[ae] Also at The Collaborative Innovation Center of Quantum Matter (CICQM), Beijing, China
[af] Also at TRIUMF, Vancouver, BC, Canada
[ag] Also at Università di Napoli Parthenope, Naples, Italy
[ah] Also at Department of Physics, University of Colorado Boulder, Colorado, USA
[ai] Also at Washington College, Chestertown, MD, USA
[aj] Also at Physics Department, Yeditepe University, Istanbul, Turkey
* Deceased